ISTANBUL TECHNICAL UNIVERSITY ★ GRADUATE SCHOOL OF SCIENCE ENGINEERING AND TECHNOLOGY

CONSTRUCTION AND CHARACTERIZATION OF SOLID-SUPPORTED LIPID BILAYERS TO INVESTIGATE CELL - SURFACE INTERACTIONS

Ph.D. THESIS

Abdulhalim KILIÇ

Department of Molecular Biology-Genetics and Biotechnology

Molecular Biology-Genetics and Biotechnology Programme

FEBRUARY 2018

ISTANBUL TECHNICAL UNIVERSITY ★ GRADUATE SCHOOL OF SCIENCE ENGINEERING AND TECHNOLOGY

CONSTRUCTION AND CHARACTERIZATION OF SOLID-SUPPORTED LIPID BILAYERS TO INVESTIGATE CELL - SURFACE INTERACTIONS

Ph.D. THESIS

Abdulhalim KILIÇ
(521112110)

Department of Molecular Biology-Genetics and Biotechnology

Molecular Biology-Genetics and Biotechnology Programme

Thesis Advisor: Assoc. Prof. Dr. Fatma Neşe KÖK

FEBRUARY 2018

İSTANBUL TEKNİK ÜNİVERSİTESİ ★ FEN BİLİMLERİ ENSTİTÜSÜ

HÜCRE – YÜZEY ETKİLEŞİMLERİNİN İNCELENMESİ İÇİN YÜZEY-DESTEKLİ LİPİD ZARLARIN OLUŞTURULMASI VE KARAKTERİZASYONU

DOKTORA TEZİ

Abdulhalim KILIÇ
(521112110)

Moleküler Biyoloji - Genetik ve Biyoteknoloji Anabilim Dalı

Moleküler Biyoloji - Genetik ve Biyoteknoloji Programı

Tez Danışmanı: Doç. Dr. Fatma Neşe KÖK

ŞUBAT 2018

Abdulhalim KILIÇ, a **Ph.D**. student of ITU Graduate School of Science Engineering and Technology student ID **521112110**, successfully defended the thesis entitled "**CONSTRUCTION AND CHARACTERIZATION OF SOLID-SUPPORTED LIPID BILAYERS TO INVESTIGATE CELL - SURFACE INTERACTIONS**", which he prepared after fulfilling the requirements specified in the associated legislations, before the jury whose signatures are below.

Thesis Advisor :	**Assoc. Prof. Dr. Fatma Neşe KÖK** Istanbul Technical University	.....
Jury Members :	**Prof. Dr. Zeynep Petek ÇAKAR** Istanbul Technical University	.....
	Assist. Prof. Dr. Deniz YÜCEL Acıbadem Mehmet Ali Aydınlar University	.....
	Assoc. Prof. Dr. H. Özgür ÖZER Istanbul Technical University	.....
	Assist. Prof. Dr. Ahu ARSLAN YILDIZ İzmir Institute of Technology	.....

Date of Submission : 19 January 2018
Date of Defense : 09 February 2018

Emeğe,

FOREWORD

First, I would like to thank to my supervisor, Assoc. Prof. Dr. Fatma Neşe KÖK with all my respect, for giving me the possibility to work in her research group, the extensive freedom in trying various experiments in my own under her tolerant guidance and support. Her critical way of thinking strengthened my scientific background and enlightened my way throughout my studies, and every time will illuminate my academic future.

I want to thank to Prof. Dr. Zeynep Petek ÇAKAR, as my respectful, precious instructor from the first years of my undergraduate education, and jury member, who guided me everytime with her attentive and kind personality. I would like to thank to Assist. Prof. Dr. Deniz YÜCEL as my jury member who guided me during my thesis. I want to express my thanks to Assoc. Prof. Dr. Hakan Özgür ÖZER for AFM studies and his students Majid F. JADIDI and Ahmed ULUCA. He opened his lab to me, which was very valuable for me to progress my thesis. I also would like to thank to Assist. Prof. Dr. Ahu ARSLAN YILDIZ who accepted to be my jury member.

I would also like to kindly thank to my labfriends, Ayşe Buse ÖZDABAK, İnas ÖZCAN, Arife KUŞBAZ, Şebnem SEHERLER who have been helpful and friendly with me. It was a pleasure to work with them. I am indebted each of them.

I am grateful to my devoted family and my beloved wife Süheyla, for their love, support, encourage and understanding.

Last, I am grateful to my university, my program and Research Center (MOBGAM) for providing me these opportunities.

This study was supported by ITU-BAP Project (36172).

January 2018 Abdulhalim KILIÇ

TABLE OF CONTENTS

Page

ABBREVIATIONS

AFM	: Atomic Force Microscopy
BSA	: Bovine Serum Albumin
DLS	: Dynamic Light Scattering
DMEM	: Dulbecco's Modified Eagle Culture Medium
DPPTE	: 1,2-Dipalmitoyl-Sn-Glycero-3-Phosphothioethanol
ECM	: Extracellular Matrix
FN	: Fibronectin
FRAP	: Fluorescence Recovery after Photobleaching
HEPES	: 4-(2-hydroxyethyl)-1-piperazineethanesulfonic acid
hfOB	: Human Fetal Osteoblastic Bone
MTS	: 3-(4,5-dimethylthiazol-2-yl)-5-(3-carboxymethoxyphenyl)-2-(4-sulfophenyl)–2H-tetrazolium
QCM-D	: Quartz Crystal Microbalance with Dissipation
PBS	: Phosphate Buffered Saline
PC	: Phosphatidylcholine
PLL	: Poly-L-Lysine
PS	: Phosphatidylserine
R_a	: Roughness Average
RGD	: Arginylglycylaspartic acid
RIU	: Refractive Index Unit
SAM	: Self-Assembled Monolayer
SaOS-2	: Human Osteosarcoma
SLB	: Supported Lipid Bilayers
SPR	: Surface Plasmon Resonance
tBLM	: Tethered Bilayer Lipid Membranes

SYMBOLS

Δf	: Frequency Change
ΔD	: Dissipation Change
$\Delta \Theta$	: Plasmon Resonance Angle
λ	: Wavelength
l_{decay}	: Decay Length
κ	: Sensitivity Factor
C	: Mass Sensitivity Constant
d_n/d_c	: Refractive Index Increment
Q	: Quality Factor

LIST OF TABLES

Page

LIST OF FIGURES

Page

CONSTRUCTION AND CHARACTERIZATION OF SOLID-SUPPORTED LIPID BILAYERS TO INVESTIGATE CELL - SURFACE INTERACTIONS

SUMMARY

Investigation of cell-cell/biomolecule and cell-surface interactions are essential to understand basic mechanisms such as cell signaling, attachment, proliferation and differentiation. Getting insight to these mechanisms also elucidates the topics such as the development and improvement of effective medical systems. Supported lipid bilayers (SLBs) when functionalized with bioactive molecules that are responsible for specific biological interactions, allow long-term experiments for many practical applications such as investigation of the basic features of biological membranes, construction of biosensors, drug screening platforms, cancer cell detection platforms and investigation of the cell–cell/biomolecule, cell-surface interactions. These biomimetic lipid bilayer platforms allow the usage of surface-sensitive characterization techniques such as atomic force spectroscopy (AFM), surface plasmon resonance (SPR) and quartz crystal microbalance with dissipation monitoring (QCM-D).

The aim of the thesis is to construct functional SLB platform to investigate cell-surface interactions and to monitor whole process in real time via QCM-D system. In this way, it is possible to investigate changes in cell-surface interactions (surface characteristics, cell type and time dependent) that can not be distinguished under the microscope. SLB surfaces were functionalized with RGD, and osteocalcin mimetic (OSN) peptides and their interaction with osteoblast cells were evaluated. RGD is the binding motif of various extracellular matrix (ECM) proteins so it is expected to promote cell adhesion whereas OSN is known to promote biomineralization rather than cell attachment so chosen as control. Similar platforms were used in parallel in cell culture environment for comparison.

The first part of the thesis focused on the construction of an SLB platform in single step. Most of the model lipid membrane studies on gold-coated sensors involve the usage of various surface-modification strategies to rupture liposomes and induce lipid bilayer formation since liposomes with polar surfaces do not interact with bare, hydrophobic gold. For this purpose, it was aimed to form SLB on gold sensor surfaces without further modification by incorporating a thiol-modified phospholipid, *1,2-Dipalmitoyl-sn-Glycero-3-Phosphothioethanol* (DPPTE) into phosphatidylcholine (PC) based liposomes. The binding kinetics of liposomes with different DPPTE ratio (0.01 to 100% mol/mol) and diameters were monitored by QCM-D. The dissipation change per frequency change, i.e., acoustic ratio, which is evaluated as a degree of the viscoelasticity, considerably decreased with the presence of DPPTE (from 162.3 GHz^{-1} for flattened PC liposomes to ca. 89.5 GHz^{-1} for 100% DPPTE liposomes) when compared to the results of two reference rigid monolayers and two viscoelastic layers. To assess the quality of SLB platform, the interpretation of QCM-D data was also complemented with Surface Plasmon Resonance. While QCM-D is sensitive to the liquid content within the layers, SPR provides liquid-independent results and thus

the results of these techniques are compared to make more realistic interpretations. The optimum thiolated-lipid ratio (1%, lower thiol ratio and higher rigidity) was then used to determine the dry-lipid mass deposition, the water content and the thickness values of the SLB via viscoelastic modelling. Further, surface characterization studies were performed by Atomic Force Microscopy with high spatial resolution. The results suggested that model membrane was almost continuous with minimum defects but showed more dissipative/soft nature compared to an ideal bilayer due to partially fused liposomes/overlapped lipid bilayers/multilayer islands. These local elevations distorted the planarity and led the increase of overall membrane thickness to ~7.0 nm. However, the construction of SLB on gold in a single step has been successfully accomplished.

In the second part of the thesis, the aim was to obtain insight about how to evaluate cell – surface interactions in QCM-D system. QCM-D is one of the powerful techniques, which allow real time, quantitative and noninvasive analysis of the interaction of different cell types with various modified surfaces. For this purpose, different surfaces were prepared without using SLB system and their interaction with the cells for 18 h were interpreted. First, the dynamic adhesion behavior of human fetal osteoblastic bone (hfOB) cell lines was monitored on untreated and hydrophilically treated gold sensor surfaces as reference substrates. Adhesion was also observed under light microscopy to facilitate the evaluation. Cells increased their surface contact area and spread more on hydrophilic surfaces, and showed distinct profile with an increased rigidity at the cell-surface interfacial layer, which is assigned to extracellular matrix remodeling. Further, the adhesion strength and kinetics were characterized on cell adhesive (poly-L-lysine and fibronectin) and repellent (bovine serum albumin) surfaces. The overall results indicated that protein-mediated specific interactions contributed mostly to the dissipation changes (ΔD) or acoustic ratio ($\Delta D/\Delta f$). Finally, the potential of QCM-D to distinguish healthy and cancerous cells were evaluated by comparing the results of hfOB cells with that of SaOS-2 (osteosarcoma) cancerous cells. Cancerous cells interacted more strongly with the surfaces and showed more viscoelastic characteristic than the healthy cells.

In the final part of the thesis, SLB activation and functionalization with RGD and OSN peptides and examination of the interactions of these systems with cells via QCM-D were aimed. First, the stability of lipid bilayers in various medium conditions were evaluated. The structural integrity was conserved until fifth day in PBS, but hole formations started to form from the first day and increase their number and size in time under serum-supplemented medium conditions. SLBs enriched with different lipids (cholesterol, PS, DOTAP) increased the stability of SLB to pure PC. Lateral mobility of the lipid bilayer was also demonstrated via FRAP (Fluorescence Recovery after Photobleaching) method. After the SLB characterization for both stability and fluidity, the kinetics of peptide attachment to SLBs were compared to their nonspecific adsorption onto gold surfaces and the characteristic of resultant layers were analyzed via QCM-D. The results indicated that conjugation to SLB provide higher structural flexibility than passive adsorption. When cells were incubated with these surfaces, it was seen that low density of mobile RGD peptides on SLB platforms preserved their biological activity and promoted cell adhesion more efficiently than high number of immobile peptides on the gold surfaces. Cell attachment and spread on RGD-fSLB surfaces were also confirmed in cell culture. Limited number of cells were attached on bare SLB surface and they remained in rounded morphology. Cells did not spread well on OSN-coated surfaces, and acoustic ratio measured on each OSN layers probably

did not originate from specific adhesion of the cells, instead the negative charge of OSN could provide electrostatic interactions between surface and biomolecules on the cell membrane, thus promoting nonspecific protein and cell attachment.

In conclusion, nonfouling SLB surfaces were successfully functionalized and constructed ^{f}SLB platforms were shown to have the potential for real time and label-free monitoring of the specific cell – surface interactions via QCM-D.

HÜCRE – YÜZEY ETKİLEŞİMLERİNİN İNCELENMESİ İÇİN YÜZEY-DESTEKLİ LİPİD ZARLARIN OLUŞTURULMASI VE KARAKTERİZASYONU

ÖZET

Hücre-hücre/biyomolekül ve hücre-yüzey etkileşimlerinin araştırılması, hücre sinyal iletimi, hücre tutunma, çoğalma ve farklılaşma gibi temel mekanizmaları anlamak için önem arz etmektedir. Bu mekanizmalara ilişkin edinilecek detaylı bilgiler, etkin tıbbi sistemlerin geliştirilmesi ve iyileştirilmesi gibi konularda da aydınlatıcı olmaktadır. Yüzey-destekli Yapay Lipid Membranlar (YLM) özgül biyolojik etkileşimlerden sorumlu biyoaktif moleküller ile işlevselleştirildiğinde biyolojik zarların temel özelliklerinin incelenmesi, biyosensör yapımı, ilaç tarama platformları, kanser hücresi tespit platformları ve hücre-hücre / biyomolekül, hücre-yüzey etkileşimlerinin incelenmesi gibi birçok pratik uygulama için uzun süreli deneylere imkân sağlamaktadırlar. Biyomimetik YLM platformlar ayrıca atomik kuvvet spektroskopisi, yüzey plazmon spektroskopisi (SPR) ve disipasyon-izlemeli kuvartz kristal mikroterazi (QCM-D) gibi yüzeye-hassas karakterizasyon tekniklerinin kullanılmasına izin verir.

Bu tez çalışması kapsamında, hücre-yüzey etkileşimlerini araştırmak için işlevsel YLM platformu oluşturulması ve tüm sürecin QCM-D sistemi kullanılarak gerçek-zamanlı takip edilmesi amaçlanmıştır. Bu şekilde mikroskop altında ayırt edilmesi mümkün olmayan hücre-yüzey etkileşimlerindeki değişikliklerin (yüzey özelliklerine, hücre tipine ve zamana bağlı) araştırılması mümkün olabilmektedir. Bu maksatla YLM yüzeyleri RGD ve osteokalsin mimetik (OSN) peptidleri ile işlevselleştirilmiş ve bu yüzeylerin osteoblast hücreleri ile etkileşimi incelenmiştir. RGD peptidi, çeşitli hücre dışı matris proteinlerinin bağlanma motifi olduğundan hücre tutunmasını teşvik ettiği için; OSN peptidi de hücre tutunmasından ziyade biyomineralizasyonu desteklediği bilindiğinden kontrol olarak seçilmiştir. Karşılaştırma maksadıyla paralel çalışmalar, benzer platformlar kullanılarak hücre kültür ortamında da gerçekleştirilmiştir.

Tezin ilk kısmı tek aşamada oluşturulacak bir YLM platformu tasarlamak üzerine odaklanmaktadır. Polar yüzeyli lipozomların, muamele edilmemiş, hidrofobik altın yüzeyler ile etkileşime girmemesi nedeniyle, altın kaplı sensörler üzerinde yapılan model lipid membran çalışmalarının çoğunda lipozomların kırılıp-parçalanması ve lipid membran oluşumunu başlatması için çeşitli yüzey-modifikasyon stratejileri kullanılır. Tezin bu bölümünde, altın sensör yüzeyler üzerinde ayrıca bir modifikasyona gerek kalmadan, *fosfatidilkolin* temelli lipozomlara thiol-modifiye bir fosfolipid olan *1,2-Dipalmitoyl-sn-Glisero-3-Phosphothioethanol* (DPPTE) dâhil edilerek YLM oluşturulması amaçlandı. Farklı DPPTE oran (% 0,01 ila % 100 mol/mol) ve çaplarında lipozomların bağlanma kinetikleri QCM-D ile izlendi. Sonuçların yorumlanması için iki rijit ve iki viskoelastik katman referans olarak kullanıldı. Viskoelastisite derecesi olarak değerlendirilen, frekans değişikliği başına düşen disipasyon değişimi, yani akustik oranın, DPPTE varlığında önemli ölçüde

düştüğü gözlemlendi (yassılaşmış PC lipozomlar için 162,3 GHz^{-1} iken, % 100 DPPTE içeren lipozomlar için yaklaşık 89,5 GHz^{-1}). YLM platformunun niteliğini değerlendirmek için, kuvartz kristal mikroterazi verilerine ek olarak yüzey plasmon spektroskopisi sonuçları da kullanıldı. QCM-D katmanlardaki su oranına da hassas iken, SPRnin su oranından bağımsız sonuçlar vermesi iki tekniğin sonuçlarının karşılaştırılarak daha gerçekçi yorumlar yapılmasına olanak sağladı. Optimum tiyollü-lipid oranı (% 1, daha düşük tiyol oranı ve daha yüksek rijitlik) ile elde edilen veriler, viskoelastik modelleme yoluyla yüzeydeki kuru-lipid miktarını, katman içi su miktarını ve kalınlık değerlerini hesaplamak için kullanıldı. Yüzey karakterizasyonu çalışmaları ek olarak AFM kullanılarak yüksek uzaysal çözünürlük ile gerçekleştirildi. Sonuçlar, model membranın minimum defektlerle neredeyse bütün/kesintisiz olduğunu, ancak kısmen kaynaşmış lipozom / üst üste gelmiş kimi lipid membran katmanları / çoklu lipid katman adacıkları nedeniyle de ideal bir lipid membrana kıyasla daha fazla disipasyona sahip olduğunu göstermiştir. Lipid membrandaki bu bölgesel yükseltiler membranın düzlemselliği kısmen bozarak genel membran kalınlığının ~ 7.0 nm'ye yükselmesine neden olmuştur. Buna rağmen tek aşamada altın üzerinde YLZ oluşturulması başarılı bir biçimde gerçekleştirilmiştir.

Tezin ikinci bölümünde, QCM-D sistemi kullanılarak hücre - yüzey etkileşimlerinin nasıl gerçek zamanlı takip edileceği ve ne gibi değerlendirmeler yapılabileceği konusunda öncalışmalar yürütülmesi amaçlandı. Bunun için YLZ sistemi kullanılmadan değişik yüzeyler hazırlandı ve hücreler ile 18 saatlik etkileşimleri takip edilerek sinyal değişiklikleri yorumlandı. İlk olarak, insan fetal osteoblastik kemik (hfOB) hücre hattının dinamik tutunma davranışı, referans substratlar olarak, muamele edilmemiş hidrofobik ve hidrofilik kılınmış altın sensör yüzeyler üzerinde izlendi. Değerlendirmeyi kolaylaştırmak için hücre tutunması ışık mikroskopisi altında da gözlemlenerek sonuçlar karşılaştırıldı. Hücrelerin hidrofilik altın yüzeylerde yüzey temas alanlarını daha fazla arttırıp daha fazla yayıldığı görülmüştür. Ayrıca hücre dışı matrisin yeniden biçimlenmesi ile ilişkilendirilen hücre-yüzey arayüzünde artan rijitlik bu yüzeylerde daha yüksek gözlemlenmiştir. Bu öncalışmadan sonra, tutunma kuvveti ve kinetiği, hücre tutucu (poli-L-lisin ve fibronektin) ve itici (sığır serum albümin) yüzeyler üzerinde de karakterize edildi. Sonuçlar, protein aracılı özgül etkileşimlerin frekans değişiminden (Δf) çok disipasyonda (ΔD) veya akustik oranda (ΔD / Δf) değişime katkıda bulunduğunu gösterdi. Son olarak, QCM-D'nin sağlıklı ve kanserli hücreleri ayırt etme potansiyeli, hfOB hücrelerinin ve SaOS-2 (osteosarkom) kanserli hücrelerin sonuçları ile karşılaştırarak değerlendirildi. Kanserli hücrelerin referans yüzeylerle daha güçlü etkileştiği ve sağlıklı hücrelere göre daha fazla viskoelastik karakteristik gösterdiği gözlemlendi.

Tezin son bölümünde, YLM'lerin RGD ve OSN ile işlevselleştirilmesi ve bu sistemlerin hücreler ile etkileşimlerinin QCM-D ile incelenmesi amaçlanmıştır. Bunun için ilk olarak, lipid membranların stabilitesi çeşitli ortam koşullarında belirlendi. PBS içerisinde, membranın yapısal bütünlüğünün beşinci güne kadar korunduğu gözlenirken, serumlu besiyeri ortamında ilk günden itibaren delikler oluşmaya başlamış, sayı ve boyutları zamanla artmıştır. Farklı lipidlerle (kolesterol, PS, DOTAP) zenginleştirilmiş YLM'lerin saf PC-YLM'a göre stabiliteleri artmıştır. Yapay lipid membranın yanal hareketliliği de FRAP yöntemi ile gösterildi. YLM'nin hem stabilite hem de akışkanlık karakterizasyonundan sonra, YLM yüzeylere peptit bağlanma kinetiği incelenerek altın yüzeylerine spesifik olmayan adsorpsiyonları ile karşılaştırıldı ve oluşan katmanların özellikleri QCM-D ile analiz edildi. Sonuçlar, YLM'ye konjüge edilmiş peptidlerin, pasif adsorpsiyonla yüzeye bağlanmışlara

kıyasla daha yüksek yapısal esneklik taşıdığını gösterdi. Hücreler bu yüzeylerle inkübe edildiğinde, YLM platformlarındaki düşük yoğunluğa sahip hareketli RGD peptidlerin biyolojik aktivitelerini korudukları ve altın yüzeylerdeki yüksek sayıda hareketsiz peptitten daha etkili şekilde hücre adezyonunu arttırdığı görüldü. RGD-^{f}YLM yüzeylerinde gözlenen hücre bağlanması ve yayılması, hücre kültüründe de doğrulanmıştır. Yalın YLM yüzeyine sınırlı sayıda hücre tutunmuş ve yuvarlak morfolojide kalmıştır. Hücreler OSN-kaplı yüzeylerde iyi yayılma göstermemiştir. Ölçülen yüksek akustik oranın hücrelerin spesifik tutunmasından kaynaklanmadığı, bunun yerine OSN'nin negatif yükü sayesinde yüzeye bağlanan proteinlerden kaynaklanan bir artış olduğu düşünülmüştür.

Tez kapsamında esas olarak protein ve hücre tutunmasına dirençli olan YLM yüzeyleri başarılı bir şekilde işlevselleştirilmiş ve oluşturulan ^{f}YLM platformlarının, özgül hücre-yüzey etkileşimlerinin QCM-D aracılığıyla gerçek zamanlı ve işaretleme olmaksızın takip edilme potansiyeline sahip olduğu görülmüştür.

1. INTRODUCTION

Investigation of cell-cell/biomolecule and cell-surface interactions are essential to understand basic mechanisms such as cell signaling, attachment, proliferation and differentiation. Getting insight to these mechanisms also elucidates the topics such as the development and improvement of effective medical systems. Supported lipid bilayers (SLBs) when functionalized with bioactive molecules that are responsible for specific biological interactions, allow long-term experiments for many practical applications such as investigation of the basic features of biological membranes, construction of biosensors, drug screening platforms, cancer cell detection platforms and investigation of the cell–cell/biomolecule, cell-surface interactions. These biomimetic lipid bilayer platforms allow the usage of surface-sensitive characterization techniques such as atomic force spectroscopy (AFM), surface plasmon resonance (SPR) and quartz crystal microbalance with dissipation monitoring (QCM-D).

The aim of the thesis is to construct functional SLB platform to investigate cell-surface interactions and to monitor whole process in real time via QCM-D system. In this way, it is possible to investigate changes in cell-surface interactions (surface characteristics, cell type and time dependent) that can not be distinguished under the microscope. SLB surfaces were functionalized with RGD, and osteocalcin mimetic (OSN) peptides and their interaction with osteoblast cells were evaluated. RGD is the binding motif of various extracellular matrix (ECM) proteins so it is expected to promote cell adhesion whereas OSN is known to promote biomineralization rather than cell attachment so chosen as control. Similar platforms were used in parallel in cell culture environment for comparison.

Detailed information about model lipid bilayer systems was presented in Chapter 2. Chapter 3 focused on the construction of the proposed SLB platform. Most of the model lipid membrane studies on gold-coated sensors involve the usage of various surface-modification strategies to rupture liposomes and induce lipid bilayer formation since liposomes with polar surfaces do not interact with bare, hydrophobic gold. In

this part of the thesis, it was aimed to form SLB on gold sensor surfaces without further modification by incorporating a thiol-modified phospholipid (DPPTE) into *phosphatidylcholine* (PC) based liposomes. The binding kinetics of liposomes were monitored by both QCM-D and Surface Plasmon Resonance (SPR). While QCM-D is sensitive to the liquid content within the layers, SPR provides liquid-independent results and thus the results of these techniques are compared to make more realistic interpretations. The optimum thiolated-lipid ratio was then used to determine the dry-lipid mass deposition, the water content and the thickness values of the SLB via viscoelastic modelling. Further, surface characterization studies were performed by Atomic Force Microscopy with high spatial resolution.

In the second part of the thesis (Chapter 4), the aim was to obtain insight about how to evaluate cell – surface interactions in QCM-D system. QCM-D is one of the powerful techniques, which allow real time, quantitative and noninvasive analysis of the interaction of different cell types with various modified surfaces. For this purpose, different surfaces were prepared without using SLB system and their interaction with the cells was followed for 18 h. First, the dynamic adhesion behavior of human fetal osteoblastic bone (hfOB) cell lines was monitored on untreated and hydrophilically treated gold sensor surfaces as reference substrates. Adhesion was also observed under light microscopy to facilitate the evaluation. Further, the adhesion strength and kinetics were characterized on cell adhesive (poly-L-lysine and fibronectin) and repellent (bovine serum albumin) surfaces. Finally, the potential of QCM-D to distinguish healthy and cancerous cells were evaluated by comparing the results of hfOB cells with that of SaOS-2 (osteosarcoma) cancerous cells.

In the final part of the thesis (Chapter 5), SLB activation and functionalization with RGD and OSN peptides and examination of the interactions of these systems with cells via QCM-D were performed. First, the stability of lipid bilayers (PC and PC enriched with different lipids such as cholesterol, PS, DOTAP) in various medium conditions were evaluated. Lateral mobility of the lipid bilayer was also demonstrated via FRAP (Fluorescence Recovery after Photobleaching) method. After characterization of SLB for both stability and fluidity, the kinetics of peptide attachment to SLBs were compared to their nonspecific adsorption onto gold surfaces and the characteristic of resultant layers were analyzed via QCM-D. Cell attachment on each surfaces were also checked in cell culture conditions.

Finally, concluding remarks are given in Chapter 6 along with future prospects and challenges.

2. BIOMIMETIC LIPID BILAYERS ON SOLID SURFACES: MODELS FOR BIOLOGICAL INTERACTIONS[1]

2.1 Introduction

Biological membranes are crucial to cell life as being selectively permeable barriers and as special sites of communication between the inside and the outside of the cellular world. The cell membrane with its complex and dynamic structure consists of a lipid bilayer (phospholipids and cholesterol), a large variety of membrane proteins (transmembrane, lipid-anchored or peripheral) and carbohydrates (in the form of glycoproteins and glycolipids). All these components are asymmetrically distributed in the two leaflets of the bilayer and move freely, as described in the fluid mosaic model. Since the cell membrane is also intimately associated with the cell skeleton and the extracellular matrix (ECM), the structure and the function of the membranes are affected by the changes in the organization of this complex network [1-2].

The major lipid constituents of cell membranes are glycerophospholipids, which have an amphiphilic nature that allows them to self-assemble rapidly and spontaneously when transferred into an aqueous solution. The aliphatic parts of each layer are positioned toward each other, and the hydrophilic heads face either the bulk water or to the inside part of the closed structure. That self-organization of the phospholipids results in the formation of the bilayer structure [3]. The other amphipathic lipid classes in the biological membranes are sphingolipids and steroids. While sphingolipids allow dense packing of lipids with limited lateral mobility, the presence of cholesterol, a sterol, can fluidize them. The local organization of these components and membrane proteins gives rise to lipid microdomains (rafts and caveolae) with variable patchiness and thickness in mammalian cell membranes [1,4]. All these variations in the composition (between two layers, two cell types, two organelles *etc*.) and in the fluidity (rafts) of the lipid bilayer are important for membrane functionality and should be

[1] This chapter is based on the paper "Kilic, A. and F.N. Kok, Biomimetic lipid bilayers on solid surfaces: models for biological interactions. Surface Innovations, 2016. 4(3): p. 141-157."

investigated to understand the cellular mechanisms based on membranes and, consequently, to mimic them realistically.

Because of this complexity of biomembranes, there is a clear need to develop model membrane systems, where one or a few membrane components can be isolated and studied not only for basic membrane studies but also for various important biological interactions – that is, cell–cell, cell–surface, membrane protein–toxin, membrane protein–drug and so on. Model lipid membranes can be constructed from various natural and/or synthetic lipids in different compositions and be enriched by different membrane biomolecule repertoires. Constructed membrane models must sustain the structure and fluidity of the lipid bilayer, mimicking the physiological reality, and should help to preserve the structure and function of reconstituted membrane proteins [5-6]. The current knowledge of the molecular processes occurring at biological membranes is mainly based on studies of the biological membrane models in different forms: micelles, bicelles, nanodisks, liposomes and giant vesicles, for example, are in solution, while some other systems could be formed between two aqueous phases or at the air–water interface as lipid monolayers and black lipid films [5]. Solid-supported lipid bilayers (SLBs), on the other hand, are constructed on planar solid surfaces such as glass, gold, silica and mica and separated from the substrate with a thin (around 1 nm) hydration layer and aqueous solution above [7].

SLBs are widely studied membrane-mimicking models that are mostly formed by Langmuir–Blodgett transfer, Langmuir–Schäfer deposition, deposition from detergent solution, spin coating and vesicle fusion techniques [5,8-9]. The most widely used, the simplest one of these techniques, is vesicle (liposome) fusion [10]. When unilamellar liposomes face a solid surface, they can deform, rupture and fuse to form a continuous lipid bilayer. The resulting structure depends on the properties of the solid support (surface charge, structure, roughness), liposomes (composition, charge and size) and aqueous solution (pH and ionic strength) [5,10]. Transmembrane proteins can also be reconstituted into liposomes to form a proteoliposome, and these can be used to construct membrane protein-incorporated bilayers [11-12].

Functionalized supported lipid bilayers are valuable in the study of the characteristics and behavior of membrane-bound proteins and membrane-mediated cellular processes such as cell adhesion and cell signaling [11-14]. The biomimetic properties of SLBs provide a suitable cell culture environment, so the protein and cytoskeleton

organization of the cells can also be studied [15-18]. Applications of supported membranes on solid surfaces potentially include biosensors, drug screening systems, surface modification of medical implants, bioresorbable material scaffolds supporting cell attachment and growth (for tissue engineering) and the production of catalytic interfaces [19-21].

2.2 Supported Lipid Membrane Models

There are several modified bilayer systems developed for chosen biomolecules of interest. Solid-supported bilayers can simply be formed on hydrophilic surfaces (glass, mica, silica) in one step or as in hybrid bilayers, using alkanethiol chemistry [10]. For the latter, a self-assembled monolayer (SAM) is first formed on gold or other widely used electrode surfaces such as silver and mercury, and then a phospholipid monolayer rides on SAM by way of vesicle fusion [19,22]. These platforms provide a suitable cell-mimicking environment for various small peripheral ligand–extracellular protein interactions or other cell membrane processes. These systems can be easily formed and are relatively stable, but they are not suitable for the incorporation of large transmembrane proteins or pore-forming toxins. Transmembrane proteins require some space on both sides of the bilayer, and a short distance between the solid support and the lipid bilayer (approximately 1 nm) causes restrictions and hampers the activity of inserted proteins that is highly dependent on their flexible three dimensional conformation [22]. This can be overcome by the modified systems named as polymer-cushioned or tethered bilayer lipid membranes (tBLMs), which elevate the bilayer from the surface, offering an aqueous layer in between [23]. Polymer-cushioned systems use a physisorbed spacer layer such as cellulose, dextran, agarose, polyacrylamide, poly-l-lactic acid, polyethylene glycol (PEG) and polyelectrolytes on the surface [24]. Soft polymers provide the necessary height and water reservoir between the support and the lipid bilayer, thus supplying a low friction interface, a more natural environment to the bilayer, and preserving the structural and functional properties of membrane spanning proteins. Moreover, non-specific adsorption of aqueous and transmembrane proteins, an important problem typically occurring at defect sites of solid-supported bilayers lacking polymer layers, is avoided [22,25].

Tethered lipid membranes are quite durable since the lipid bilayer is covalently attached to the surface by various methods using different tethering molecules [12,23-

33]. Short spacer molecules (*e.g.,* tetraethylene glycol) generally provide enough space for the insertion of small membrane proteins or pore-forming peptides such as gramicidin and melittin [28,34]. In order to construct an artificial tethered bilayer lipid platform for the incorporation of transmembrane proteins with a large extra membrane domain, on the other hand, longer spacers are needed. For the incorporation of multidrug resistance protein 1 (MDR1), for example, a modified *lipid (1,2-distearoyl-sn-glycero-3-phosphoethanolamineN-[amino(polyethylene glycol)-2000]* (DSPE-PEG)) (Figure 2.1b) with long PEG spacer was utilized to elevate lipid membrane from the preactivated (Figure 2.1a) gold sensor surface and generate the necessary water reservoir underneath. MDR1-containing liposomes were then spread on top of that surface for protein incorporated bilayer formation (Figure 2.1c). For tethered lipid membranes, it should be considered that while tethered layers are much less affected by solution conditions (pH, ionic strength), an increased level of tethering can hinder the mobility of the membrane [22].

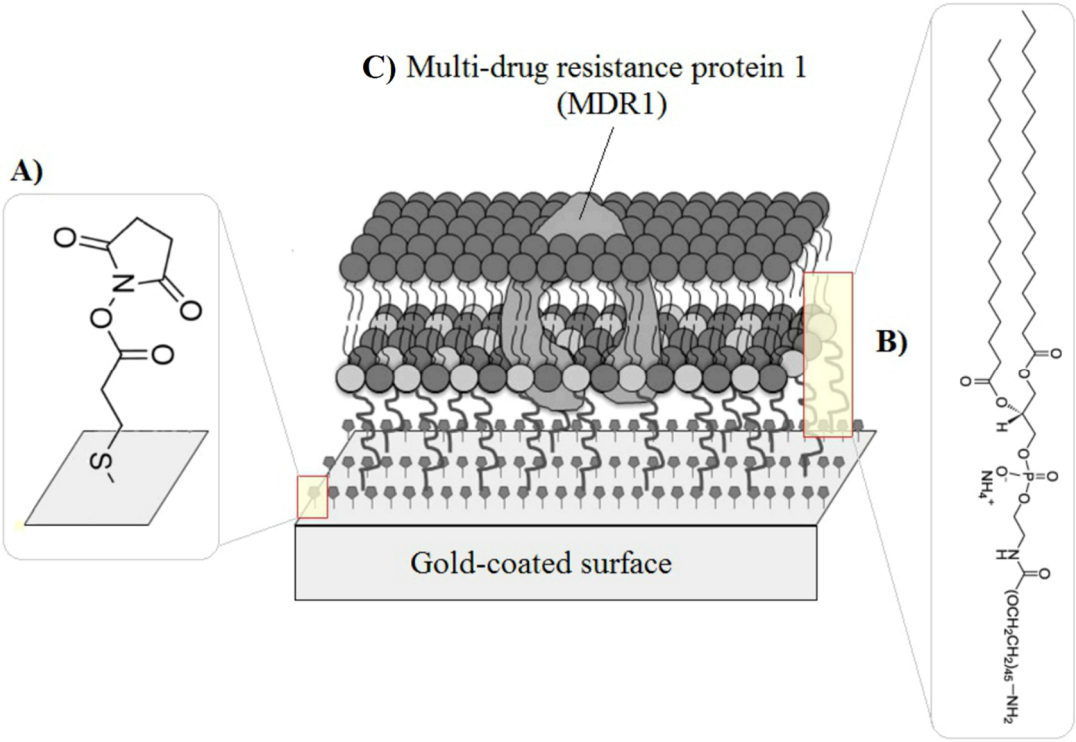

Figure 2.1 : Example of a tBLM constructed on a gold-coated surface. (a) Gold sensor surface is activated with a substance with a succinimide end group. (b) DSPE-PEG spacer layer is attached. (c) Protein-incorporated tBLM is formed by liposome spreading. Adapted with permission from Inci *et al.*[12]. Copyright © 2015 Elsevier.

2.3 Characterization of SLBs

SLBs can be easily manipulated and have high robustness and stability, unlike black lipid membranes, and they remain largely intact even when subjected to high flow rates or vibration [34]. In addition, the presence of holes and surface irregularities does not cause the destruction of the entire bilayer. Their mechanical stability allows long-term experiments, and since they are constructed on flat solid surfaces, they can be characterized by surface-sensitive characterization tools. High-resolution images can be obtained by atomic force microscopy (AFM) or near-field fluorescence microscopy [6], and even small defects ranging from 10 to 500 nm can therefore be detected, which is not easy by standard wide-field optical microscopy. Both surface plasmon resonance (SPR) and ellipsometry, being optical techniques, and a quartz crystal microbalance with dissipation (QCM-D), an acoustic sensor, can provide information about adsorption events on surfaces and the properties of the resulting films [35-36]. In particular, both SPR and QCM-D techniques can quantify adsorbed masses in real time. Binding of proteins to supported bilayers can be studied quantitatively by total internal reflection fluorescence microscopy [37]. The secondary structure and the orientation of membrane proteins in supported bilayers are conveniently determined by polarized Fourier-transform infrared spectroscopy [38]. These techniques employing optical or mechanical sensing are among the popular methods for physical, chemical and structural characterization of lipid layers within aqueous environments [5].

The quality, stability and integrity of SLBs under different conditions can simply be examined on a standard fluorescence microscope, and several artifacts can be easily detected and eliminated [8]. Although testing the stability of SLBs is important for all applications, the enhanced stability may be required in some cases such as their application as cell culture platforms. The interaction of the cells with the biomimetic lipid bilayer challenges the integrity of the platform, so the stability must be enhanced to a point where the SLBs should remain intact during the experiment [9]. Another important characteristic of a bilayer is the lateral mobility of its constituting lipids since the physiological function of the membrane depends on the dynamics of its components. Model membranes should therefore maintain their fluidity to mimic the natural membrane environment to be able to perform all of its functions. Fluorescence recovery after photobleaching is one of the most common techniques used for this

purpose, and it determines the membrane fluidity by monitoring the diffusion rate of fluorescently labeled lipids or proteins in supported bilayers [8]. Intense light is focused onto a small field of the bilayer to bleach labeled molecules, then recovery of fluorescence in the bleached area caused by lateral diffusion is monitored over time. The diffusion coefficient is then calculated from the mobile and immobile fractions obtained.

The roughness of the support surface is another important parameter for SLB formation and has an important contribution to the formation of homogeneous adlayers. It is well known that rough or hydrophilic surfaces hold more liquid in their small cavities, namely the wettability is high, and this could also be detected by the sensed mass and dissipation on a QCM-D [39-41]. Research on surface topography showed that lipid bilayer formation in the presence of hydrophilic surface curvatures between 1.2 and 22 nm yields loss of integrity, and since a continuous lipid bilayer has a hydrophobic inside and the hydrophilic nature of the curvature is thermodynamically unfavorable, the most probable structure in SLB is pore formations around these curvatures (Figure 2.2a) [41]. In case the curvature is under 1.2 nm and above 22 nm in diameter, the lipid membrane envelops the curvature and follows/repeats the topographical features of the underlying substrate (Figure 2.2b). Deep and irregular cracks on surfaces may also act as diffusion barriers to lipid lateral motion by preventing the spread of the bilayer, and lipids are not uniformly distributed and divided regions are seen. Further, increased roughness results in a larger surface area and ends with an additional mass of adlayer to some degree [40]. On the other hand, it was observed on nanoporous surfaces that, while bilayers span the pores in a size smaller than two times the bilayer thickness, the lipid layer invaginates into the pores and increases the membrane surface area when the pore sizes are much larger than the bilayer thickness [42].

Techniques such as QCM-D and SPR give high time resolution and allow obtaining an idea about the global characterization and the layer formation of the vesicle adsorption process, but they are limited to determination of structural properties such as bilayer thickness and defect formation. AFM, on the other hand, supplies images with high spatial resolution. AFM probes the sample surface by using an atomically sharp tip mounted on a spring cantilever. The tip–sample interaction is monitored with an optical system to be mapped at very high spatial resolution in the most common

operational modes (contact, non-contact and tapping) [43]. AFM is a very powerful technique that also provides information on the local nanoscale organizations, intermediate structures, topographical changes such as the lateral extent of lipid domains, the roughness and the height of patches relative to the substrate and the biomechanical properties of the adlayer [44-45]. Since topography maps are actually two-dimensional surface maps, it is sometimes difficult to understand whether the surface is completely covered with single bilayers, multilayers and/or a bare solid substrate; all of them give the same featured image. Fortunately, this obstacle is overcome by the phase signal property, which reflects the differences in the mechanoelastic and surface chemical properties of the material (composition, adhesion, friction, viscoelasticity *etc*.). Due to the different interactions of materials with the AFM tip, it can be distinguished whether an adlayer, a multilayer mass, or an underlying substrate is observed. That discrimination is also possible by running time series experiment to observe samples with slightly increased incubation times (Figure 2.3).

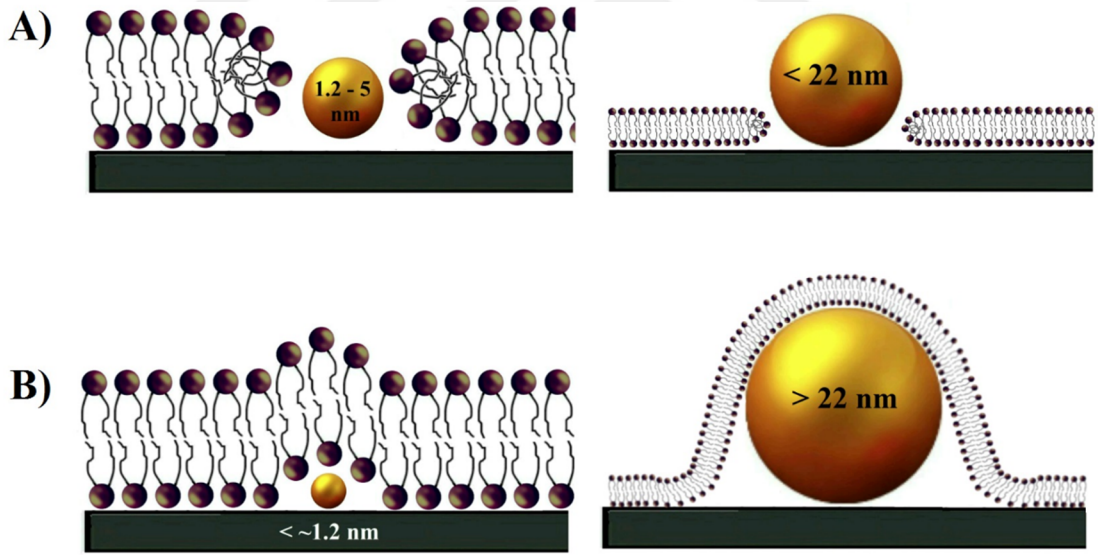

Figure 2.2 : Lipid bilayer formation in the presence of particles. The size is critical in the (a) disruption and (b) continuity of the lipid bilayer. Adapted with permission from Roiter *et al*. [41]. Copyright © 2008 American Chemical Society.

2.3.1 QCM-D

Studying lipid membranes on solid surfaces by using the QCM-D technique was initiated by Keller and Kasemo [13] and Keller *et al*. [14] and vesicle fusion became an established tool to form SLBs. QCM-D not only provides an opportunity to characterize the entire process in a label-free manner and in real time without

compromising the data quality but also allows the kinetic analysis of the bilayer formation [46].

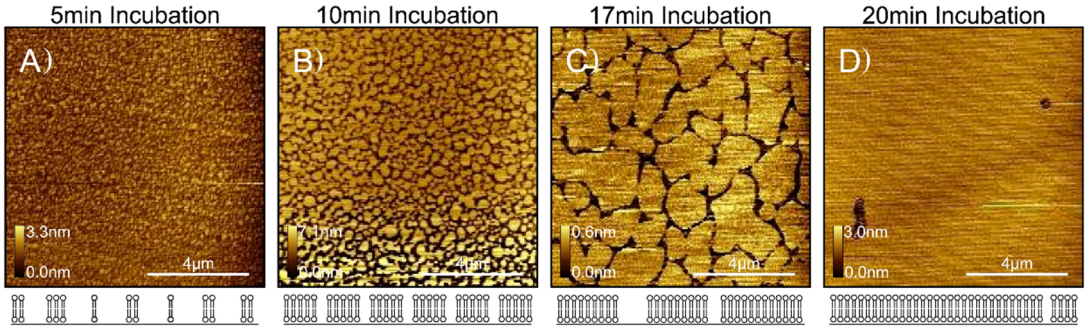

Figure 2.3 : An example of a time series experiments of lipid bilayer formation observed using AFM. Samples were incubated on mica substrates for (a) 5, (b) 10, (c) 17 and (d) 20 min. The images below the panels are illustrations of the lipid coverage state for each panel. Reprinted from Attwood *et al*. [44]. Copyright © 2013 MDPI.

Applying a sufficient alternating voltage with a frequency close to the resonant frequency (f_0) of the quartz crystal, a mechanical oscillation can be excited [47-49]. Taking advantage of the piezoelectricity of quartz, QCM-D senses all material that is mechanically deformed and provides a simple way of characterizing the adsorption kinetics of intact liposomes or fused bilayer/multilayer formation since the frequency change in the sensor (Δf) reflects the film mass, while the dissipation change (ΔD) correlates with viscoelastic properties [35-36]. According to the basic theory of QCM developed by Sauerbrey [47] in 1959, the frequency change (Δf) of a quartz crystal resonator is a linear function of the adsorbed mass (Δm) (equation 2.1) [47-48] if the film is evenly distributed over the active area of the crystal (uniform), thin compared to the thickness of the crystal and rigid and coupled to the crystal such that it can be treated as an extension of the quartz crystal [47] where C, the mass sensitivity constant, equals $C. -17.7$ ng/(Hz.cm^2) for a 5-MHz crystal depending on the thickness and the density of quartz [50]. However, the incorporation of viscosity and elastic contribution (dampening of the resonator) to the frequency change of the liquid phase violates the assumption of the Sauerbrey relation and has led researchers to new ways of reinterpreting the data and characterizing mass deposits with frictional dissipative losses because of their viscoelastic character [49].

$$\Delta m = C\Delta f \qquad (2.1)$$

One approach addressing the dissipative losses due to viscoelastic adsorption is to monitor the decay of a crystal's oscillation. Oscillating quartz crystals sense a layer as a viscoelastic 'hydrogel' when the liquid couples to the adsorbed material as an additional dynamic mass by way of direct hydration and/or entrapment within the adsorbed film. If a film layer is viscoelastic or 'soft', it will not couple fully to the oscillation of the crystal and will dampen the crystal's oscillation, resulting in a decrease in the quality factor Q of the crystal. The Q factor contains all the information about how well the quartz crystal is resonating in the surrounding media. This means that the influence of all kinds of adsorbed layers on the quartz crystal or liquids in contact with the quartz crystal surface is reflected in the Q factor [48-49,51]. The damping or dissipation (D), which is the inverse of Q, includes information on the film's viscoelasticity. D is defined as the ratio of the energy lost (dissipated) during one oscillation cycle to the total energy stored in the oscillator (equation 2.2) [49].

$$D = E_{lost}/2\pi E_{stored} \tag{2.2}$$

Thus, the rigidity or viscoelasticity (softness) of the adsorbed film and the structural differences between different adsorbed systems or the structural changes in the same film during the actual adsorption process can be determined by QCM-D. More concretely, if a rigid structure, such as a lipid membrane, is formed on the surface, a low amount of water would couple to the molecules and the film would have a low dissipation value (Figure 2.4). Positively charged vesicles, for example, rupture immediately upon contact with a silica surface, resulting in low dissipation. On the other hand, if a viscoelastic/soft layer formed on the surface (*e.g.,* negatively charged vesicles form a vesicular layer on a silica surface, *i.e.*, liposome adsorption on the surface, as shown in the first part of Figure 2.4), it would be highly dissipative [5,49].

Another advantage of QCM-D is the usage of overtones to make a depth-dependent analysis. The propagated acoustic wave through the sensor is affected by changes in the fluid containing the analyte of interest. The penetration/sensing depth or decay length in the medium is limited to a region extending ~250 nm at the fundamental frequency (5 MHz). However, the penetration depth can be adjusted by changing the frequency (overtones); by increasing the frequency or overtones (f_n), the penetration depth decreases. In some cases, the adsorbed film could be so soft that the upper region away from the crystal surface does not couple to the oscillation of the crystal sensor. Measuring both dissipation and frequency at several overtones/harmonics (n = 3, 5,

…, 13) allows viscoelastic modeling of the experimental data and determining parameters such as mass, thickness, density or viscoelasticity [51]. The detection range decreases with increasing overtone number. Therefore, the different overtones supply data about the homogeneity of the adsorbed films and it is possible to solve the properties of different layer combinations.

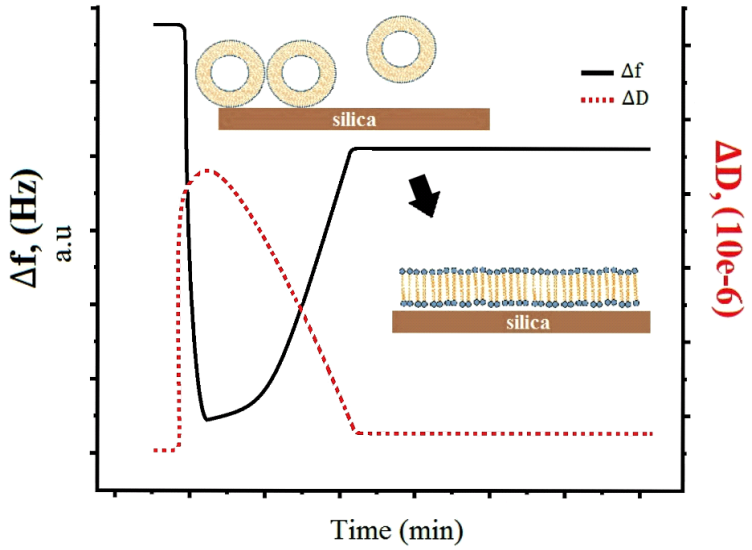

Figure 2.4 : Representative QCM-D Δf and ΔD curves for liposome adsorption and successive bilayer formation.

2.3.2 SPR

SPR is also one of the most widely used optical techniques for various artificial lipid bilayer studies [20,43]. The method takes its name from surface plasmons, which are electromagnetic waves confined to the metal surface and penetrate a short distance, propagating parallel along a dielectric interface, and they are extremely sensitive to the refractive index n and its changes. The exact position of resonance provides information on the optical properties near the surface, and this could be related to the mass/ coverage/thickness of the interfacial layers. The interactions at the gold surface alter the surrounding environment of the thin metal film, leading to shifts in the plasmon resonance condition and in the refractive index of the surface. Change in the refractive index is simultaneously detected by a sensor and plotted as response (resonance units – RU) against time. By using SPR, optical properties (refractive index, dielectric constants, extinction coefficient) and thickness, porosity and conductivity of thin layers; surface density/concentration of molecules; surface reactions (binding/interaction kinetics, affinity, specificity, binding/interaction

enthalpy and activation energy); and surface adsorption/desorption (biomolecules, polymers/polyelectrolytes, surfactants and lipids) can be characterized [52-54].

2.3.3 Combination of QCM-D and SPR data

The coupled or entrapped water within the membrane is also an important aspect of biomimetic membrane studies. Frequency changes in QCM-D include the adsorbed lipid and water as a mechanically coupled mass to the surface. If it is an intact liposome adhesion, the water is trapped inside and between adsorbed vesicles, and a small amount of water is found adjacent to adsorbed vesicles. In the case of lipid bilayer formation, bound or dynamically coupled water involves water molecules within the bilayer, water associated with the lipid head groups, water trapped between the surface and the bilayer and probable water trapped in the small number of intact vesicles [14,35]. On the contrary, refractive index changes near the sensor surface in the SPR technique are the result of replacement of water molecules with adsorbed lipid molecules. Since SPR does not detect water and the morphology of the adlayer through the extinction depth, the method only supplies information about the lipid mass on the surface. So the total mass of water entrapped within the layer can be inferred from both complementary QCM-D viscoelastic modeling and SPR results [35]. The frequency (Δf; Hz) and dissipation change (ΔD) detected in QCM-D and the refractive index changes ($\Delta\mu$RIU) monitored in SPR are converted to mass per area, implementing the viscoelastic model simulation of the software provided by QCM-D. For SPR, the equivalence of 1 μRIU is either calibrated using a large amount of different biomolecules or provided by the manufacturer. The total mass of water trapped at the surface within the lipid layer can be determined by comparing the mass uptake acquired from QCM-D measurements and SPR experiments. When the hydration content of the film is known, the exact density and thickness of the film could be easily calculated [51,55-57].

2.4 Biomimetic lipid membranes as models for various membrane-related functions

Mammalian cells continuously interact with each other and other surfaces through biomolecules, so these interactions are important for basic mechanisms such as cell signaling, cell attachment, proliferation and differentiation. Impaired interactions play

an important role in the development of diseases such as cancer. Understanding these mechanisms also sheds light on issues such as the development of new and more efficient medical systems. The surface of tissue engineering scaffolds and implants, for example, can be manipulated based on the mechanisms learned from artificial systems to achieve better tissue–implant interaction and connection. Supported lipid membranes functionalized with bioactive molecules provide a passive and biocompatible surface, allow long-term experiments and mimic the cell membrane, keeping its fluid structure, and, finally, they could be easily modified by the integration of molecules that are responsible for specific interactions in the cells. Thus, they have been tested for many practical applications such as investigation of the basic features of biological membranes and biomolecules that compose them, construction of drug screening platforms targeting membrane components and investigation of the cell–cell and cell–biomolecule interactions [6,12,17-20,23,58].

As in biological membranes, protein adsorption onto model membranes can be supplied by simple electrostatic interactions, anchoring by a short segment or by covalent binding to lipid molecules. Supported phospholipid bilayers are generally composed of neutral *phosphatidylcholine* (PC) lipids resisting the adsorption of water-soluble proteins. This has a practical value since it provides protein-resistant surfaces to prevent biofouling [59]. This passivity can be altered by incorporating electrically charged lipids on the constructed layer. Addition of negatively charged *phosphatidylserine* (PS) lipid molecules besides PC in a membrane model has been shown to increase the enzymatic activity of blood coagulation factors at lipid membrane interfaces [60]. These interactions between PS-containing supported lipid membranes and blood coagulation proteins (prothrombin, annexin A5) have been demonstrated by different groups by using QCM-D, SPR and AFM at SLBs [61] or by using surface-bound liposomes [62]. A different work revealed surface-induced self-assembly of G-actin into filament polymerization on a positively charged lipid bilayer followed by QCM-D and AFM [63]. Charged lipid ratio, lipid mobility and buffer conditions were reported as important parameters for the dynamics at the nanoscale to control the self-assembly of the actin filaments. Since these filaments play active role in cell motility, mechanical stability and cell division, the parameters affecting their polymerization are important to understand the mechanism behind these functions.

Apart from changing the phospholipid content of SLBs, their surfaces can be enriched by proteins. Eukaryotic cells modify their surface proteins at the C-terminus with *glycosylphosphatidylinositol* (GPI) to serve as an anchor to the plasma membrane. This modification was mimicked for alkaline phosphatase which was anchored into the model lipid membrane by GPI to comprehend the partition of GPI proteins into rafts by AFM imaging [64]. Rafts, which are functionally important membrane microdomains rich in sphingolipids and cholesterol, have an essential function in membrane-related events, so studying them in a controlled artificial environment gives important insights into the mechanism of partitioning of different membrane components – for example proteins – into rafts.

Another interesting example is the incorporation of water channel proteins – that is, aquaporins –, which are exceptionally permeable to water but highly retentive of solutes, into SLBs. Aquaporin incorporated biomimetic membranes have been studied for their potential to be used in water filtration applications such as water reuse and desalination [65-66]. Aquaporin Z (AqpZ) incorporated on planar, biomimetic membranes holds a great potential, but the difficulties in the production of robust and defect-free SLBs in large surfaces limit their application. Ding *et al*. [67] addressed this challenge by forming amide bonds between an AqpZ-incorporated SLB and a microporous substrate and obtained a forward-osmosis membrane with a large area of 36 cm^2. Control SLBs without any covalent bonding were reported to show higher roughness possibly because more intact vesicles adsorb on the surface without rupture and more defects form due to the lack of covalent bond. Covalently bound biomimetic membranes were found to exhibit high water flux with very low solute permeation due to the formation of an SLB with few defects. Taking into consideration the difficulties in purification of membrane proteins in functional form, as a remarkable example, AqpZ has been synthesized in an artificial cell-free expression system (protein synthesis machinery of a cell extract). This method allows the synthesis and insertion of the protein into an already formed tethered membrane system (Figure 2.5). tBLM was produced by vesicle fusion by using phospholipid–PEG molecules as a spacer. After tBLM construction, the cell-free aquaporin expression system was directly incubated onto the tBLM for expression and insertion and the whole process was characterized by using QCM-D, SPR, and AFM [26].

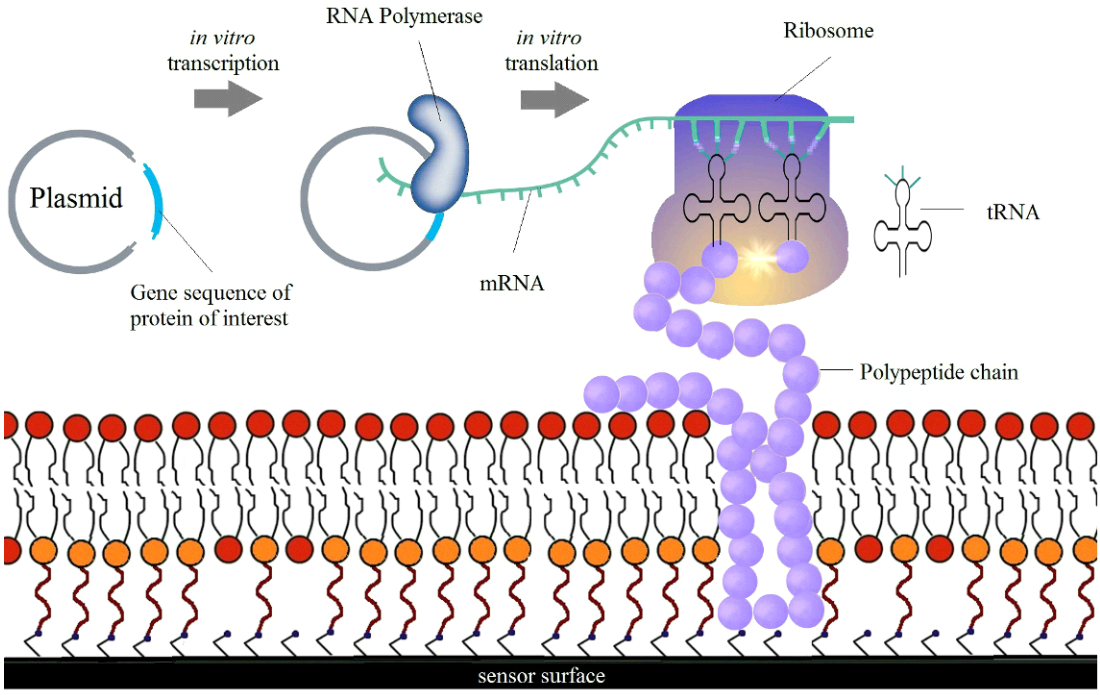

Figure 2.5 : A membrane protein is synthesized by an artificial cell-free expression system and inserts itself into already formed tethered bilayer system.

Biomimetic SLB platforms have also been utilized for biophysical studies, in particular in the recording of selective ion passage across the membrane by way of ion channels [68]. Freestanding lipid bilayers have generally been preferred over SLBs for these types of measurement since the ion passage between two large reservoirs is easier to monitor than restricted free ion movements between the membrane and the solid support. There are still some remarkable examples for SLB usage in ion channel activity monitoring, usually using tBLMs [68]. Electrical impedance spectroscopy studies on gramicidin channels in tBLMs showed that the magnitude of ionic conductance varies substantially in reservoirs with different chemical structures and ion selectivity in tBLMs was different from that reported for free BLM containing same ion channels [69]. In order to obtain the similar behavior, ester type linkers were found to be replaced with ether linkers. Even single channel recordings could be obtained with the careful choice of tethering molecule and after optimization of experimental conditions [70]. In another example, a different ion carrier protein, valinomycin, incorporated to a tBLM system displayed high discrimination between potassium (K^+) and sodium (Na^+) ions' translocations across the hydrophobic barrier [25]. Since intact tBLMs showed low background current in the absence of an ionophore, they even allowed the recording of current fluctuations upon the opening

and closing of a single channel protein shown with a mimic of the transmembrane part of the nicotinic acetylcholine receptor, a synthetic M2 peptide.

Investigation of membrane protein–ligand interactions is essential to understanding various complex cellular processes. In addition, the interaction of membrane proteins with the ECM could be mimicked using ECM components as interaction partners. An integrin-incorporated peptide-tethered lipid membrane system, for example, offers the advantages of experimental monitoring of the interaction of integrin with ECM components (Figure 2.6a) [71]. For this, an integrin receptor was incorporated into the optimized system and its functionality was monitored in real time by SPR with fluorescent detector attachment. Correct assembly, orientation and functional incorporation of integrin receptors were confirmed by specific and reversible binding of ligands and monoclonal antibodies. Binding of the ECM component vitronectin (Figure 2.6b) on the integrin-incorporated bilayer resulted in a significant change in both SPR and fluorescence signal, indicating that integration of integrin receptors did not hamper their binding capacity [71]. It is important to note that the fluorescence signal obtained by surface plasmon activation enhanced the signal obtained from the binding event (reflectivity against fluorescence signal in Figure 2.6b).

Not only do regulatory ligands take part in cellular processes but synthetic drugs and toxins also interact with membrane proteins to exhibit their effects. Evaluation of the interaction of drugs with membrane proteins by using biomimetic lipid membrane systems is important since the majority of known drugs target membrane proteins. Monitoring binding affinities by traditional methods in the pharmaceutical industry is limited to screening and profiling drugs. These artificial systems using surface-sensitive techniques could potentially revolutionize current technologies in drug screening and development [19]. The interaction of a cholesterol-lowering drug, pravastatin, with MDR1 was evaluated in a tethered bilayer lipid system by using both SPR and QCM-D [12]. MDR1 is a transmembrane protein, which is essential in cellular defense mechanism and pumps several toxic compounds out of the cell. Therefore, it is important to evaluate the interactions of MDR1 with several drugs/toxins for medical and pharmaceutical studies. One important challenge is that MDR1 has a large membrane-spanning part and therefore requires a considerable area between the lipid bilayer and the surface. To address this problem, a long spacer, namely DSPE-PEG (2000) molecules, was used as a spacer molecule to elevate the

lipid bilayer (Figure 2.1b). The spacer layer was found to exhibit viscoelastic behavior, considerably holding water, and showed structural transitions between 'mushroom-like' and 'brush-like' conformations depending on its concentration on the surface. Dissipation analysis by QCM-D also indicated that the presence of MDR1 protein led to the formation of more rigid layers, probably by restricting the movement of phospholipids. The orientation and presence of the MDR1 protein in lipid bilayers was proved by selective binding of anti-MDR1 human monoclonal antibody on MDR1-containing bilayers as opposed to MDR1-free ones. Finally, the interaction of pravastatin with MDR1-containing and MDR1-free bilayers showed the specific interaction of the drug with the protein (Figure 2.7).

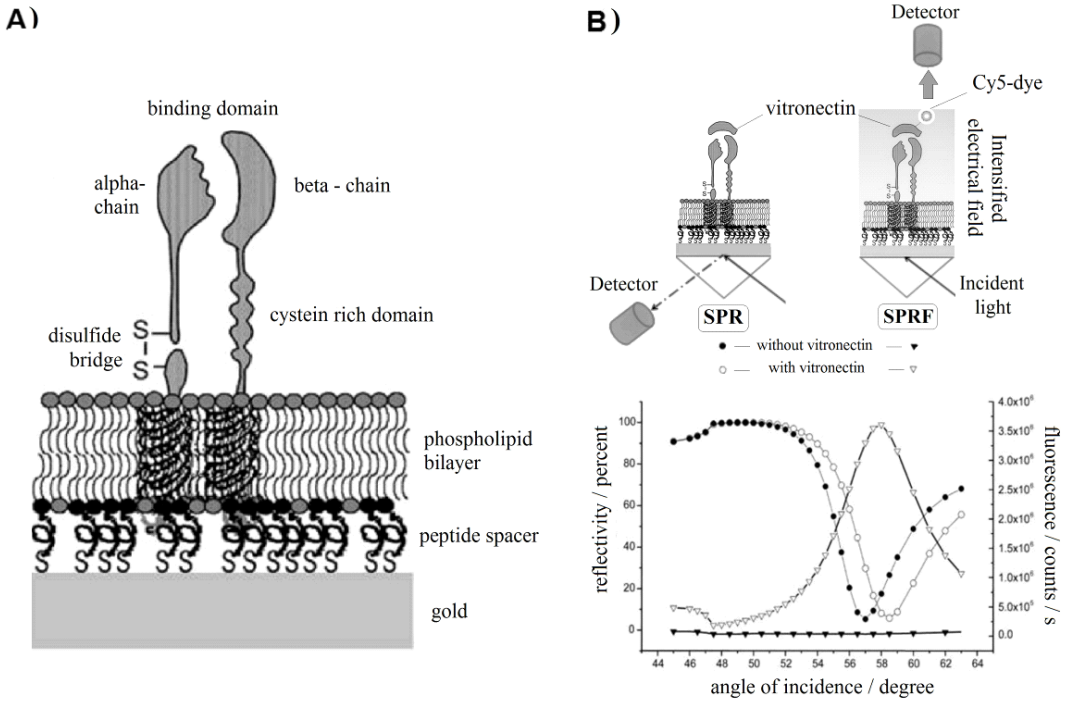

Figure 2.6 : (a) Integrin-incorporated peptide-tethered lipid membrane on gold and (b) vitronectin binding to functionalized membrane detected by both reflectivity and fluorescence signal. Adapted with permission from Sinner *et al*. [71]. Copyright © 2004 Elsevier.

For multiplexed analysis, however, arrays of supported lipid bilayers (SLBs) should be developed. Kaufman *et al*. [72] proposed a novel way to produce SLB arrays based on non-contact dispensing of liposomes to a substrate through a thin surface-confined water film. The proposed method addressed the delamination and lipid redistribution problem, which occurs due to evaporation of the spotted solution when SLBs are printed on dry substrates. These spatially separated and addressable micropatterns can allow choosing different functionalities at different locations needed for drug

screening studies. Another interesting application is the development of antiviral drugs that target the viral lipid envelope by using information obtained from biomimetic membranes [73]. For this, interactions of viral proteins with model membranes were used for target identification and characterization, using similarities between lipid vesicles and the lipid envelopes of virus particles. These studies led to the discovery of a hepatitis C virus (HCV) protein with an amphipathic, a-helix (AH) component that can rupture lipid vesicles in a size-dependent manner. When the AH peptide was added to the vesicle-adsorbed platform, the intact vesicle layer was transformed into a planar bilayer, indicating induced vesicle rupture, and the whole process was monitored by QCM-D and AFM. A synthetic AH peptide was then synthesized, and its antiviral activity was validated against HCV, the human immunodeficiency virus, the herpes simplex virus and the dengue virus [73].

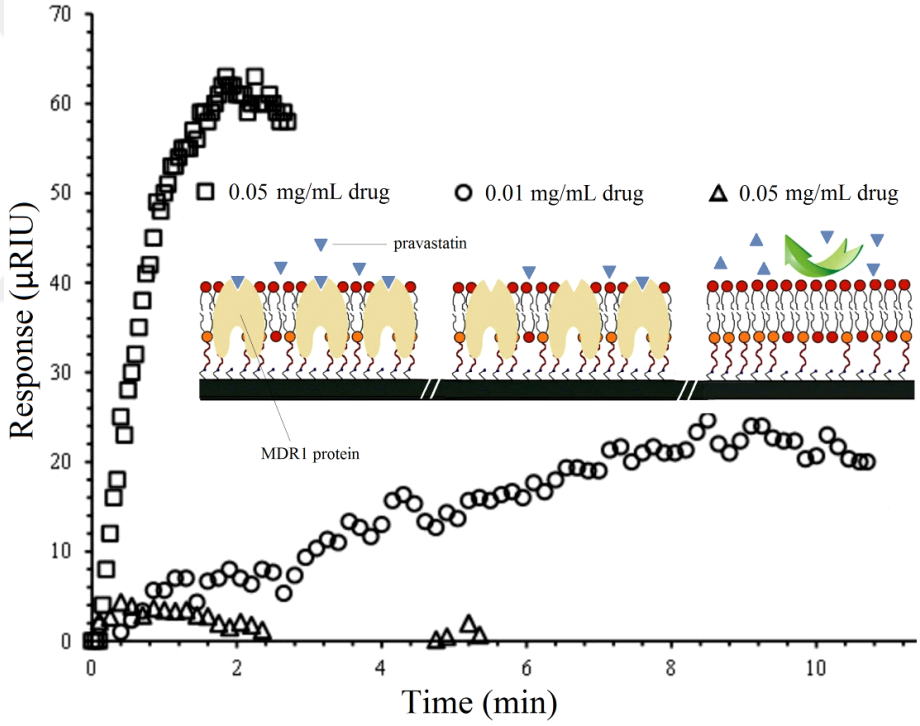

Figure 2.7 : Binding of 0.05 mg/mL (squares) and 0.01 mg/mL (circles) pravastatin solutions on MDR1-incorporated tBLM and binding of 0.05 mg/mL of pravastatin (triangles) on MDR1-free bilayers. Adapted with permission from Inci *et al*. [12]. Copyright © 2015 Elsevier.

Not only ligand or drug interactions but also the mechanism of the function of regulatory proteins that should interact with membranes for activity can be studied in SLB systems. The phosphatase and tensin homologue (PTEN), a tumor suppressor protein with a lipid phosphatase function, exhibits its enzymatic activity only after

associating itself with the membrane, and it is known to interact with at least three different components [74]. The binding kinetics of PTEN on SLBs with different contents has been analyzed by various techniques such as TIRFM, SPR and stopped-flow spectrophotometry, and the results showed that important insights could be obtained when using these platforms.

Nanoparticles (NPs) have been explored for various medical applications, but their safety and possible interactions with cell components are still unknown. SLBs can be used as model systems to evaluate the interaction of NPs with cell membranes and their potential to disrupt membrane integrity as part of nanotoxicology. The interaction of gold NPs with different dimensions ranging from 2 to 40 nm, for example, has been analyzed in PC lipid bilayers and monitored by QCM-D [75]. The contribution of natural organic matter on the binding event has also been tested in the presence of polymethacrylic acid. Only a marginal loss was reported for citric acid-stabilized NPs, whereas in the presence of polymethacrylic acid, the 40-nm NP induced a significant mass loss. In another study, silver NPs that are known for their antimicrobial activity were analyzed in SLB systems by using impedance spectroscopy and AFM [76]. Only a slight reversible perturbation of SLB was reported, indicating that 2–3-nm silver NPs only weakly bound to the bilayer surface and did not deeply penetrate into the membrane. The interaction of NPs with biomimetic membranes can also be studied in high-throughput lipid bilayer arrays [77]. Lipid bilayer membranes with varying lipid compositions and charges were prepared, and their interactions with 60-nm aminated and carboxylated polystyrene NPs were analyzed. Aminated NPs were found to rupture lipid bilayers, while the carboxylated ones did not. The disruption efficiency of aminated NPs was reported to be highly correlated with membrane and NP charge and ionic strength, indicating an electrostatic interaction. These studies were performed for over 1000 lipid bilayers, indicating the great potential of the bilayer array platform to measure a large number of NP and membrane parameters rapidly.

2.5 Biomimetic Lipid Membranes as Cell–Cell and Cell–ECM Interaction Models

Biomimetic lipid membranes designed as cell culture substrates have been utilized to study cell behavior on different surfaces and to understand the contribution of different membrane components on cell–cell interactions. Cells cannot adhere to pure PC SLBs simply because these are protein and cell resistant, probably as a result of surface

electrostatics, surface hydration and lateral mobility of the lipid molecules [78]. This is a positive aspect, which helps to minimize non-specific interaction of cells or other molecules on the surface. Lipid bilayers can be specifically modified by positively charged mixed lipid bilayers if the usage of non-specific interactions are needed [9,18] or functionalized by adhesive short peptide motifs such as RGD (arginylglycylaspartic acid) [79-80] and IKVAV (Ile-Lys-Val-Ala-Val) [81] and ECM proteins such as collagen promoting specific cell adhesion [82].

RGD amino acid sequence is found in several ECM proteins and mimics their bioactivity through specific recognition by cellular receptors. Different RGD-containing synthetic peptide amphiphiles (peptide–lipid conjugate molecules) can be used for the construction of functionalized bilayers to evaluate their potential to enhance adhesion of hippocampal neural stem cells (NSCs) [79]. After a few days in culture, only the longer (15-residue) RGD-containing peptide derived from bone sialoprotein seemed to support a monolayer of single cells, whereas neurosphere-like aggregation was observed on bilayers with a shorter (six-residue) sequence derived from fibronectin. NSCs, however, maintained their differentiation ability into neurons and astrocytes in both cases. The study encourages the use of short peptides to develop synthetic model systems for stem cell engineering to control stem cell fate by mimicking the native microenvironment artificially [78]. Similar findings were reported for a laminin-derived IKVAV pentamer presenting bilayers for the attachment, growth and differentiation of adult rat-derived hippocampal progenitor cells [81]. The results showed that there was a minimum IKVAV concentration required for cell attachment (1%), while saturation in cell binding was recorded at 3% IKVAV. When a jumbled peptide sequence was used, cell attachment was reduced tenfold. In another study, *1-palmitoyl-2-oleoyl-snglycero-3-phosphocholine* (POPC), a phospholipid with desired fluidity at room temperature, was chosen for SLB construction [83]. A recombinant chimeric protein was synthesized in which two molecules of ephrin A5 (EA5), a neuronal adhesion protein, was connected to one fragment crystallizable (F_c) domain of immunoglobulin G and inserted in SLBs (Figure 2.8). The F_c domain served as an anchoring molecule to orient EA5 proteins and ensure their mobility to increase accessibility for specific recognition. These features seemed to allow aggregation and clustering of the EA5 proteins induced by interaction with the cell, consequently leading to cortical rat neuron maturation. When

neuron growth on EA5–F_c-coated surface without SLB was observed, the number of cells was found to be much less than that for EA5–F_c in SLB. This also showed the importance of mimicking the natural environment of the cell to ensure its proper functioning in artificial conditions.

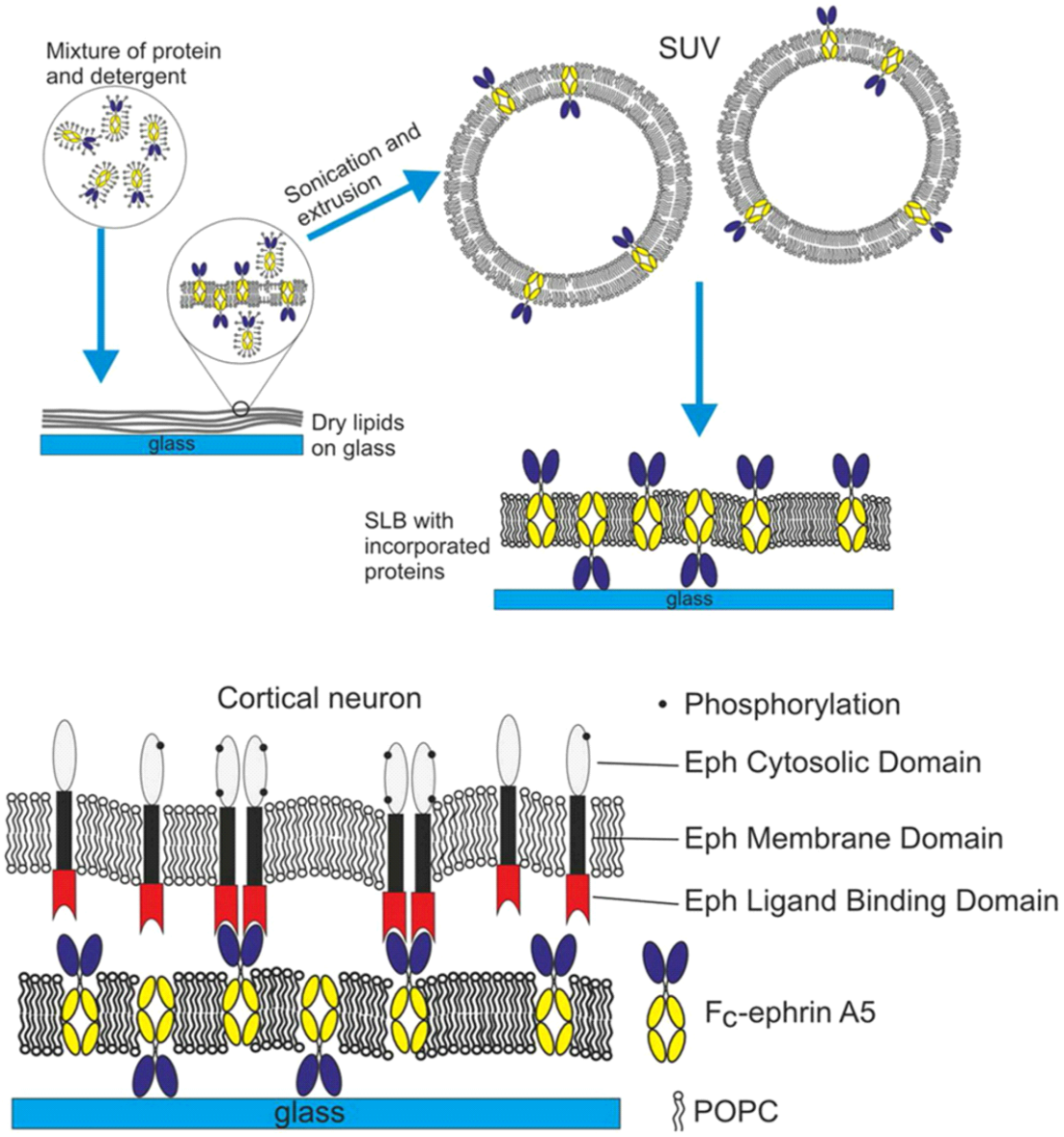

Figure 2.8 : Top: reconstitution of chimeric EA5–F_c protein into SLB by fusion of small lamellar vesicles (SUV). Bottom: cortical neurons recognizing EA5–F_c embedded in SLB through their ephrin A5 receptors. Reprinted with permission from Moulick *et al*. [83]. Copyright © 2016 American Chemical Society.

Another cell type, smooth muscle cells (A10), displayed normal growth behavior on the type I collagen-functionalized supported phospholipid bilayer, but not on bare POPC lipid without collagen [82]. Cell–cell junctional proteins such as N-cadherin can also be used to create SLBs to mimic native cell–cell interactions and to drive emergent

tissue behavior by human multipotent cells from the periosteal niche [21]. Lipid bilayers can also be patterned as cell-repellent and cell-adhesive areas to ensure the presence of cells in desired locations and allow creation of controlled surfaces [16,84]. When two different cell lines, namely HeLa (human cervical carcinoma) and NIH 3T3 (mouse fibroblast), were cultured on micropatterned membrane arrays with different lipid compositions and charge densities, it was seen that all examined membrane compositions blocked cell adhesion except those containing PS [12]. Cell interactions with SLBs have been mostly investigated with microscopy techniques using fluorescently labeled molecules, but the combination of QCM-D data with these conventional methods helps to obtain additional information about these interactions [17,78-88].

The interface between a cell and its substrate is around or less than 100 nm, so while images of two cells look very similar under microscopy for different situations/conditions, they may have actually very different interfacial features in the attachment and spreading process [89]. Traditional methods are endpoint assays and supplies just a ‘snapshot’ of the adhesion process. Also, they are laborious and cost intensive, and techniques such as prelabeling or postlabeling of the cells and fixation–permeabilization steps destroy the cells before analysis [90]. While conventional methods used in cell interaction studies may result in manipulations affecting the cell behavior and physiology and cause data loss, QCM-D allows to monitor changes in cell morphology without any manipulation or labeling. Since QCM-D enables analysis of mechanical properties at the cell–surface interface in real time with high-sensitivity temporal resolution, the cell adhesion process can be non-invasively followed on various surfaces [91]. QCM-D gives very different corresponding profiles for different stages of cell adhesion process, making it popular for studying cell–surface interactions and cells at surfaces [89]. In one of these studies, QCM-D profiles of a supported lipid bilayer with different clustered RGD-containing ligand densities were analyzed to evaluate the average RGD interligand spacing to trigger cell adhesion and spreading with complementary optical microscopy technique. Experiments were conducted using human embryonic kidney cells (HEK-293), and the results revealed that estimated RGD spacing for cell adhesion was nearly 80 nm, while 10 nm was necessary to observe flattened cells on a fluid surface such as a lipid bilayer [85].

QCM-D can directly detect the effect of small molecules, such as drugs, on established cell layers [58,92]. In the QCM-D method, the frequency change (−Δf; Hz) reflects direct interaction of the cell with the substrate, which is related to the cell mass adsorbed onto the sensor surface in the penetration depth of the acoustic wave of the crystal sensor (250 nm at the fundamental frequency, 5 MHz). On the other hand, the energy dissipation change (ΔD) reflects membrane and cytoskeletal rearrangement above the membrane in close contact with the substrate [35,93]. In a cell adhesion experiment, the increase in the surface area of spreading by means of focal adhesion formations and cytoskeletal arrangements causes frictional losses at the sensor–cell layer interface, so the experiment ends up with an increase in ΔD values. But at the same time, the cell membrane of the flattened cells comes closer to the surface and increases the sensed mass and, consequently, Δf [92]. These values are assembled as $-\Delta D/\Delta f$ (GHz^{-1}) for each time point to identify the adhesion maturation of cells. The cells, therefore, do not exhibit pure mass-load behavior such as that of a rigid film, but behave more like a viscoelastic material with considerable dissipation of energy [58]. Plots of $-\Delta D/\Delta f$ can also be used to compare the different outcomes and create fingerprints for the adhesion process of the different cell lines since the energy dissipation change (ΔD) is related to the viscoelasticity/softness/ stiffness of the sensed cell layer. Thus, the intrinsic viscosity of the adsorbed cell layer can be quantified, and the flatness of cells can be identified. To put it simply, spherical, rounded cell morphologies give higher $-\Delta D/\Delta f$ values, whereas flattened cells give lower $-\Delta D/\Delta f$ values [58,91-92]

The adhesion behavior of cancer cells differs from that of normal cells, so development of faster and effective experimental techniques is needed for better understanding of the mechanisms behind cancer development. QCM-D has the potential to study the dynamic adhesion behaviors of healthy and cancerous cell lines on the lipid membrane platform. Toxicity studies on healthy cells that are attached to biomimetic lipid platforms and interactions of cancerous cells with drugs that target the cytoskeleton can also be performed by QCM-D [92]. SLBs can be decorated with specific antibodies (Ab) and used as a ‘smart coating’ to capture circulating tumor cells (CTCs) and circulating tumor microemboli directly from whole blood [94]. Non-specific adsorption of blood cells and proteins was eliminated thanks to the non-fouling nature of the lipid bilayer. While a conventional surface (Ab–silane) had 15% capture

efficiency with over 2000 white blood cells (WBCs) being non-specifically bound on the chip, the Ab–SLB-coated chip significantly enhanced capture efficiency and reduced nonspecific WBC adhesion. Since the platform was inspired from the cell membrane and mimicked its fluidity, dynamic clustering of lipid-tethered antibodies to antigens on CTCs was promoted, and due to antibody–antigen clustering, cells adhered more firmly on the surface compared to those on a conventional antibody immobilized surface. This led to an additional advantage: while antibody-conjugated lipids were concentrated underneath CTCs, non-functionalized lipids migrated away from the target cells, leading to greater resistance to non-specific binding. All these showed the power of the biomimetic approach over conventional fabrication techniques in differentiating cancer cells in a complex environment such as blood.

Another interesting example is the construction of a layer-by-layer polypeptide-adsorbed supported lipid bilayer (SLB) platform for the isolation and maintenance of rare populated stem cells [95]. QCM-D data showed that the constructed platform was protein resistant compared to the polypeptide multilayer films without an underlying SLB, promoting selective binding of fetal liver stem/ progenitor cells from the primary culture. These cells were also found to form colonies, which can be maintained for an 8-d period, a promising result that could be tested for other kinds of stem cell selections.

2.6 Challenges and Outlook

Although various model membrane architectures have been explored and successful models have been proposed for specific applications, the commercialization of these systems is often limited due to challenges related to both lipid bilayers and membrane proteins. Biomimetic membranes generally suffer from structural defects, causing non-specific leakage of solutes across the bilayer. This is significant in particular in screening any specific effect of particular membrane protein-mediated ion translocation since to determine the protein-mediated ion flux across a lipid bilayer, a defect-free membrane over the entire sensing area is required [96-97]. The vesicle fusion method appears as a simple method for SLB formation, but optimal vesicle rupture and bilayer formation is influenced by many experimental parameters and is therefore prone to defect formation [98]. When a scale-up is needed, the challenge in the preparation of defect-free membranes becomes more pronounced, in particular

when membrane protein-based biomimetic membranes studies are considered [99]. Membrane fabrication is difficult to replicate at higher scales since many fabrication approaches are in the bottom–up direction, depending on self-assembly. The stability of the formed bilayer should be retained for sufficiently long periods of time for commercial applications, and although directly supported bilayers are more stable, a 1-nm distance between the bilayer and the solid substrate is not enough to retain the required mobility and function of many integral membrane proteins [22,97]. In addition, some economic challenges arise from the inherent nature of membrane proteins. Purification of membrane proteins is expensive, and preparation of sufficient amounts of correctly folded fully functional target proteins and their incorporation into artificially formed lipid bilayers is technically challenging because of their delicate nature, which causes their quick denaturation and consequent loss of activity when purified from their native systems [97,100]. On-site cell-free protein synthesis has therefore been explored by different groups to overcome this limitation [26,100]. The adaptation of cell-free expression systems for high-yield and cost-effective membrane protein synthesis has a great potential to design diverse high throughput applications in the future. Development of new techniques, in particular automated membrane protein transfer techniques, will be a key advancement in the construction of high throughput platforms involving different proteins. Usage of synthetic channel-based biomimetic membranes has also been explored since these non-protein channels can offer higher stability and scalability compared to their natural counterparts [99].

The complexity and the diversity of biomembranes are two other issues to be addressed in this field. Model membrane systems have been designed with one or two lipid types to mimic the main structure and dynamics of the plasma membrane; but for precise modeling, this is not sufficient to catch the actual, extensive lipid diversity often involved in biofunctions. Trials to increase SLB complexity by cholesterol, charged lipids or phase-separating lipid compositions often prevent successful SLB formation, leading to their negligence or underrepresentation in biomimetic membranes [10]. There are different approaches and experimental optimization techniques to produce improved SLBs with various lipid types; however, the manipulations (*e.g.,* changing temperature, buffer type, fusion peptide supplement) applied in preparation methods have the possibility of leaving residual effects on SLB properties [10]. Moreover, in such cases when vesicles are prepared with more than one lipid type, the obtained SLB

composition and structure may not be the same as that of the vesicles because of the different nature and responses of each lipid types to the experimental protocols commonly used in this area [98].

SLB technology is predicted to carry on a key role in the development of sensors and nanodevices in the future. For instance, the usage of spatially arrayed supported bilayers ensures exceptionally rapid and powerful data collection in parallel measurements [22]. This development can also be used for biosensing systems, such as artificial tongues, wherein several receptors should be displayed and recorded simultaneously to create the response [19]. When commercialized by further advances in economical manufacturing, miniaturization and packaging technologies, SLB arrays may also accelerate proteomic research based on membrane-associated proteins, which are targets of approximately half of the known drugs. Different combinations of SLB array systems in microfluidic platforms can also be attractive for developing early-warning sensors for biological warfare agents and the discovery of novel drugs [22]. Special manufacturing techniques have been applied to construct patterned SLBs, and the common methods involve production of physical barriers to compartmentalize membranes prior to SLB formation, deliberate defect formation to confine membrane regions after SLB formation and direct deposition of lipid bilayers onto a substrate by microcontact printing [101]. These techniques allow the construction of high-throughput systems, but often the modulation of the asymmetric lipid composition is difficult and/or time and labor intensive, so other techniques still have to be explored to overcome these challenges [19,102].

Another interesting potential application is the construction of more complex platforms with the use of actual cell membrane fragments. Although single-protein research is attractive in many ways, understanding and mimicking signaling networks requires the existence of protein–protein and protein–lipid interactions [19]. In addition, expensive and elaborate protocols are avoided when vesicle fusion protocols involving native membrane fragments are used. Not only plasma membrane fragments but also endoplasmic reticulum-derived microsomes can offer a window toward more complex artificial systems to mimic cellular functionality [100].

2.7 Conclusions

Biomimetic lipid bilayer platforms constructed in many forms ranging from simple liposomes to SLB arrays have been extensively used to study the fundamental properties of biological membranes and their constituent lipid and protein molecules. SLBs are in particular attractive since they can be designed to have different properties and functionalities and they are relatively stable, keeping their fluid nature. They also allow the usage of surface-sensitive characterization techniques such as AFM, SPR and QCM-D. These techniques can supply information about binding events on surfaces in real time without labeling and allow the determination of membrane-related events in high resolution. In recent years, the potential of SLBs in numerous practical applications, such as drug screening or cancer cell detection platforms, has been explored. These platforms address some of the important challenges faced in cell membrane research and help to develop systems to be used in cell membrane-related applications.

3. THE EFFECT OF THIOLATED PHOSPHOLIPIDS ON FORMATION OF SUPPORTED LIPID BILAYERS ON GOLD SUBSTRATES INVESTIGATED BY SURFACE-SENSITIVE METHODS[2]

3.1 Introduction

Supported lipid bilayer systems prepared by surface-mediated liposome fusion allow researchers to isolate and study one or few biological membrane components. These non-fouling biomimetic surfaces that resist cell/protein adhesion can be modified/functionalized by changing their lipid composition or incorporating membrane-associated proteins or molecules. Functionalization by different components helps to develop biosynthetic systems such as drug-screening platforms, membrane-based molecular biosensors, and then utilized in medical diagnostics, biomaterial improvement, and various other biomedical assays [11-12,19,21,79,103-105]. Taking the advantage of high stability and flat geometry, SLBs make long-term experimentation possible and allow the usage of surface sensitive characterization tools such as quartz crystal microbalance with dissipation monitoring (QCM-D), surface plasmon resonance (SPR), atomic force microscopy (AFM) and fluorescence recovery after photobleaching (FRAP) within aqueous environments [8,43-44,46,104].

Silica, mica and glass are well-established and most commonly employed solid supports for the preparation of SLBs since their hydrophilicity and negative charge at neutral pH provide liposomes a surface to adsorb, deform, flatten and finally rupture to form a bilayer [105]. In that case, the lipid layer is attached to the support by noncovalent bonds. These systems generally have high fluidity because of underlying water layer, but low stability due to weak interactions [106]. Liposomes with polar surfaces, on the other hand, neither interact with bare, hydrophobic gold surfaces [107], nor rupture on oxidized gold surfaces [13]. However, to take the advantages of

[2] This chapter is based on the paper "Kilic, A., et al., The effect of thiolated phospholipids on formation of supported lipid bilayers on gold substrates investigated by surface-sensitive methods. Colloids Surf B Biointerfaces, 2017. 160: p. 117-125."

the attractive properties (such as biocompatibility, electrical conductance) of gold [108-109], an efficient chemisorption method, gold-thiol bond chemistry is often used. For that, a self-assembled monolayer (SAM) is first formed onto the gold using this chemistry, and then a single phospholipid monolayer is attached on that tightly packed and well-ordered SAM. These type of strategies yield higher stability, but might hamper the fluidity of SLB, and in turn may hinder the dynamics or electrochemical characteristics of the formed bilayers [22,110-112].

The majority of lipid membrane studies on gold surfaces involve the usage of various surface-modification strategies to induce lipid bilayer formation. These surface-based constraints can be eliminated by the direct formation of SLB on bare gold. In this study, a synthetic phospholipid functionalized with thiol-anchors at the lipid headgroups, *1,2-Dipalmitoyl-sn-Glycero-3-Phosphothioethanol* (DPPTE) (Figure 3.1), was used together with phosphatidylcholine (PC) to enable spontaneous lipid bilayer formation on gold. In this way, the optimized ratio of DPPTE phospholipids can supply the sufficient stability by chemical adsorption to solid support, and PC components mainly give the fluidity to the constructed lipid adlayer.

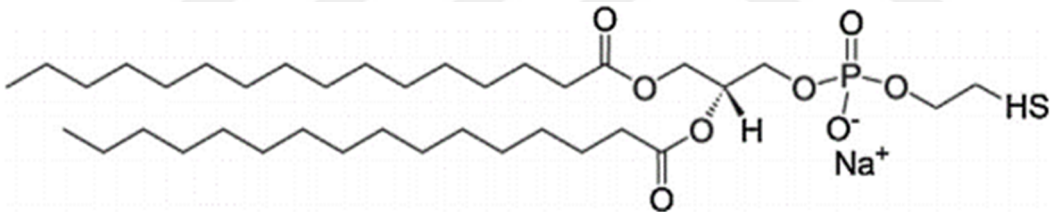

Figure 3.1 : Chemical structure of DPPTE [113].

There are few examples of the usage of thiolated phospholipids within zwitterionic liposomes to avoid the need of a premodified gold surface [111,114]. Pera and Fritz [114] reported that lipid bilayer with DPPTE showed stronger mechanical coupling to the surface as to the physisorbed bilayers. Having used thiolated liposomes at three different ratios, bilayer formation had been detected by nanomechanical bending of cantilever sensors in AFM. Despite their well-grounded approach, the main limitation is the lack of real-time monitoring of lipid bilayer formation. It is an end-point application and supplied just a snapshot of the whole adhesion process. Further, lipid bilayer formations were characterized only through their mechanical properties. However, the characterization of the bilayers need a more detailed information concerning real-time monitoring of bilayer formation, the amount of adsorbed lipid

mass on the surface, hydrodynamically coupled or mechanically trapped solvent (water content) within the bilayer. To our knowledge, the binding kinetics and characterization of this type of liposomes with both temporal and spatial resolution was thoroughly investigated for the first time by our study employing three different methods (QCM-D, SPR and AFM). For this purpose, different liposomes at varying DPPTE ratios and at different diameters were tested and the results were discussed for a better understanding.

QCM-D allows real-time, in situ monitoring and label-free qualitative and quantitative assessment in SLB characterization. It provides data on adsorption kinetics using the frequency change in the sensor (Δf) that reflects mass deposition, and also senses energy losses from the system into the surrounding environment as a result of the soft or loose nature of the adlayer by measuring changes in the dissipation factor (ΔD) [35,46,104,115]. Hence, the rigidity/stiffness or viscoelasticity/softness of the adsorbed film and structural differences between different adsorbed systems (intact liposomes or bilayer/multilayer formation *etc*.), or structural changes in the same film during the actual adsorption process can be determined by the evaluation of both signals [49]. Furthermore, the quantitative results on deposited mass and layer thickness can also be extracted using multiple frequency overtones/harmonics of crystals' resonance frequency since these different harmonics probe the adlayer at different depths that are inversely proportional to the frequency of the wave [116]. Higher overtones are qualitatively more related for the processes closer to the sensor surface whereas lower overtones are representative for the liquid-film interface [117]. SPR is an optical technique based on the changes in surface plasmons confined onto the metal surface that are extremely sensitive to changes in refractive index in close vicinity of the surface. Thus, SPR can provide information about adsorption behavior of liposomes on surface, the properties of the resulting films and quantify adsorbed masses in real-time [52-53]. AFM, on the other hand, is a very powerful technique that provides information on the local organizations, topographical changes and biomechanical properties of the adlayer [44-45]. In this study, to obtain a comprehensive understanding on water content, and roughness of the adlayer, QCM-D data was combined with SPR and AFM results.

3.2 Materials and Methods

3.2.1 Materials

L-α-phosphatidylcholine (Egg, Chicken PC, 840051), *1,2- Dipalmitoyl-sn-Glycero-3-Phosphothioethanol (Sodium Salt)* (DPPTE, 870160P), and liposome extrusion accessories (610000) were purchased from Avanti Polar Lipids (USA).

SPR sensor chips (chromium (1 nm) and gold (50 nm) coated BK7 glass slides) and AT-cut gold coated quartz crystals with a fundamental frequency of 5 MHz and a diameter of 14 mm were purchased from NanoDev (Turkey) and Q-Sense (Sweden), respectively. We used commercial silicon cantilevers (Nanosensors, type: PPP-NCL-50 & PPP-NCHR) with resonance frequencies of 163080 Hz and 335710 Hz and spring constants of 50 N/m and 42 N/m, respectively. The radius of curvature of tips were less than 10 nm.

Purified water was used throughout the experiments with a minimum resistivity of 18.2 MΩ.cm. Phosphate buffered saline (PBS) (0.01 M, pH 7.4, containing 137 mM NaCl) was prepared and filtered through 0.2 m filters, and degassed before each QCM-D and SPR experiments.

3.2.2 Preparation of unilamellar liposomes

Phosphatidylcholine (PC) and *1,2-Dipalmitoyl-sn-Glycero-3- phosphothioethanol* (DPPTE) lipids were dissolved separately in chloroform at +4 ◦C (2.5 mg/mL), aliquoted and stored at −20 °C. To prepare thin lipid film layer, 40 µL of lipid solution with different molar PC/DPPTE ratios (0.01 to 100%) was poured into a round bottom flask. Chloroform was evaporated by manually rotating the flask and using a dry nitrogen stream in a fume hood. The formed thin lipid film was left overnight at nitrogen atmosphere at +4 °C to ensure the removal of all solvent residues. The dried lipid film layer was hydrated by phosphate buffered saline (PBS, 0.01 M, pH 7.4) to a final lipid concentration of 0.02 mg/mL. The flask was agitated vigorously for 10–15 min until a clear solution was obtained. To obtain unilamellar liposomes, hydrated and vortexed lipid solutions were extruded 21 times through a polycarbonate membranes with three different pore sizes (50, 100 and 200 nm). The extrusion method yielded normal distributions with mean diameter of 92 ± 3, 142 ± 7 nm and 174 ± 3 nm, respectively, measured by dynamic light scattering (DLS) (Malvern, Zetasizer).

The obtained unilamellar liposomes were collected in a falcon tube and stored at +4 °C overnight to be used on the following day. Liposomes were produced freshly for each adsorption kinetic measurements and used within the 24 hours of preparation.

3.2.3 Preparation of sensor surfaces

Immediately before each use, clean QCM and SPR gold-coated surfaces were rinsed with ultrapure water, and dried under nitrogen gas. After each measurement, the crystals were cleaned with H_2O:NH_3(25%):H_2O_2 (30%) (5:1:1) solution for 5 min in 75 °C to remove the thiol residuals from the gold surfaces, then they were treated under UV-Ozone chamber for 15 min. Then the crystals were rinsed with Milli-Q water, dried under nitrogen, and stored in a desiccator until reuse.

3.2.4 QCM-D and SPR measurements

QCM measurements were performed using a dissipative QCM instrument (QCM-Z500, KSV Instruments, Finland) using a flow through system provided with a peristaltic pump. The frequency (Δf) and dissipation change (ΔD) data with different overtone frequencies, *i.e.*, harmonics at 15, 25, 35, 45, 55 MHz were obtained. The change in normalized frequency (f_n/n, with n is the overtone number) of the third overtone (n = 3, *i.e.*, 15 MHz) was generally presented unless otherwise stated. SPR measurements were performed with SPR-Mini Surface Plasmon Resonance system (Nanodev Scientific Inc., Turkey) and the shifts in the resonance angle were monitored in real time as degree (°).

All of the buffers and suspensions were first equilibrated thermally at room temperature (22–24 °C) then introduced to the measurement cell at a rate of 100 µL/min by peristaltic pump. Following the initiation of the system, first PBS was passed through the measurement cell to tune the resonant frequency of the crystal, and take a stable baseline (generally after 15–20 min.) before each measurement. Then, liposome solution was allowed to flow over the gold sensor until the frequency and dissipation signals stabilized. PBS was then used to wash out the unadsorbed or loosely bound liposomes. Each experiment was repeated at least three times.

3.2.5 AFM characterization

In order to investigate the physical properties and changes in morphology of samples, topography images were acquired using Atomic Force Microscopy (AFM). The

images were obtained using the AFM (NanoMagnetics Instruments) operated in tapping mode. For AFM studies, PC – DPPTE (1% mol/mol) layers at different concentrations were used to determine the dynamic adhesion profile and to evaluate the film thickness of the lipid layer.

3.2.6 Statistical analysis

Statistical analyses of the data were performed by Student's t-test in Microsoft Office Excel. Significant difference was considered at the level of $p < 0.05$ ($n = 3$).

3.3 Theory/Calculation

3.3.1 Viscoelastic modelling of QCM-D data

The basic theory and equation of QCM developed by Sauerbrey suggested a linear relation of the adsorbed mass per unit area (m, measured in $ng.cm^{-2}$) with the decrease in the normalized frequency change (negative f, in units of Hz) of a quartz crystal resonator for thin, rigid and compact films or molecules [48]. In that case, the dissipation change (ΔD) is close to zero so the adlayer can be treated as an extension of the crystal and 1 Hz frequency changes quantified to 17.7 $ng.cm^{-2}$ added areal mass for 5-MHz crystal sensors [118]. However, since the contribution of soft or loose materials (*i.e.,* viscoelastic effects) to the frequency change violate Sauerbrey assumption; the equation is modified [116] accounting the viscoelastic properties of the adsorbed material. Viscoelasticity or rigidity is related to ΔD, which is defined as the ratio of the energy lost (loss modulus) from the system into the bulk to the total energy stored (storage modulus) during one oscillation cycle in the system [49]. Thus, these type of dissipative adlayers are alternatively defined within viscoelastic models with an effective thickness, density and complex shear modulus (shear viscosity and shear elasticity) [119]. If the density is independently known or specified by the user, using at least the data of 3 harmonics solve the equations and supplies the modeling the experimental data to estimate these unknown parameters (density, thickness, viscosity and elasticity) [49,120]. In this case, the sensed mass per area (effective density × effective thickness) can be calculated by the modelling. These quantitative data in this study was obtained by viscoelastic modelling implemented by QCM-Z500 Data Analyzer software (KSV Instruments, software version 3.40) in QCM-D device.

Viscoelastic modelling uses effective parameters (thickness, density) of the film, which means that the dry mass part within the film and the trapped water part cannot be separated below the shear-plane [57]. When performing the modelling in QCM-D, an assumed reasonable effective lipid film density, $\rho_{effective}$, which should be between density of the buffer (~ 0.995 g.cm^{-3}) and the lipid molecules (~ 1.1 g.cm^{-3}) was used as a fixed input in the modelling (ρ_{film} = 1.06 g.cm^{-3}) to obtain adsorbed mass, m_{wet}. The thickness and density parameters are dependent variables and the total mass from the modelling does not change by varying the density within this plausible interval [55,57]. Initial liquid bulk parameters (density (ρ_{buffer}), viscosity (η_{buffer})) were hold constant; and film thickness (d_{film}), viscosity (η_{film}) and elasticity (μ_{film}) values are fitted. Start values for the modeled parameters used were t_{film} = 10 nm, μ_{film} = 0.1 MPa, η_{film} = 1 mPas, and η_{buffer} = 1.05 mPas [118]. The agreement of the calculated (fitted) values from the viscoelastic modeling with the measured value of the overtones was checked each time.

3.3.2 SPR measurements

The sensed mass of QCM-D (so called wet mass) refers to the biomolecules, hydrodynamically associated/bound water in the lipid membrane (as in hydration layers), mechanically trapped water in cavities and viscous drag [35,115,121]. For that reason, to obtain the accurate effective layer thickness, the amount of entrapped water so the density of the lipid film should be determined independently as mentioned above part. This could be achieved exploiting SPR in parallel to QCM-D since the refractive index changes are just the result of the adsorbed lipid molecules and disregard the water molecules through its extinction depth (dry or optical mass, mdry).

In the SPR-Mini Surface Plasmon Resonance system (Nanodev Scientific inc, Turkey) utilized in the studies, the dry – optical mass density (ng.cm^{-2}) calculations came from the change in the plasmon resonance angle ($\Delta\Theta$) by the equation 3.1 given for the thin films ($d_{film} << l_{decay}/2$) [55],

$$m_{\mathrm{dry}} = \frac{l_{decay}}{2} \frac{\mathrm{d}c}{\mathrm{d}n} \kappa \Delta\Theta \qquad (3.1)$$

where l_{decay} is the decay length of the evanescent field (characterized by exponential intensity decay) of the excited surface plasmon polaritons. $l_{decay}/2$ is the probe (or sensitivity) depth of the evanescent field, and κ is the sensitivity factor of the system. d*n*/d*c* is the refractive index increment for the adsorbed molecules, and in a standard

buffer solution, an approximation of 0.20 $cm^3.g^{-1}$ for lipid bilayer studies [57,122] was accepted in our calculations.

A reasonable estimate for l_{decay} equals to 37 ± 13 % of the light wavelength (λ) at the SPR minimum, where in the present study the excitation wavelength is 850 nm. However, more accurately, l_{decay} comes from the following equation 3.2 as 376 nm.

$$l_{decay} = \lambda/2\pi/Re\left\{-n_{eff}^4/(n_{eff}^2 + n_{metal}^2)\right\}^{1/2} \qquad (3.2)$$

where $n^2_{metal} = \epsilon_{metal}$ is the complex dielectric constant of the metal, in this case gold (n^2_{gold} = 25.86 [123]), at that wavelength (λ = 850 nm) and η_{eff} is the effective index of refraction of the medium (n_{eff} =1.33 for water [124]).

κ, the sensitivity constant of the system, is estimated according to the equation 3.3 where 1000 micro refractive index units (μRIU) approximately correspond to an angle change of 0.1 deg [119], was calculated as 9.9337×10^{-3} deg^{-1} for thin film limit ($d << l_{decay}/2$).

$$\kappa = \frac{\Delta n}{\frac{\Delta\theta}{1-e^{-2d/l_{decay}}}} \qquad (3.3)$$

Using calculated and known values in equation 3.1, an equivalence of 0.1 ° = 1 μRIU = 93 $ng.cm^{-2}$ mass density for lipids was found to be used in conversion of SPR response to the adsorbed mass.

Thus, employing both QCM-D viscoelastic modelling and SPR results deduce the total mass of water entrapped within the lipid adlayer. The water content ratio (H) comes from the mass differences between QCM-D and SPR data (equation 3.4),

$$H = \Delta m_{wet} - \Delta m_{dry}/\Delta m_{wet} \qquad (3.4)$$

Knowing the hydration content of the film, the exact effective density ($\rho_{effective}$) of the film could be easily calculated (equation 3.5).

$$\rho_{effective} = (1 - H)\,.\,\rho_{lipid} + H\,.\,\rho_{buffer} \qquad (3.5)$$

This calculated value was replaced with the assumed density input at the beginning of the modelling. Since QCM-D mass from the modelling does not change, the exact effective thickness ($d_{effective}$) of the film was also calculated using equation 3.6 by assuming a highly flat sensor surface, uniform thickness and uniform density.

$$d_{effective} = \frac{\Delta m_{wet}}{\rho_{effective}} \quad (3.6)$$

3.4 Results and Discussion

The subsequent definitions are provided to clarify the content. When the liposomes suspended in solution bind to the surface, this is referred interchangeably as "adhesion" or "adsorption". If the liposomes adsorbed remain as intact spheres, they are called "not deformed". If they lose their hard-sphere forms, they are "deformed". "Flattened" refers to higher deformations and especially to noticeable decrease in the height of the adsorbed liposome. In addition, "rupture" is the transition from an adsorbed liposome to a bilayer patch. The unruptured liposomes among bilayer patches are called as "trapped" liposomes whereas unruptured but partially fused liposomes on top of a bilayer are mentioned as "partially fused liposomes".

3.4.1 Adsorption behaviors of PC- x % DPPTE liposomes

Experiments with liposomes containing both PC and DPPTE phospholipids at different molar ratios (0.01 to 100%) were conducted on bare, untreated (*i.e.,* hydrophobic) gold surfaces. When working with thiolated liposomes, the adhesion occurred in one-step kinetics as anticipated. The frequency and dissipation changes grow monotonically (Figure 3.2) because highly strong gold-thiol interactions induce liposomes to rupture immediately and individually after adsorption. This behavior does not resemble to lipid bilayer formation via two-step kinetics including a first critical surface coverage (a significant frequency minimum, *i.e.,* maximum in coupled mass, and corresponding dissipation maximum) and then spontaneous liposome rupture (increase in frequency and decrease in dissipation) [13].

The dissipation change per frequency change (in absolute values), *i.e.,* acoustic ratio, $|\Delta D/\Delta f|$ (GHz^{-1}) were calculated for each experimental setup as it is practical to directly compare the energy losses per coupled unit mass [125]. Simply, the relatively high values indicate highly viscoelastic layers (high water content), in that case a liposomal layer, whereas relatively low ratio point out the deformation degree of the liposomes and may suggest the flattened or eventually ruptured liposomes, and finally formation of a lipid bilayer (low water content). Using the quantitative acoustic ratio results, the state of the bilayer, *i.e.,* the degree of the liquid trapped within the formed layer, or between the layer and the surface, can be predicted. To assess the success of bilayer

formation and compare acoustic ratios in our experimental system, two representative rigid and two viscoelastic layers were characterized and used as reference (Table 3.1, for details of layer characterizations see supporting information, Appendix A). It could be seen that the expected acoustic ratio is lower than that of a highly flattened liposomal layer (162.3 ± 10 GHz^{-1}) and higher than a rigid lipid monolayer (59.3 ± 5 GHz^{-1}) for bilayer formation.

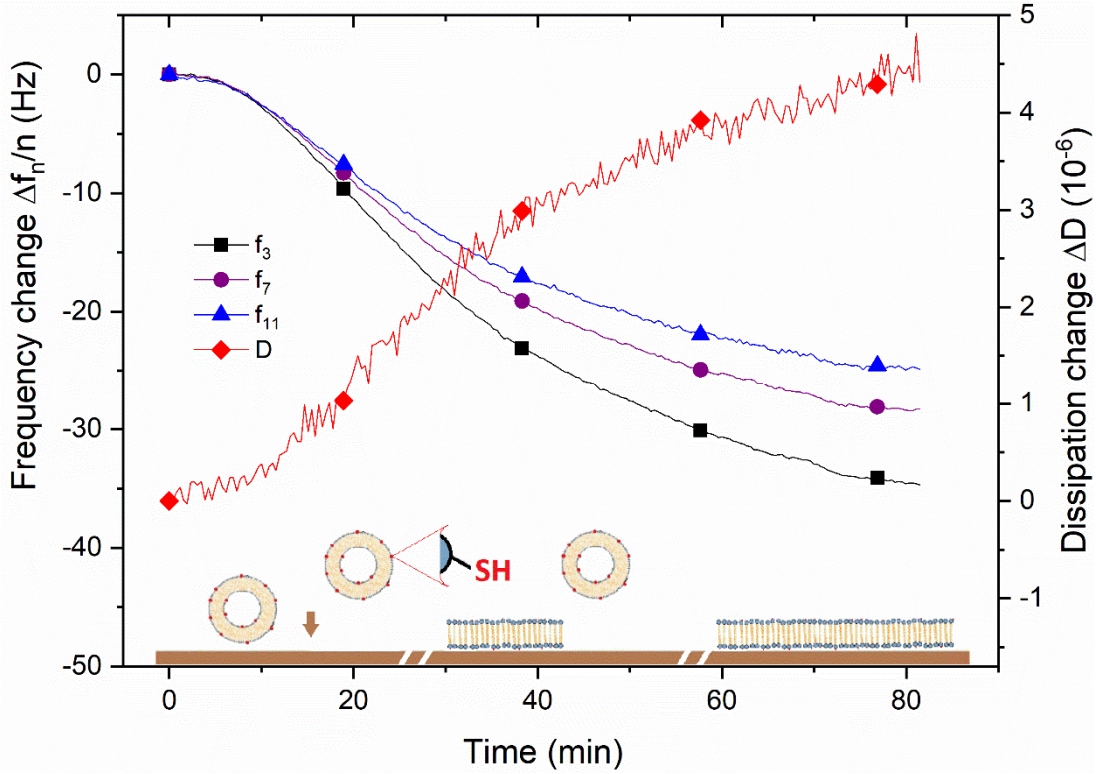

Figure 3.2 : A typical frequency (in various harmonics) and dissipation changes versus time for the adsorption of 1% DPPTE-PC liposomes on unoxidized gold sensor surface monitored by QCM-D. Below, illustration of thiolated liposome adhesion (not to scale).

The outcomes for liposomal binding during the whole process were evaluated using |Δf|, ΔD and acoustic ratio. Keeping in mind that pure PC liposomes cannot interact with unoxidized (hydrophobic) gold surfaces [107], it was noticed that even minor amounts (0.01% mol/mol) of DPPTE lipids in liposomes provided adsorption on the surface thanks to the strong interaction between gold and thiol groups (Figure 3.3). The graph of viscoelastic, flattened PC-liposome layer, which was built up on oxidized – hydrophilic gold surface with the same lipid concentration, was also added to the figure for easy comparison. In comparison with flattened PC liposomes, a decrease in ΔD (6 ± 0.5 × 10^{-6}) and |Δf| (40 ± 2 Hz) in half might be interpreted as the rupture of

some liposomes to release their trapped water. However, this decreased value could be originated either from a decrease in the number of the adsorbed liposomes or their flattening while the liposome number was similar. When acoustic ratio was taken into consideration (150 ± 5 GHz^{-1}), a value similar to flattened liposome layer (162.3 ± 10 GHz^{-1}) was observed. This shows that the relative water content per adhered mass of both liposome layer resembles each other, though the deformation of the thiolated ones' are slightly higher. Since the deformation degrees are close to each other, the decrease at the overall areal mass could not be attributed to release of water because of decrease in the thickness of the adhered liposomes, but rather to the weak liposomal adsorption. When the scarce thiol amount (0.01%) is considered, it can be claimed that most of the thiolated liposomes could not interact with the surface and easily rinsed so a low density of liposomes attached to the surface.

Table 3.1 : Acoustic ratios of representative rigid and viscoelastic layers on sensor surfaces.

Layer characteristic		Acoustic ratio (GHz^{-1})	
Rigid	Protein monolayer	41.7 ± 4	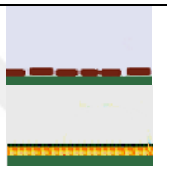
	Lipid monolayer	59.3 ± 5	
Viscoelastic	Flattened liposomes	162.3 ± 10	
	Intact liposomes	298.0 ± 21	

When DPPTE ratio was raised tenfold (to 0.1%), the chemical forces between liposome and the gold surface were enhanced which should increase the liposome density and mass on the surface. For this sample, decreased ΔD ($3.4 \pm 0.4 \times 10^{-6}$) and |Δf| (28 ± 2 Hz) values were obtained. There was also a significant decrease ($p < 0.05$) in acoustic ratio to 121.4 ± 6 GHz^{-1}. The measured frequency drop reported in the literature for a flat, rigid ($\Delta D < 0.5 \times 10^{-6}$) and continuous PC lipid bilayer, the response is around 26 ± 1 Hz [13-14,126]. The frequency change of 0.1% DPPTE – PC liposomes is very close to that value, however, higher ΔD indicates that the sensed mass includes significant amounts of water, thus the percentage of lipid mass on the surface was probably under 26 ± 1 Hz when the contribution of water was excluded from the total value. It may be suggested that while this thiol ratio caused to highly

deformed, even ruptured liposomes, the sensor surface was not entirely covered by phospholipids. The results are clear indication of an incomplete bilayer coverage beside unruptured liposomes and weak liposome – surface interactions.

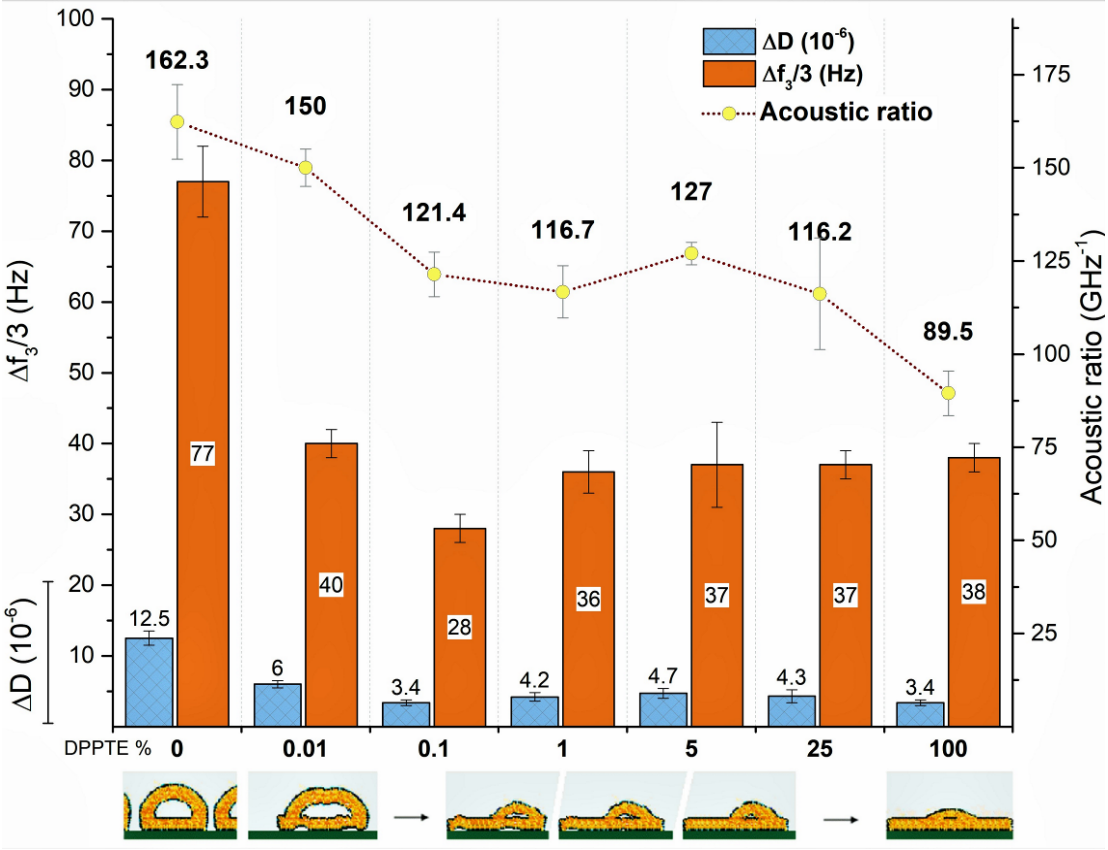

Figure 3.3 : ΔD, |Δf| and acoustic ratio values and representative figures (not to scale) of estimated structures of liposomes containing PC and DPPTE at different ratios. Statistically significant differences in acoustic ratios were labelled with brackets on graph for $p < 0.05$ ($n = 3$).

When DPPTE ratio was further increased tenfold (to 1%), acoustic ratio decreased to 116.7 ± 7 GHz^{-1} showing an increase in the rigidity of the layer but the decrease was statistically not significant. ΔD ($4.2 \pm 0.6 \times 10^{-6}$) and |Δf| (36 ± 3 Hz) were however noticeably higher than those of previous concentration (0.1% DPPTE) indicating an increased mass density. When the thiolated lipid ratio was kept increasing, no significant differences can be determined among 1, 5 and 25% DPPTE ratios. It can be said that the attachment acquired via 1% DPPTE is enough to saturate the sensor surface by phospholipids. To confirm whether phospholipids covered the entire gold surface or not, Bovine Serum albumin (BSA) protein solution (0.05 mg/mL) was used as a reporter of accessible gold surface since BSA molecules interacts with gold surface, but not with PC phospholipid layers [59]. The control experiments with BSA

indicated the strong adsorption onto the naked gold surface as a rigid monolayer with 12.0 ± 1 Hz frequency shift ($\Delta D \sim 0.5 \times 10^{-6}$). On the contrary, the frequency response of BSA with 1% DPPTE – PC layer was too low ($\Delta f = \sim 1.0$ Hz). This indicated that the layer was almost continuous with minimum defects.

The decreasing tendency of acoustic ratio in parallel to increased thiol percentage might suggest that increased thiol mediated attachment led majority of the liposomes to rupture fully. However, $\Delta D > \sim 0.5 \times 10^{-6}$ values for each set confirm that beside bilayer formation there are also some unruptured liposomes preventing continuous and planar bilayer formation. After each liposome solution, the measurement cell was subsequently rinsed thoroughly by PBS, so the possibility of a second or more adsorbed liposome layer on the underlying bilayer was eliminated. Therefore, these unruptured liposomes include either trapped liposomes or partially fused liposomes (or both of them) resulting multilayer islets and increase in the viscoelasticity on the surface. This inference can also be checked from the signals obtained via different frequency overtones (harmonics) since they provide a three-dimensional information about the adlayer [115]. Signals obtained at harmonics did not overlap for each thiol ratio (as shown in Figure 3.2) indicating a softer intra-structure because of the trapped liquid within different depths throughout the continuous layer [125]. Furthermore, frequency shifts at the normalized third overtones were the largest and at the 11^{th} ones, the smallest. This discrepancy confirms that the mass sensed at the bulk-lipid bilayer interface was higher than the mass at the sensor surface proximity. Although the liquid trapped over the depth of the bilayer indicates the presence of trapped liposomal structures, the more water trapped on the lipid bilayer – bulk interface validates the dominancy of the incompletely ruptured liposomes as the multilayer formations as represented in bilayer illustrations in Figure 3.3 (for 0.1 to 25%). The degree of the fractional bilayer coverage (α) and unruptured liposomes amounts on the surface can be roughly estimated since the bilayer does not contribute significantly to dissipation ($\Delta D_{bilayer} = 0.1 \times 10^{-6}$) whereas unruptured liposomes do. As an approximation of the quantification, the following equation 3.7 and 3.8 could be used [11,127]:

$$\alpha = 1 - \frac{\Delta D_{measured} - \Delta D_{bilayer}}{\Delta D_{saturated} - \Delta D_{bilayer}} \tag{3.7}$$

$$\Delta D_{saturated} = \beta . s \quad (3.8)$$

assuming that there is a linear relationship between the dissipation change at saturation ($D_{saturated}$) when the surface is fully covered by intact liposomes and pure PC liposome sizes (s) varying from 25 to 200 nm. β is the constant ratio of $D_{saturated}$ to the liposome size, equals to 0.15 [127]. $D_{saturated}$ is 21.3×10^{-6} for our liposomes (s = 142 ± 7 nm) and gives 81% fractional bilayer coverage for 1 % DPPTE – PC lipid bilayer and remaining fraction contains unruptured intact liposomes. This percentage decreases as the number of the flattened liposomes increased.

When pure DPPTE liposomes were used, they gave significant decrease in acoustic ratio when compared to 25% DPPTE ratio. This value (89.5 GHz^{-1}) is closer to the values obtained for the rigid lipid monolayer (59.3 ± 5 GHz^{-1}), also presenting the decreased entrapped water through the layer. Since all of the phospholipid molecules within liposome have thiol groups, complete rupture of all of the liposomes in one-step could be predicted due to the strongest gold-thiol group interactions. However, it was interesting to observe that ΔD value was $3.4 \pm 0.4 \times 10^{-6}$, which means that there is still entrapped liquid. In addition, overlapped frequency overtones except the third one indicates the presence of partially fused liposomes instead of trapped ones for pure DPPTE samples (Figure A.2). Despite the relative rigidity of pure DPPTE liposomes, using that ratio is not suitable when mimicking natural biomembranes. Beside, high proportion of thiol groups will decrease the fluidity of the bilayer, and the lateral diffusion of phospholipid molecules.

3.4.2 The effect of liposome size on its rupture

The effect of liposome size on its rupture was examined with liposomes formed by three different pore sized polycarbonate membranes, namely 50, 100 and 200 nm, keeping the thiol ratio constant (1% DPPTE). Average diameters of the liposomes were determined as 90 nm, 140 nm and 175 nm, respectively. The final asymptotic values of QCM-D signals and calculated acoustic ratios for each liposomes are presented in Figure 3.4.

Both frequency and dissipation values showed sharp increase when liposome size increased from 140 to 175 nm as expected, but stayed almost unchanged when decreased to 90 nm. The latter result might be explained with two competing factors at a certain diameter interval, packing coverage and deformation degree of liposomes.

Simply, increased liposome sizes lead higher shape deformation [14]/surface contact area, but at the same time, their overall packing coverage ("steric effect") at saturation reduces [128]. This compensation may result in similar frequency changes in our case.

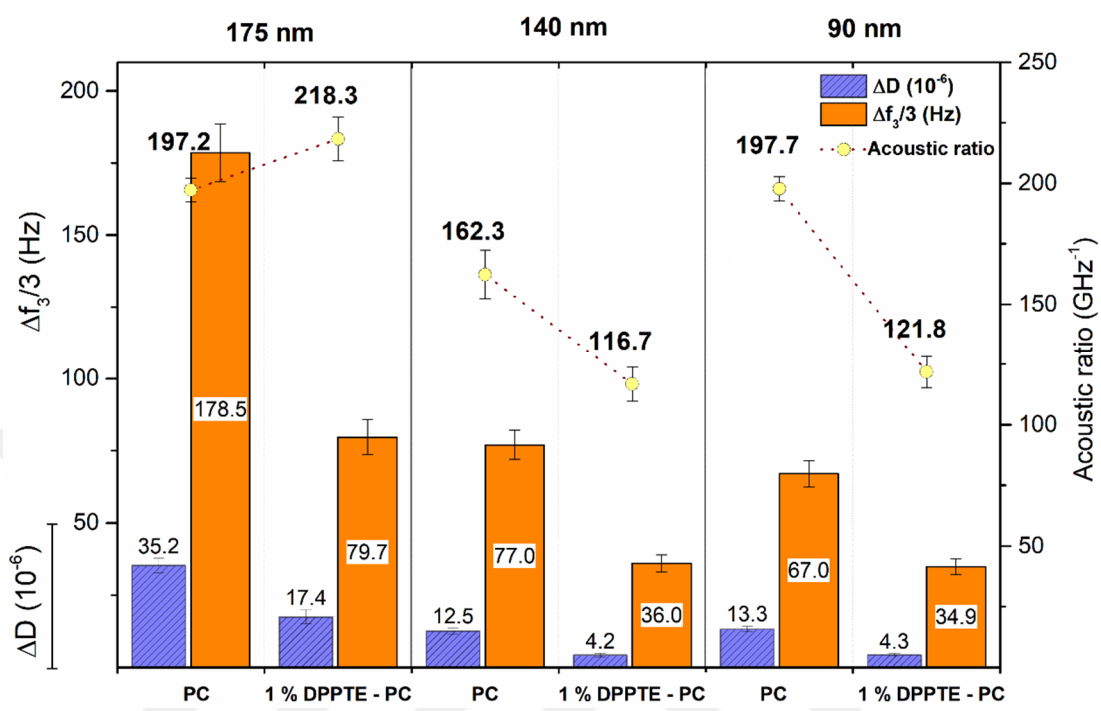

Figure 3.4 : ΔD, |Δf| and acoustic ratio values of liposomes of different sizes.

In all sizes, pure PC liposome layers showed higher mass adsorption (Δf) and viscoelasticity (ΔD) as to thiolated ones. When thiolated lipids were involved, both values decreased significantly demonstrating the high deformation degree of liposomes. Liposomes with 90 and 140 nm sizes were deformed and further ruptured similarly. However, when the size increased to 175 nm, both frequency (79.7 Hz) and dissipation changes (17.5×10^{-6}) were considerably higher proposing unruptured liposome adsorption on the surface. The acoustic ratio was also higher (218.3 GHz^{-1}) when compared with the other sizes.

Another interesting result is the increased acoustic ratio of larger liposomes (from 197.2 to 218.3 GHz^{-1}) with the addition of 1% DPPTE since a decrease was observed for the others. Both lowered Δf and ΔD values for 1% DPPTE – PC liposome layer suggested highly deformed liposomes with lower amounts of solvent compared to pure PC liposome layer, whereas acoustic ratio is higher. This behavior could be attributed to poor steric packing efficiency of larger liposomes, which prevents close packing on the substrate as demonstrated recently in [128].

3.4.3 SPR & QCM-D data modelling

Viscoelastic modelling was further studied with 1% DPPTE as the optimized ratio (low thiol ratio and more rigidity). For this, complementary experiments were conducted with SPR for better qualification of the adlayer (Figure A.3). The water content and the thickness of 1% PC – DPPTE lipid adlayer was calculated using both SPR and QCM-D data. The results were also compared to pure DPPTE lipid adlayer, flattened PC liposomes and also ideal planar PC bilayer model constructed on silica surface (based on literature data [57]). The whole data combined and graphed with illustrations of final expected liposome behavior in Figure 3.5.

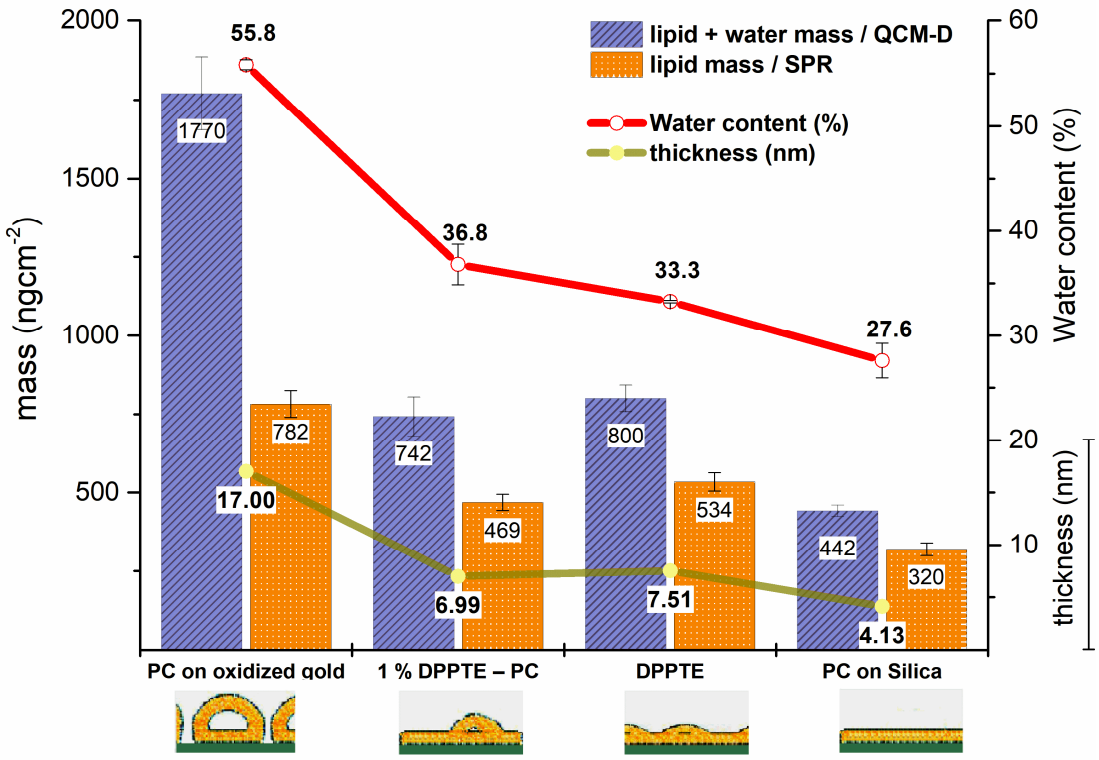

Figure 3.5 : The sensed mass per area on QCM-D & SPR surfaces, the calculated water percentage and average layer thickness. Below illustrations of the adlayers as an approximation (not to scale).

The differences between the adsorbed mass sensed with QCM and SPR show that there is significant amount of water associated with either the liposomal layer and even with ideal bilayer. PC liposomes on hydrophilic gold surface have high water content (~55.8%) as expected. This ratio is lower when an intact, hard-sphered, non-deformed, closely packed liposomal layer is considered (pure theoretically ~80% for liposomes' weight at 140 nm diameter). Because the strong electrostatic attraction between the polarized gold surface and the head groups of the lipids, deformed and flattened

liposomes leads their effective diameters to be smaller to their nominal diameters [13,129]. Viscoelastic modelling provided the possibility to calculate the effective thickness of this highly flattened PC liposome monolayer to be about 17 ± 1.1 nm. On the other side, an ideal, highly rigid lipid bilayer (d_{film} = 4.13 ± 0.2 nm) on a negatively charged silica surface contains ~27.6% water based on literature data [57]. Since the bilayer is highly rigid, planar and uniform as authors reported, this amount originates from the water bound to the lipid membrane (*i.e.,* hydrodynamically coupled), and not be treated as the bulk medium above the bilayer. It was reported that although hydrodynamic hydration layers are probed by QCM-D, they do not contribute to the dissipation [57]. From QCM-D studies mentioned in section 3.4.1, ΔD values for 1 – 100% DPPTE liposomes were between 3.0 and 4.7 × 10^{-6}. When hydrodynamically coupled water on silica sensor was taken into account, additional water amounts found for 1% DPPTE – PC (~37%) and DPPTE liposomes (33.3%) indicates the mechanically trapped liquid either in trapped flattened liposomes, and/or partially fused liposomes. Because of extra water load within the lipid bilayer, the overall thickness was calculated as ~7.0 nm for both samples.

Higher dry-lipid mass of thiolated bilayers compared to ideal bilayer (PC on silica) also points out formation of overlapped lipid bilayers/multilayer island and the distortion from the planarity.

Pure DPPTE liposomes resulted in a layer with lower water content/higher rigidity compared to 1% DPPTE – PC, confirming QCM-D results. In addition, high dry-lipid mass (534 ± 29 ng/cm^2) of DPPTE lipid layer compared to that of 1% DPPTE – PC (469 ± 26 ng/cm^2) displays the presence of more multilayer island, which led to an increase in average film thickness. As a conclusion, these results lead us to comment that the constructed bilayer via thiolated lipids is not fully planar, and implies some local elevations as illustrated something like in Figure 3.5.

3.4.4 Surface characterization of lipid adlayer with AFM

While combination of QCM-D/SPR method gives high time resolution, AFM supplies high spatial resolution. QCM-D/SPR allows us to get information as global characterization methods for layer formation, but it is limited in the detection of local structural properties such as bilayer thickness and defects. AFM is a very useful technique that provides information on the local organizations, topographical changes

and biomechanical properties of the adlayer [43-45]. For this purpose, a series of experiments with optimized thiol ratio (1% PC – DPPTE) liposome solutions were conducted at the standard liposome concentration (20 g/mL) with two different incubation durations (5 and 45 min). Thus, the initial and further progress of the adlayer formation was tried to be captured. First the topography image of an intact liposome layer in liquid was acquired (Figure 3.6a) to compare with the results of 1% PC – DPPTE lipid bilayer. The roughness average (R_a) of the bare quartz crystal – gold sensor surface was found around 0.8 nm for a scanned 1 μm^2 area. The liposome solution was incubated at least 45 min, and the results showed roundish structures with the noticeably increased heights between the peaks and valleys as seen in cross-section analysis having R_a as 2.96 nm (Figure 3.6a). In the thiolated liposome case, R_a lowered to 1.03 nm (Figure 3.6b) and to 0.84 nm (Figure 3.6c) at the end of 5 min and 45 min, respectively. The R_a approached to the roughness of the bare gold in time, and a smoother surface formed when compared with the liposome layer, which indicates the rupture and further fusion of liposomes as commented within QCM-D/SPR results.

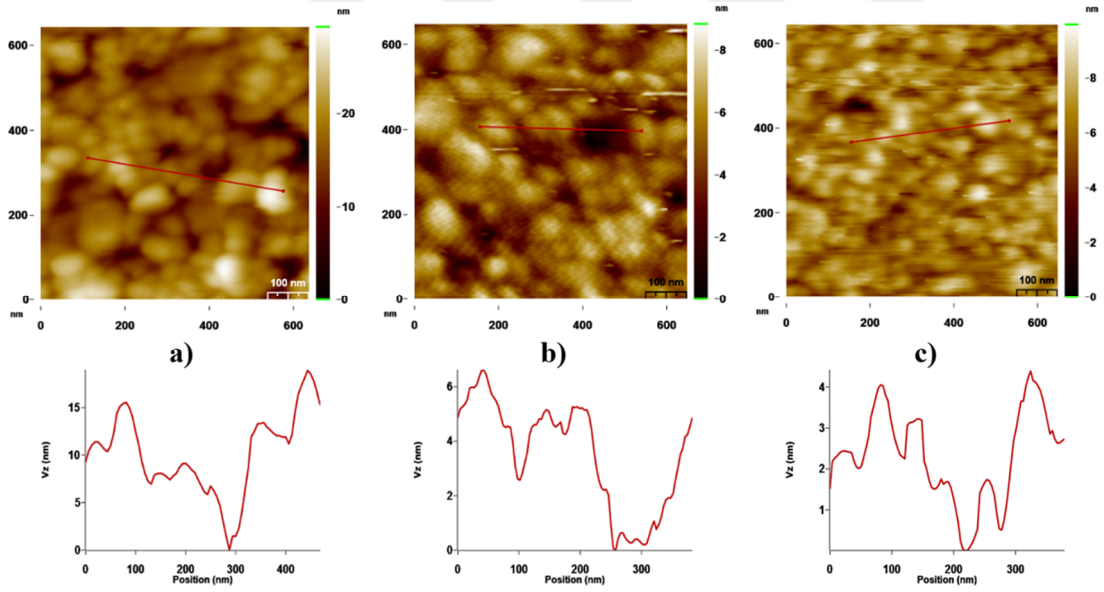

Figure 3.6 : Tapping-mode AFM topography images (top) and cross-section analysis (below) of (a) PC liposome layer (R_a = 2.96 nm), b) 1% DPPTE (thiolated)-PC liposomes after 5 min (R_a = 1.03 nm) and c) 45 min incubation (R_a = 0.84 nm).

In addition to topography (height), AFMs record phase data simultaneously that allows to compare surface structure and material domains directly. The phase signal shifts during scanning of regions with different composition. Phase shifts are recorded as bright and dark regions in phase image, similar to the indication of height changes in topography image. The phase is a measure of the energy dissipation due to the

interaction between the tip and the sample, which is determined by a number of factors such as viscoelasticity, adhesion and contact area. Despite the difficulties of interpretation, phase imaging is one of the most commonly used techniques for mechanical and compositional characterization of sample surface.

The partial patchy coverage structure that was ambiguous to realize in the topography image of thiolated liposomes for 5 min incubation (Figure 3.6b) is clearly detectable in the phase image (Figure 3.7a). Phase shifts showed the lipid layer edges with different softness/stiffness levels of the same material, and vary around 40–50 degrees (insert). The diameter distribution of the patches fit to the size distribution of liposomes acquired by DLS. In time (45 min, Figure 3.7b), patch edges became more ambiguous (phase shift variation is 10–15 degree) that could be commented as an indication of the fusion of highly deformed thiolated liposomes through the scanned area. Incompletely ruptured liposomes led local elevations as multilayer islands, which were mentioned in sections 3.4.1 and 3.4.2, are also confirmed via AFM results.

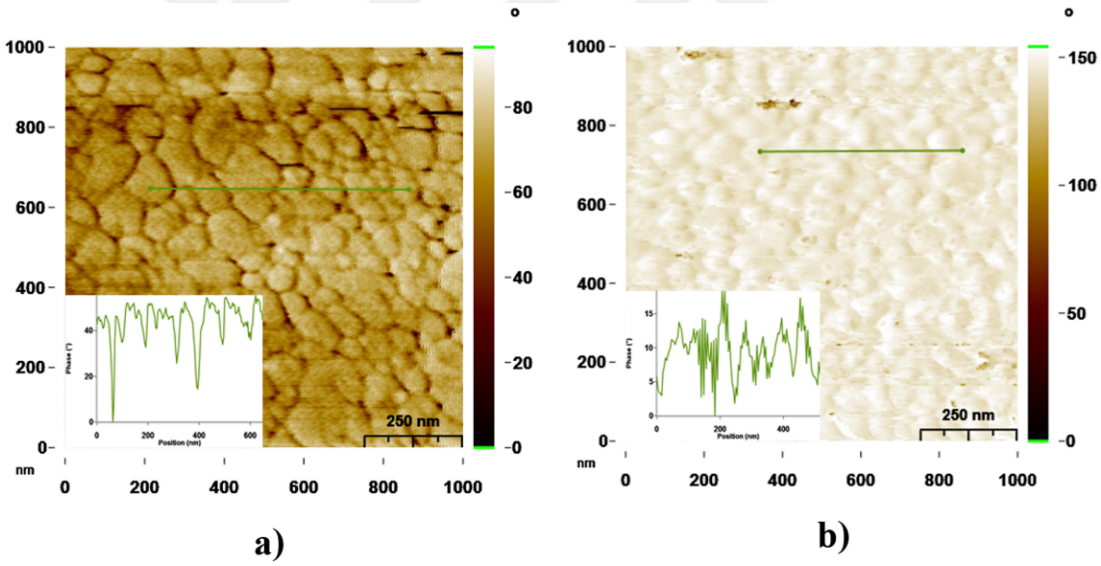

Figure 3.7 : Tapping-mode AFM phase images and cross-section analysis (inserts) for a) 5 min and b) 45 min incubated 1% DPPTE-PC liposomes.

3.4.5 Conclusion

A series of unilamellar liposomes with different DPPTE percentage (0.1 to 100%) was employed to investigate the effect of thiol-terminated phospholipid presence on liposomal behavior and on the effectiveness in SLB formation. The assessment of the quality of the constructed SLB platform was mainly interpreted via QCMD. Using the quantitative |ΔD/Δf| results, the degree of the liquid trapped within the formed layer,

or between the layer and the surface was predicted. PC liposomes are washed from bare gold surfaces but DPPTE containing ones could interact even at minor amounts (0.01%) thanks to the strong interaction between gold and thiol groups. Lower thiol ratio (0.01 to 0.1%) usage resulted with low density of liposomes attached to the surface and incomplete bilayer coverage beside unruptured liposomes, respectively. Whereas higher ratio (1–25%) yielded to the saturation of the surface and rupture of liposomes, not only as bilayer but also as multilayer islets in different depths through the continuous layer. Liposomes with 1% DPPTE was chosen as the optimized ratio since this is the lowest thiol content that generated appropriately rigid layer. The size of liposomes affected their behavior on the surface and there seemed to be a critical size in between 140 and 175 nm for them to rupture and form bilayer; bilayer formation is favored under 140 nm, whereas the liposomes seemed to flattened but not ruptured when the size is further increased (*ca.* 175 nm). The viscoelastic modelling results were combined with SPR and AFM experiments suggested that the SLB was almost continuous but showed higher water content compared to an ideal bilayer due to partially fused liposomes. These partial fusions led the increase of membrane thickness average to ~7.0 nm. In sum, direct bilayer formation on bare gold surfaces can be achieved by well-known thiol-gold chemistry using low ratio of thiolated lipids on liposomes. This procedure has a different dynamics than bilayer formation on modified gold and can further be explored by incorporating different membrane elements (different phospholipids, cholesterol, *etc.*) on the structure.

4. QUARTZ CRYSTAL MICROBALANCE WITH DISSIPATION AS A BIOSENSING PLATFORM TO EVALUATE CELL–SURFACE INTERACTIONS OF OSTEOBLAST CELLS[3]

4.1 Introduction

Investigation and control of cell–surface interactions are not only essential in understanding cell-signaling pathways, but also to evaluate the effect of drug treatments and environmental stimuli to the cell adhesion and to assess cancer cell behavior [130]. This knowledge is critical in the development, improvement, and optimization of cell-based biosensors, biomaterials, tissue-engineering scaffolds, and for various biomedical and biotechnological applications [131-132]. During in vitro cell adhesion process, the initial attachment occurs loosely with nonspecific interactions and when sufficient proximity is obtained, cells start to flatten and then spread its membrane over the surface with increasing adhesive strength with subsequent membrane receptor-mediated specific interactions. The cell height decreases and contact area increases during the continuous flattening and spread beyond the projected area of round cell. Simultaneously, the increased number of integrin binding, clustering, and formation of adhesion complexes connect extracellular matrix (ECM) with cytoskeleton. Cells anchor firmly to the surface through reorganization and distribution of the actin skeleton with the formation of focal adhesion points between the cell and its substrate [130].

Traditional methods are informative to study cell adhesion, but are end-point assays and supplies just a "snapshot" of the adhesion process. They are qualitative in measurements, laborious, cost-intensive due to prelabeling or postlabeling of the cells, and manipulating the cell behavior and physiology as a result of fixation–permeabilization steps causing data loss [133]. Further, the membrane-associated

[3] This chapter is based on the paper "Kilic A, Kok FN. Quartz crystal microbalance with dissipation as a biosensing platform to evaluate cell-surface interactions of osteoblast cells. Biointerphases. 2017 Dec 12;13(1):011001."

events take place at the cell–surface interface in which the distance is around or less than 100 nm, so difficult to probe directly. Therefore, while images of two cells look very similar under microscopy for different situations/conditions, they may have very different interfacial features in the attachment and spreading process [58,89]. The significance of cell adhesion led researches to develop label-free and noninvasive methods to evaluate cell adhesion process. Among various tools, quartz crystal microbalance with dissipation (QCM-D) has been utilized by different groups to study the attachment and spreading of different mammalian cell lines on various sensor surfaces with or without precoated protein layers. This technique helps to monitor changes in cell morphology, cellular responses to various soluble factors, and analysis of the mechanical properties at the cell–surface interface in real time and quantitatively [58,89,92-93,134-143]. Due to the piezoelectric feature of quartz crystal, applying an alternating voltage excites a mechanical oscillation through the quartz crystal and the frequency and dissipation of this oscillation depend on the mass and viscoelasticity of the layer on the surface [104]. The penetration/sensing depth or decay length of the propagated acoustic wave through the sensor in water is limited to a region extending 250 nm at the fundamental frequency (5 MHz) and no more than 100 nm at 35 MHz [138]. For this reason, QCM only senses the cells that are in direct contact with the sensor surface, (*i.e.*, ECM, cell membrane, and in some extent the cell cytoplasm) [58] and is not sensitive to changes in the top of the adhered cells [144].

Throughout the cell adhesion at the sensor surface, the interfacial interactions are reflected in QCM-D signals, *i.e.*, the frequency change (Δf) and energy dissipation change (ΔD). Δf reflects a more direct interaction of the cell with the substrate, and comprising the adsorbed cell mass [93] and secreted proteins (microexudates) [145], fractional surface coverage of the cells [138], and cell membrane–surface separation distance/thickness of interfacial layer [146]. ΔD is the changes in the viscoelasticity/softness of the sensed layer, but there is not a complete consensus in the literature about the information content of the signal yet, and the source of the energy loss is considered as composite of many different events. Generally, it was asserted that changes in cell mechanical properties [146], thickness of interfacial layer [144,146], microexudates [145], cell membrane and cytoskeletal rearrangements above the membrane in close contact with the substrate [93], and contribution of extracellular matrix [144] are linked with that phenomena. These values are assembled

and quantified in acoustic ratio (ΔD/Δf plots) [147] that depend on effective deposited mass, viscoelastic properties, and internal structure and morphology of the cells for each time point to identify the adhesion maturation of cells independent of their positions on the surface [135,137]. QCM-D gives very different corresponding profiles, creates fingerprints for different cell lines making it popular for studying cell–surface interactions [89].

In this study, the aim was to characterize the dynamic adhesion behavior of human fetal osteoblastic bone (hfOB) cell lines by simultaneously measuring frequency and energy dissipation changes on various model surfaces. Among the metal surfaces, the gold is employed as a standard reference; therefore, the experiments were first conducted on both untreated and hydrophilically treated gold sensor surfaces. Corresponding adhesion stages observed under light microscopy were also presented to facilitate the evaluation. Further, the adhesion strength and kinetics of the cells on cell adhesive [poly-L-lysine (PLL) and fibronectin (FN)] and repellent surfaces [bovine serum albumin (BSA)] were examined for more thorough understanding. Finally, the potential of QCM-D to distinguish healthy and cancerous cells were also evaluated by comparing the results with that of SaOS-2 (osteosarcoma) cancerous cells.

4.2 Materials and Methods

4.2.1 Materials

Purified water was used with a minimum resistivity of 18.2 MΩ·cm for all solutions. Phosphate buffered saline (0.01 M phosphate buffer, pH 7.4, containing 137 mM NaCl, 2.7 mM KCl) was used as filtered through 0.2 µm filters (Millipore), degassed for QCM-D, and also autoclaved for cell assays.

Gold-coated BK7 glass slides and gold-coated AT-cut quartz crystals with a fundamental frequency of 5 MHz and a diameter of 14 mm were purchased from Reichert and Q-Sense (Sweden), respectively.

4.2.2 Surface preparations

Before each use, clean gold-coated AT-cut crystals and BK7 glass slides were rinsed with ethanol (70%), ultrapure water, and dried under nitrogen gas. In the case of

hydrophilically treated samples, the surfaces were oxidized with UV-ozone exposure for 15 min, then rinsed with water, dried under nitrogen, and used immediately since hydrophilicity obtained by this treatment is not permanent and lost with time in ambient air. The contact angle of clean, untreated gold coated AT-cut crystals and BK7 glass slides were measured as 58.81° ± 0.34° and 65.22 ° ± 0.28° (KSV Cam Goniometer system with Attension Theta analysis software, Biolin Scientific) while immediately after the treatment, these values were 27.04° ± 0.10° and 24.20 ° ± 0.18°, respectively.

Surface coatings with PLL (100 µg/mL) (Sigma-Aldrich), FN (2.5 µg/mL) (Sigma-Aldrich) and BSA (200 µg/mL) (Sigma-Aldrich) on hydrophilic gold surfaces were obtained by passing the filtered biomolecule solutions through QCM-D chamber until the signals were stabilized. After rinsing, and stabilization of the signal, the cells were introduced into the system.

In order to clean the surfaces, the crystals/slides were soaked and sonicated in sodium dodecyl sulfate (SDS), ethanol (70%), and ultrapure water, then dried under nitrogen. Finally, in order to rule out the organic contaminants at the molecular level, they were exposed to UV-ozone for 15 min and stored in a desiccator until reuse.

4.2.3 Cell culture

Human fetal osteoblastic healthy (hfOB, ATCC CRL- 11372) and SaOS-2 (human osteosarcoma, ATCC HTB-85) cancerous cell lines were maintained with routine subculturing in a humidified incubator with 5% CO_2 at 37°C. They were grown on 25 cm^2 cell culture flasks in Dulbecco's modified Eagle culture medium (DMEM) (Thermo Fisher Scientific, Inc., 21885025) supplemented with 10% (v/v) fetal bovine serum (Sigma-Aldrich), containing low glucose (1 g/L), sodium pyruvate (3.7 g/L), and 1% (v/v) of penicillin–streptomycin (Sigma-Aldrich). The cells were detached by trypsinization with 0.25% trypsin–EDTA solution (Sigma-Aldrich) at 37°C for 5 min. Excess amount of serum-supplemented culture medium was added to inactivate trypsin and the cells were centrifuged at 1000g for 5 min. The pellets were suspended in serum-free medium and viable cell amount was counted on hemocytometer with Trypan Blue exclusion.

4.2.4 QCM-D setup for cell adhesion assay

QCM measurements were performed by a dissipative QCM instrument (QCM-Z500, KSV Instruments, Finland) using a flow-through system provided with a peristaltic pump. The frequency (Δf) and dissipation change (ΔD) data with different overtone frequencies, *i.e.*, harmonics at 15, 25, 35, 45, and 55 MHz, were obtained but only the (normalized) third overtone results for frequency shift ($\Delta f_3/3$) and dissipation change (ΔD_3) were shown. Before each experiment, QCM-D system, the reaction chamber, and tubings were cleaned with SDS (1%), ethanol (70%), and degassed ultrapure water successively. Following the cleaning, the reaction chamber was dried with N_2 gas, and the sensor slide was mounted.

Real time QCM-D experiments were conducted in normal atmosphere (not in CO_2 incubator), so 25 mM *4-(2-hydroxyethyl)-1-piperazineethanesulfonic acid* (HEPES) was added as supplemental buffering system to the previously used growth media to keep pH at 7.2–7.6, and 1% (v/v) of penicillin–streptomycin solution was used to prevent bacterial growth. The cell adhesion experiments were performed in flow mode at least three times at 37 °C.

QCM-D sensors were inserted into the instrument and then deionized water was sent into the chamber with a speed of 100 µL/min until a stable baseline was reached. Then, the serum-free medium was introduced into the channels. When the signals were stabilized, defined number of cells in serum-free medium was passed through the chamber with a speed of 100 µL/min for 1 h (6 mL) to monitor cell adhesion. The pump was stopped 1 h later, and cells were left in no flow conditions for 17 h. Rinsing steps were performed at the end of all experiments to wash dead or detached cells.

To check the strength and specificity of the cell adhesion, two different control experiments were run. In the first one, an additional rinsing step at the end of 1 h was performed for both untreated and hydrophilically treated surfaces and the changes in signals were monitored. To test the specificity of the cell attachment, competition experiments were performed, incubating cells with soluble RGD peptides (Abbiotec, 350362; 100 µM) and observing the change in the signal.

The corresponding morphological changes of cells were simultaneously followed under identical conditions on gold-coated BK7 glass slides placed in a chambered system maintaining the flow conditions and allowing to take images under an inverted

light microscopy (BEL Photonics®, Brazil). Normalized spreading area of the cells was measured using an image processing software (ImageJ Version 1.51n, National Institutes of Health).

4.2.5 Cell viability assay

3-(4,5-dimethylthiazol-2-yl)-5-(3-carboxymethoxyphenyl)-2-(4-sulfophenyl)–2H-tetrazolium (MTS, inner salt) cell proliferation assay (CellTiter 96® AQueous One Solution Cell Proliferation Assay, Promega) was used to evaluate the viability of osteoblast cells on hydrophobic and hydrophilically treated sensor surfaces.

Cleaned sensors were first sterilized under UV-light in laminar flow for 15 min and then placed in a 48-well plate. The surface of the tissue culture plates were used as control. hfOB cells were seeded at a density of 10,000 cell onto the sensor surfaces and control wells. HEPES buffered serum-free medium (500-µL) was added to each sample and cell proliferation assay (MTS) assay was performed at the end of 18 h of incubation. For that, the surfaces were first washed with medium and transferred to a clean 48-well plate. Mixed solutions of medium and MTS (5:1) were poured onto the samples (600 µL per sample) and incubated for 2.5 h at 37 °C. At the end of incubation, 5 × 100 µL of each solution on the samples were transferred to a 96-well plate and optical densities were measured at 490 nm using Elisa Plate Reader. The viability percentage of proliferating cells was calculated according to the control well.

4.2.6 Statistical analysis

Statistical analyses of the data were performed by Student's t-test in Microsoft Office Excel. Significant difference was considered at the level of $p < 0.05$ ($n \geq 3$).

4.3 Results and Discussion

All experiments were conducted in serum-free medium to rule out the effect of surface– and cell–serum proteins interactions and the other factors on QCM-D signal and to observe the adhesion behavior of cells more clearly. Before QCM-D studies, cell survival was checked in serum-free medium (buffered with HEPES) for 18 h. As expected, cells were alive but their growth was slowed down and limited spreading was observed. To avoid cell stacking, an initial cell amount of 600×10^3 (0.1×10^6 cell/mL concentration) was chosen in flow system (see details in supplementary

material, Appendix B section B.1 and Figures B.1 and B.2). In this way, cells were expected not to exceed the confluency during the adhesion period.

4.3.1 Cell adhesion on untreated and hydrophilic gold surfaces

The surface characteristics have profound effect on the cell adhesion since the conformational state and orientation of proteins mediating adhesion process were affected. It is known that mammalian cells prefer to adhere on hydrophilic surfaces rather than hydrophobic ones [131,148] and untreated gold surfaces are relatively more hydrophobic (contact angle: 65°–70°) than hydrophilically treated surfaces [148]. In our case, the surfaces become oxidized [13] and the contact angle was reduced to ~25° after treatment and adhesion to both surfaces were determined and compared.

4.3.1.1 On untreated gold sensor

A typical QCM-D signal monitored on untreated gold sensor and corresponding cell morphologies taken under light microscopy could be seen in Figure 4.1. Cell morphologies in tissue culture well plate with similar density (in serum-free media) were presented for comparison (Figure B.3). After the cell suspension was passed through the chamber, a continuous increase in ΔD and a decrease in Δf were observed as an indication of the initial cell sedimentation. The cell flow was stopped at the end of 1 h, and Δf and ΔD signals reached plateau value, showing that the cell adsorption was almost completed (Figure 4.1a, inset). When the chamber was rinsed with cell-free medium as a control, minimal or no cell detachment was monitored, indicating the irreversible adhesion of the cells onto the surface.

When the cells were left in no flow conditions, it was seen that the signal remained almost unchanged for another 2 h, and then ΔD started to increase and Δf to decrease. According to sedimentation rate calculations, cells settle down to the surface in maximum 10 min in no-flow conditions [137]. For this reason, additional cell attachment from supernatant can only be seen within the first 10 min in no flow conditions, so the monitored change could not be attributed to further cell attachment, but to the rearrangements on the cell–surface interface. The increased signal due to increased contact area of the cells has been reported in previous findings [138,146]. The adhesion of secreted proteins, flattening of cell body, the approach and direct contact of the cell membrane to the surface presented increased cell–surface interface in the penetration depth (250 nm for fundamental resonance frequency, at 25 °C in

water [39]) of acoustic wave of crystal sensor and led to increase in both signals. The minimum distance between the surface and ventral cell membrane during initial cell attachment is 50 nm, and the proximity decreases to 10–20 nm afterward through integrin receptors binding to surface [137].

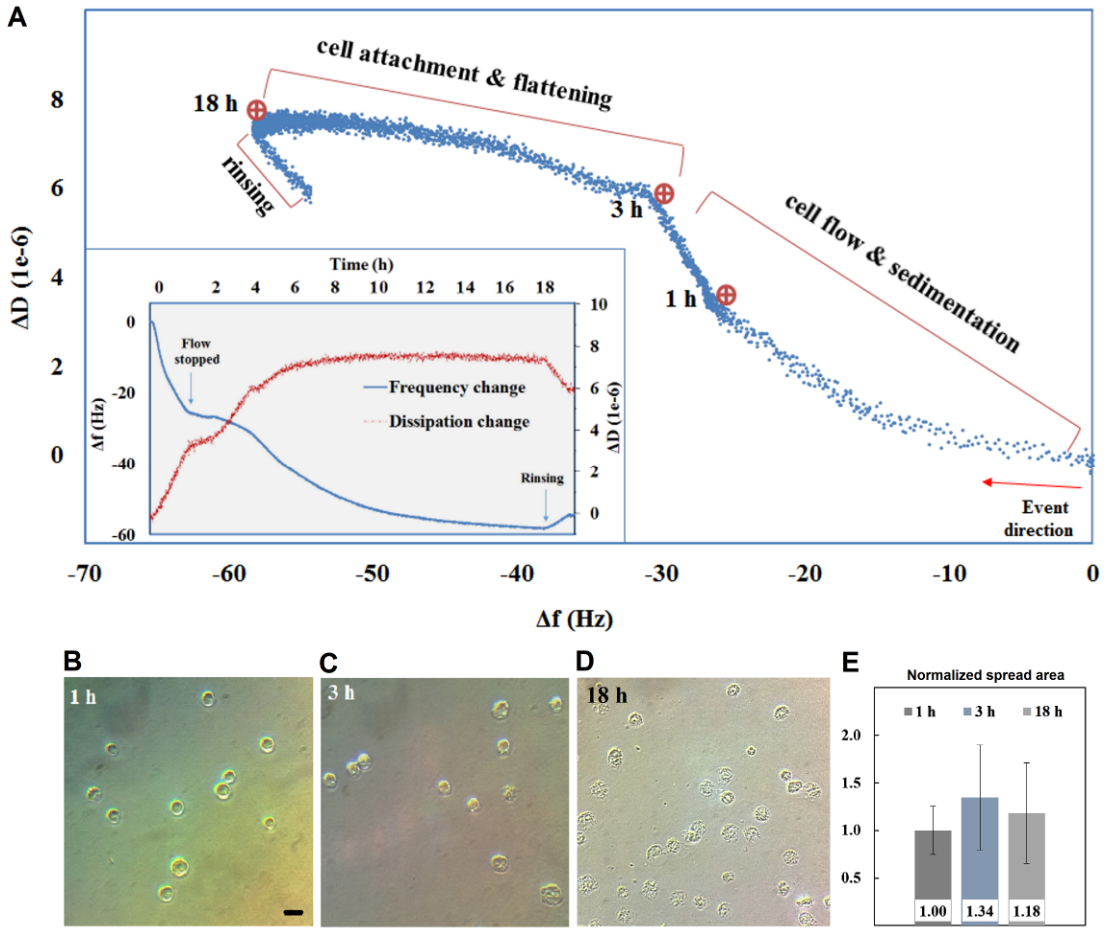

Figure 4.1 : (a) Both implicit time and in time QCM-D signals (inset) monitored on untreated gold sensor. At the implicit time graph, sparse point clouds indicate a rapid kinetic and the dense point cloud is the reverse. At t = 1 h, cell seeding was stopped. At t = 3 h, cell attachment almost completed. Below, cell morphology snapshots at corresponding time points (b) 1, (c) 3, and (d) 18 h were presented. (e) Normalized spreading area for each time points, 11 cells were measured from the images. Scale bar is 10 µm.

Microscopy images and area calculations showed that the cells started to show a more flatten appearance nearby the projected area of round cell beginning from third hour (Figure 4.1c). The average area of the cells was increased by 134 ± 55% when first and third hour results were compared. At the end of 18th hour, however, the average area decreased to some extent (118 ± 53%) (Figure 4.1e) probably due to decrease in cell viability, which could be understood from their unhealthy round shapes (Figure 4.1d) compared to healthy, spread cells grown in tissue culture plates (Figure B.3). In

parallel, acoustic ratio reached to its steepest point (*i.e.*, highest viscoelasticity per adhered mass) in the third hour (Figure 4.1a). Subsequently, the slope slowly decreased in time meaning that the increase in ΔD was lower. Even after 9 h, the dissipation value remained stable whereas Δf continued to decrease slowly (Figure 4.1a, inset). The decrease in acoustic ratio on untreated surface is consistent with previous finding [145]. It can be said that during the initial contact for 1 h, the maintenance of spherical cell morphology matches with the increase in acoustic ratio and subsequent flattening correlated with the decrease of the slope. The cells apparently did not spread beyond the projected area of round cell. Even after sufficient proximity supplied through nonspecific interactions, and possibly by integrin mediated specific interactions, the hydrophobicity of the surface seemed to hinder cells to form more adhesion sites, and structural reorganizations for further stages of complete spreading.

The presence of alive cell monolayer and specific, protein-mediated anchorage was confirmed in an experiment using trypsin solution in QCM-D flow cell (supplementary material, Appendix B section B.3, Figure B.4). After the cell adhesion and rinsing steps, trypsinization decreased the sensed mass and signals approached to the initial values indicating the enzymatic cleavage of proteins and the complete detachment of the cells.

4.3.1.2 On hydrophilically treated gold sensor

The figure of typical QCM-D signals (both implicit time and in time) monitored on hydrophilic gold sensor and corresponding cell morphologies can be seen in Figure 4.2. Cell flow was stopped at the end of 1 h, and the experiment was continued in no flow condition. As a control experiment, the chamber was rinsed with cell-free medium at the end of 1 h and minimal or no cell detachment was monitored indicating the irreversible adhesion of the cells onto the surface as in the case of untreated surfaces. The direction of Δf, ΔD signals (Figure 4.2a, inset) and acoustic ratio (Figure 4.2a) at third hour (arrow-1) was unlike the untreated, more hydrophobic surface. While Δf increased, ΔD and acoustic ratio values noticeably decreased displaying an obvious increase in rigidity at the interfacial layer. The increase in Δf (mass loss) could be attributed to the release of entrapped water between the cells and surface throughout the spreading process [137].

Microscopy results showed that most of the cells had already begun to spread beyond the projected area within the third hour (Figure 4.2c) as opposed to untreated surfaces. The normalized average area of the cells was found to increase by 160 ± 97% when images at first and third hours were examined (Figure 4.2e). The spread of the cells require the aid of ECM remodeling and cytoskeletal changes, particularly the actin concentration at the edge of the cells, and it had been already shown that these steps increase the rigidity of the focal adhesion points [134,137].

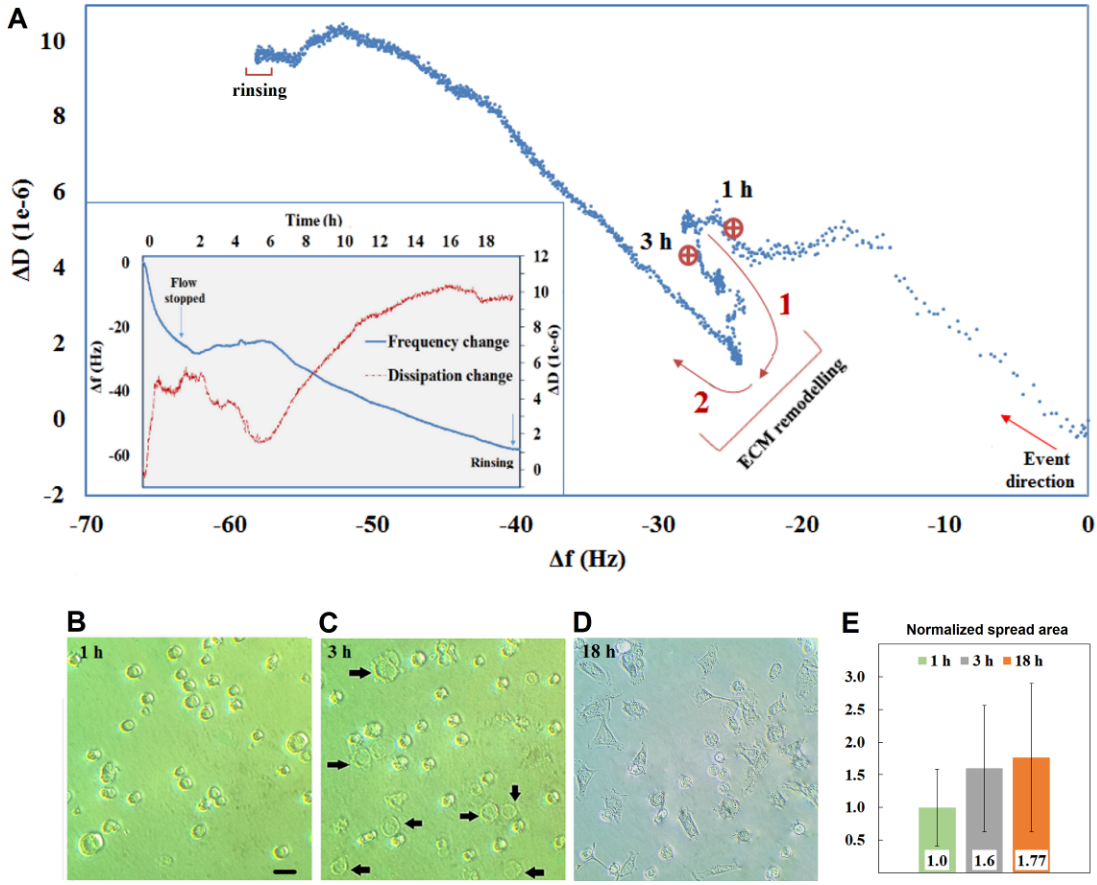

Figure 4.2 : (a) Both implicit time and in time QCM-D signal (inset) monitored on hydrophilic gold sensor and below corresponding cell morphology snapshots at the end of (b) 1, (c) 3, and (d) 18 h and (e) normalized spreading area of the cells. For both time points, 25 cells were measured from the images. Scale bar is 20 µm.

Interestingly, after reaching deep, -ΔD/Δf slope reversed its direction again (arrow-2) and even began to increase steeply, indicating an increased viscoelastic behavior at the interfacial layer. This increase on hydrophilically treated surface is consistent with a previous finding [145]. This behavior was not originated from the reversal in cell morphology from spread form to round shape as confirmed using microscopy. Acoustic ratio not only provides information about the internal structure and morphology of the cell, but also involves the dynamic processes occurred throughout

the cell spreading. While acoustic ratio increased almost until the end of the experiment, cells took different polygonal shapes (Figure 4.2d), and no significant increase was seen in the average spread area (177 ± 113%) at 18 h. Conclusively, if the signal for initial attachment step was left aside, this observation was consistent with the finding that the progress of acoustic ratio reflects focal adhesion maturation and associated cytoskeletal changes, more than the cell spreading area [93].

All the above results for untreated and hydrophilically treated surfaces are presented in Figure 4.3 for better comparison.

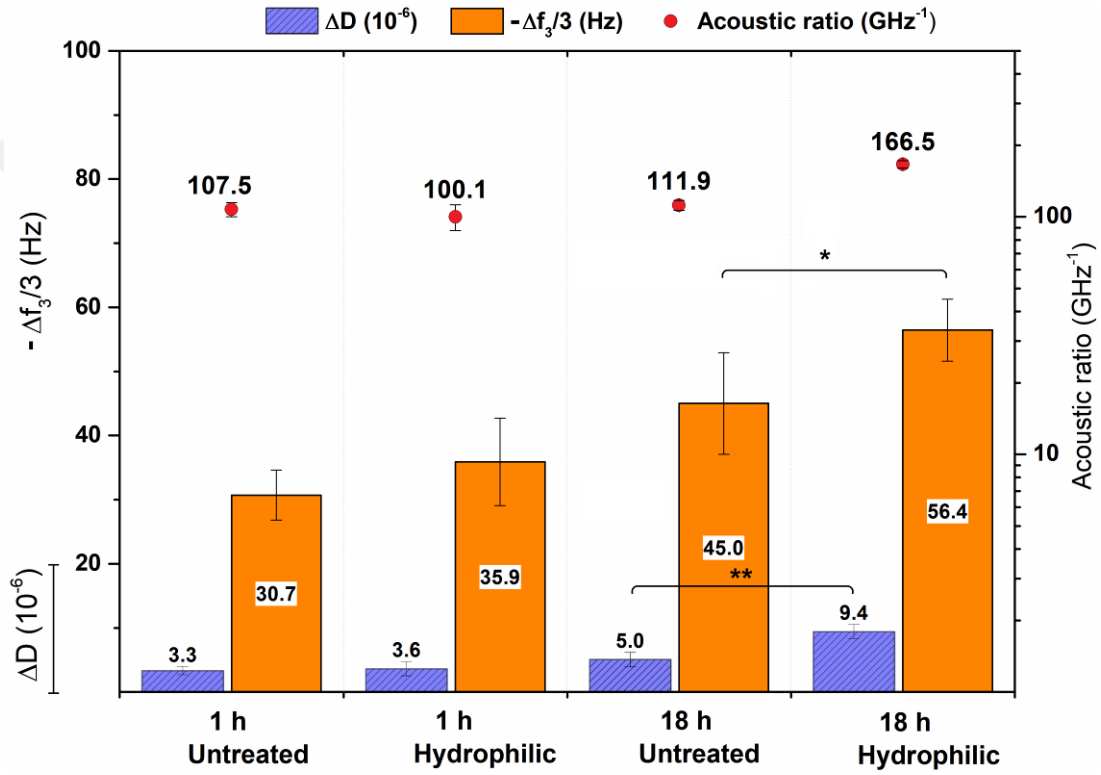

Figure 4.3 : -Δf, ΔD and acoustic ratio values at the end of 1 and 18 h for both untreated and hydrophilically treated gold surfaces. Statistically significant differences were shown with * and brackets for $p < 0.05$ ($n \geq 3$).

The acoustic ratio did not change significantly on the untreated surface in time, whereas both ΔD and -Δf values were higher for the cells at the end of 18 h. This supports that despite the flattening of the cells, integrin-mediated specific interactions was not too strong to change the viscoelasticity of the interfacial layer. The decrease in Δf and increase in ΔD signals are mostly the result of passive flattening of the cells, including adhesion of some excreted protein molecules. On the other hand, the acoustic ratio values were similar for both surface types at the beginning, indicating similar morphology and/or interfacial viscoelasticity. The initial physical contact (first hour)

seemed to be slightly stronger on the hydrophilic surface (though statistically insignificant), sign of stronger attachment during the cell flow. At the end of 18 h, the distinction was more clear and ΔD, -Δf, and remarkably acoustic ratio showed statistically significant increase on the hydrophilic surface, suggesting that the cells increased their surface contact area and spread more with the aid of protein-mediated specific interactions.

4.3.1.3 MTS viability test

The viability of cells in HEPES supplemented growth media was further checked on untreated and hydrophilically treated gold surfaces by MTS assay (Figure 4.4). At the end of 18 h, cell viability on hydrophilic surfaces was comparable to that of the tissue culture plate (control) and higher compared to the untreated surfaces. The majority of the cells were still alive on the untreated surfaces (80% viability compared to control) although they do not spread like healthy cells. These data support QCM-D results discussed in section 4.3.1.2.

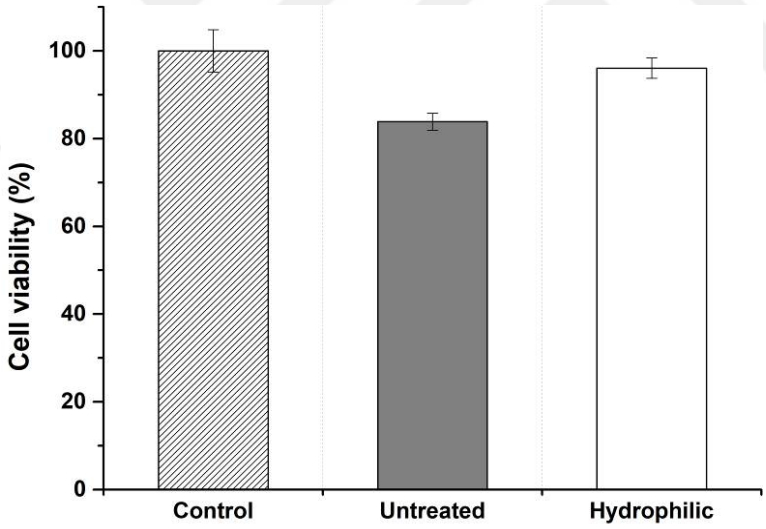

Figure 4.4 : Viability test of hfOB cells on untreated and hydrophilically treated gold surfaces.

4.3.1.4 Effect of RGD peptide saturation on cell adhesion

Short RGD (Arg-Gly-Asp) peptide sequence is the binding motif of various ECM proteins to cell adhesion molecules such as integrin. Free RGD molecules within the solution interacts with integrin proteins of cells and hinder specific cell attachment to the surface by saturating the cell binding proteins [93]. In order to confirm the presence of protein-mediated specific interactions, competition experiments performed with

soluble RGD peptides (100 μM). Substantial drop in both signals was monitored when compared to the results of hydrophilic surface, indicating that cell attachment was significantly hampered (Table 4.1). The signal was considerably affected at the end of 1 h, which is a clear sign that integrin-mediated specific interactions have already begun within the first hour. These results supported that the integrin-mediated specific interactions have considerable contribution to QCM-D signals on the hydrophilic surface.

Table 4.1 : Δf and ΔD changes for RGD saturated cell adhesion at the end of 1 and 18 h.

	In the absence of RGD		In the presence of RGD	
	Δf (Hz)	ΔD (10^{-6})	Δf (Hz)	ΔD (10^{-6})
1 h	35.9 ± 6.8	3.6 ± 1.1	11.9 ± 2.3	0.1 ± 0.1
18 h	56.4 ± 4.8	9.4 ± 1.1	19.4 ± 1.7	2.5 ± 0.3

4.3.2 Cell behavior on poly-L-lysine, fibronectin, and bovine serum albumin coated sensor surfaces

Further trials were conducted on PLL, FN, and BSA coated gold sensor surfaces to comprehend the contribution of specific interactions to the frequency and dissipation changes. They were chosen since they have the ability to promote (PLL, FN) or reduce (BSA) cell adhesion. The signal changes (Δf and ΔD) and calculated adsorbed areal mass for each protein coating were given in the supplementary material, Appendix B, section B.4 (Table B.1). The adhesion kinetics (Figure 4.5) and the overall values were compared at the end of one (initial attachment) and 18 h (cell spreading) (Figure 4.6).

The kinetics of cell adhesion on PLL and BSA surfaces (Figures 4.5a) and 4.5b) resemble to that on the hydrophilic gold surface (Figure 4.2a), *i.e.*, a temporary increase in rigidity at the interfacial layer could be tracked from the drop in the acoustic ratio, followed by a decrease and finally a steady increase, indicating the increase in viscoelasticity. However, no abrupt decrease was observed in the acoustic ratio for FN-coated surfaces (Figure 4.5c). It was probably because of the rapid increase in ΔD (up to 50×10^{-6}), which continued until third hour. Indeed, when FN concentration was lowered fivefold, an increase in rigidity was observed, which is marked by an arrow on the graph (Figure 4.5c), inset).

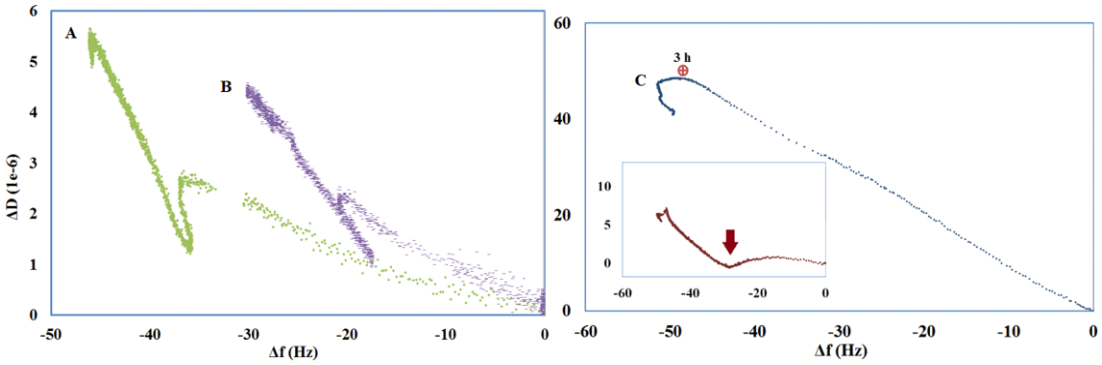

Figure 4.5 : Δf vs ΔD plots for (a) PLL, (b) BSA, and (c) high and low concentration (inset) FN-coated surfaces.

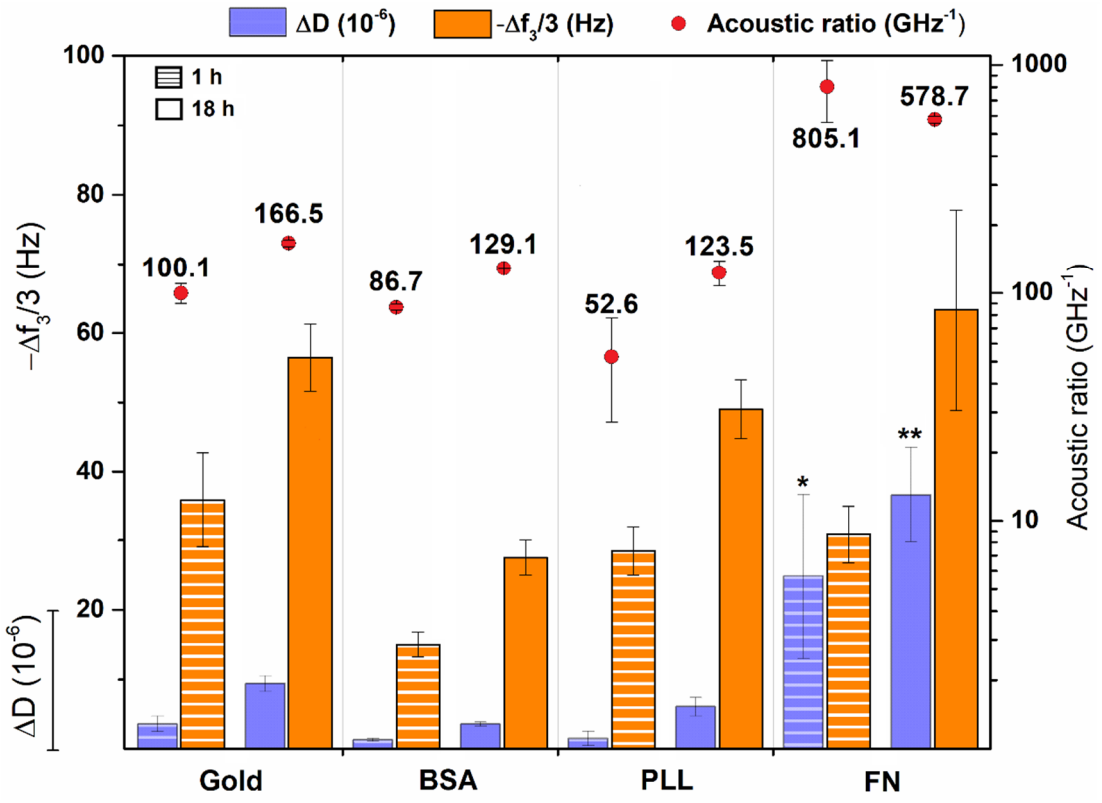

Figure 4.6 : -Δf, ΔD and acoustic ratio values at the end of 1 and 18 h for treated gold, PLL, BSA, and FN-coated surfaces. Statistically significant differences were shown with * for $p < 0.05$ ($n \geq 3$). * and ** compared to ΔD results of other surfaces for 1 and 18 h, respectively.

As expected, the number of cells was significantly reduced and the cell adhesion process was hindered on albumin-coated surfaces (Figure 4.6). Similar Δf values (for initial attachment and surface contact area) were obtained for the FN-coated surfaces when compared to the hydrophilic gold ones. However, noticeably high and sudden ΔD shifts were measured at the end of 1-h even at low FN concentrations (2.5 µg/mL).

Fibronectin is known to improve cell attachment and adhesion by specific RGD cell-binding domain so immediate interactions between these sequences and the adhesive proteins (integrin) probably led to this rapid shift. The lack of precoated ECM components on other surfaces caused a lag time in which the cells first secrete the appropriate matrix proteins and subsequently start remodeling. Fivefold lower FN concentration did not have major effect on Δf, whereas ΔD was lowered considerably, which supports that protein mediated specific interactions mostly contribute to the dissipation changes. This is also consistent with the results of positively charged PLL coated surface that is known to enhance cell adhesion by electrostatic interactions with negatively charged cell membrane. Despite similar Δf results (PLL vs FN), ΔD values were significantly low, indicating that the spread of cells occurred mostly in nonspecific manner since PLL does not contain RGD sequences. In another study [149], however, cell binding was found to be stronger on polylysine coated gold surfaces compared to both fibronectin coated and uncoated ones. In that study, the gold sensor surfaces were cleaned successively in different chemical solutions (piranha, *etc*.) to increase the hydrophilicity and poly-D-lysine, which is more suitable for some of the cell types, was utilized. The cell type (NIH 3T3 fibroblasts) and incubation conditions also differed. All these confirm that cells are extremely sensitive to the changes on the surfaces and understanding this behavior is useful in distinction of different cell types.

Measuring the dissipation changes beside the frequency provides an important advantage over QCM systems without dissipation property [139,150] since changes in frequency could be related both with physical contact of the cells or their spreading and different dynamic situations resulted in similar Δf values. As mentioned above, although similar Δf results were obtained for uncoated and FN-coated surfaces, ΔD is obviously differs when protein-mediated interactions are involved, which was also supported by earlier research [140]. The correlation between the increase in dissipation with increasing number of cell attachment and cell coverage area regardless of cell, surface type, and surface coating is the consensus of the previous studies18 and it is also shown in our work. The correlation with the frequency, on the other hand, is not strong, especially when the cells are introduced into the system in serum-supplemented medium. Serum components, mainly proteins, adsorbed on the sensor surface forms a layer with a thickness of about 35–40 nm (the so-called Vroman effect). The thick

protein layer represents a considerable proportion of the maximal penetration depth of the acoustic wave, hence likely attenuating the frequency signals resulting from the upper cell layer [138]. Even positive frequency shifts implying mass detachment had been reported when cells were added in serum-supplemented medium [89]. This positive shift is attributed to the released water originating from the structural rearrangements of the underlying protein layer. In this case, dissipation gives more reliable results and positive dissipation shifts had been the clear indication of the cell attachment and spreading. Increase in rigidity of the cell layer is associated with the extracellular matrix remodeling [134]. Viscoelastic states at different time points, on the other hand, can only be followed from the acoustic ratio (Figures 4.1a, 4.2a), and 4.5), but not from the frequency signals.

4.3.3 Cancerous cell adhesion on untreated and hydrophilic gold surfaces

The adhesion characteristics of SaOS-2 cancerous cells, which are known to overexpress certain integrin subtypes [151], were also monitored on both untreated and hydrophilic gold sensor surfaces (supplementary material, Appendix B, section B.5; Figure B.5). The initial physical contact and the last adhesion degree were higher on hydrophilic surfaces compared to that of healthy cells (Figure 4.3). In addition, the acoustic ratio values obtained on both surfaces and both time points were significantly higher than the healthy cells pointing out the viscoelastic or softer nature of cancerous cells.

SaOS-2 cells interacted with each type of surfaces stronger than the healthy ones, which is not distinguishable under microscopy. Indeed, when SaOS-2 cells were trypsinized, a longer duration was required (~15 min vs ~5 min) in the same experimental conditions. Integrin overexpression on SaOS-2 cell membranes secure strong surface interaction and this could be considered as the cause of higher ΔD values and acoustic ratio as discussed previously.

When the cluster of the average values for healthy and cancerous cells are plotted with the standard deviations, the discrimination of each cell types could be seen more clearly (Figure 4.7).

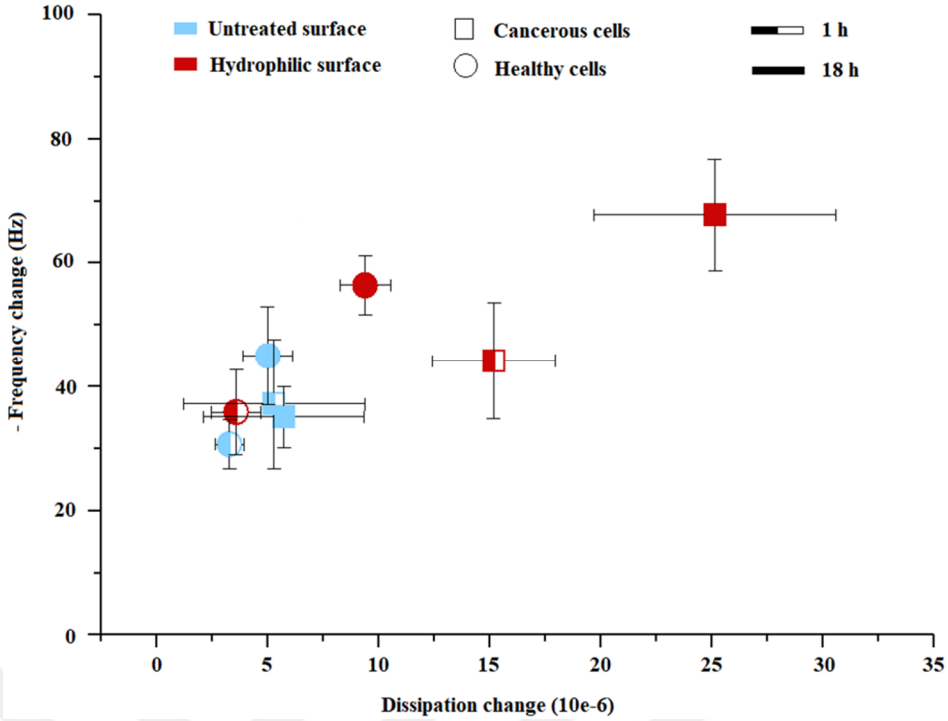

Figure 4.7 : Cluster of QCM-D signal values obtained at the end of 1 and 18 h on both untreated and hydrophilic gold surfaces.

While the data cluster acquired for untreated surfaces does not allow a distinct profile needed for a screening test, healthy and cancerous cells could be clearly distinguished on hydrophilic surfaces even at the end of 1 h without any specific protein coating. Rapid probing and sensitivity of QCM-D offers a possibility to distinguish normal and cancerous cells in a heterogeneous population, *e.g.*, within a biopsy tissue [152]. This, however, requires more thorough studies using different cells at different ratios on various substrates. If the surfaces are further functionalized specifically for the recognition of various cancer biomarkers, QCM-D signal variations could be exploited for the detection of metastatic potential of the cancerous cells. In a recent study [153], evaluating the affinity of lectins to glycans, in which the expression level on the cell surfaces has crucial roles in melanoma progression, the interaction kinetics had been probed in a quantitative manner. Larger affinity of lectin to metastatic cells had been shown and ΔD-Δf slopes provided a clear distinction of various cell types having different metastatic potential. Further, QCM-D had been used to detect the early morphological changes of cancerous cells entering apoptosis in response to anticancer drug exposure [154]. The analysis had been completed in less than 4 h, which was not possible with flow cytometry even at higher drug dosage. Consequently, QCM-D has the capability to discriminate different adhesion stages of the cells, various cell types,

and give fingerprints for each of them. These patterns can be employed to track the cancer progression, morphological changes during programmed cell death, and to develop cell-screening tests.

4.4 Conclusion

Being a label-free method, QCM-D monitors the cell adhesion process in real time and noninvasively, thus enables the analysis of mechanical properties at the cell–surface interface and provides very distinct corresponding profiles/ fingerprints for different interfacial features in the attachment and spreading process of the cells. QCM-D method was used to investigate the dynamic adhesion behavior of human fetal osteoblastic bone cell lines on reference gold and various model surfaces. The initial cell sedimentation on various surfaces increased the acoustic ratio, which is the indication of nonspecific cell interactions on the surface. The increase of the signals when no other cells were introduced to the system was attributed to increasing surface contact area of the already attached cells. Extracellular matrix remodeling of the cells could be tracked from the adhesion kinetics as temporary increase in the rigidity at the interfacial layer. It was seen that while passive flattening also decreases Δf and increases ΔD signals, the acoustic ratio is not significantly affected. On the other hand, for protein mediated specific interactions, higher acoustic ratios were observed due to increased contribution of the dissipative changes over frequency changes. RGD competition and trypsinization studies confirmed specific protein-mediated binding of cells to the surface. Finally, QCM-D results showed that cancerous cells interacted stronger with the hydrophilically treated surface and had higher viscoelastic characteristics than the healthy cells. The cluster of the average values was plotted to obtain fingerprints for both cell types and clear distinction of cancer cell signals from the healthy ones suggest potential use of this method in cell screening tests.

5. INTERACTION OF MAMMALIAN CELLS WITH FUNCTIONALIZED SUPPORTED LIPID BILAYERS

Functionalization of surfaces with bioactive substances (e.g. proteins) is an essential step in the development of biointerfaces for several medical applications. Commonly used substrates such as glass, tissue culture polystyrene (TCP), metals promote nonspecific passive protein adsorption; therefore non-selective protein layers are formed on their surface in contact with physiological fluids. These protein layers would be immobile and even denatured depending on the interaction strength between proteins and the surface. In this respect, non-fouling but selective functionalizability of SLBs provide specific adsorption/attachment and lateral mobility to biomolecules, in this way preserving their biological activity. This opens the possibility of designing SLBs as biomimetic platforms to study specific cell – surface interactions of interest. Moreover, employing SLBs overcome the frequently encountered difficulties with biocompatibility, adhesion properties and stiffness of designed artificial materials.

In this thesis, RGD and osteocalcin mimetic (OSN) peptides were used as model peptides for functionalization of SLBs to evaluate osteoblast cell (hfOB) interactions with different peptides. RGD peptide (Mw 346.344 g/mol) is the binding motif of various extracellular matrix (ECM) proteins (fibronectin, vitronectin, etc.) to cell adhesion molecules (such as integrin) [155]. OCN peptide (LEPRREVCELNPD; Mw 1568.8 g/mol), on the other hand, is found in the first helix of osteocalcin protein which is a non-collagenous protein and a major component of mineralized bone ECM. OCN peptide is hydrophilic and is negatively charged at pH=7.4 and it is known to promote biomineralization rather than cell attachment [156].

Cell interaction studies were carried out in real time in QCM-D in both peptide adsorbed gold surfaces and peptide-modified SLB surfaces. A parallel study was carried out using same platforms in standard cell culture environment.

5.1 Materials and Methods

Materials, sensor surface preparations, preparation of unilamellar liposomes, cell culturing, QCM-D setup for cell adhesion assay were used and performed in the same way mentioned in materials and methods sections of Chapter 3 and 4 unless otherwise stated.

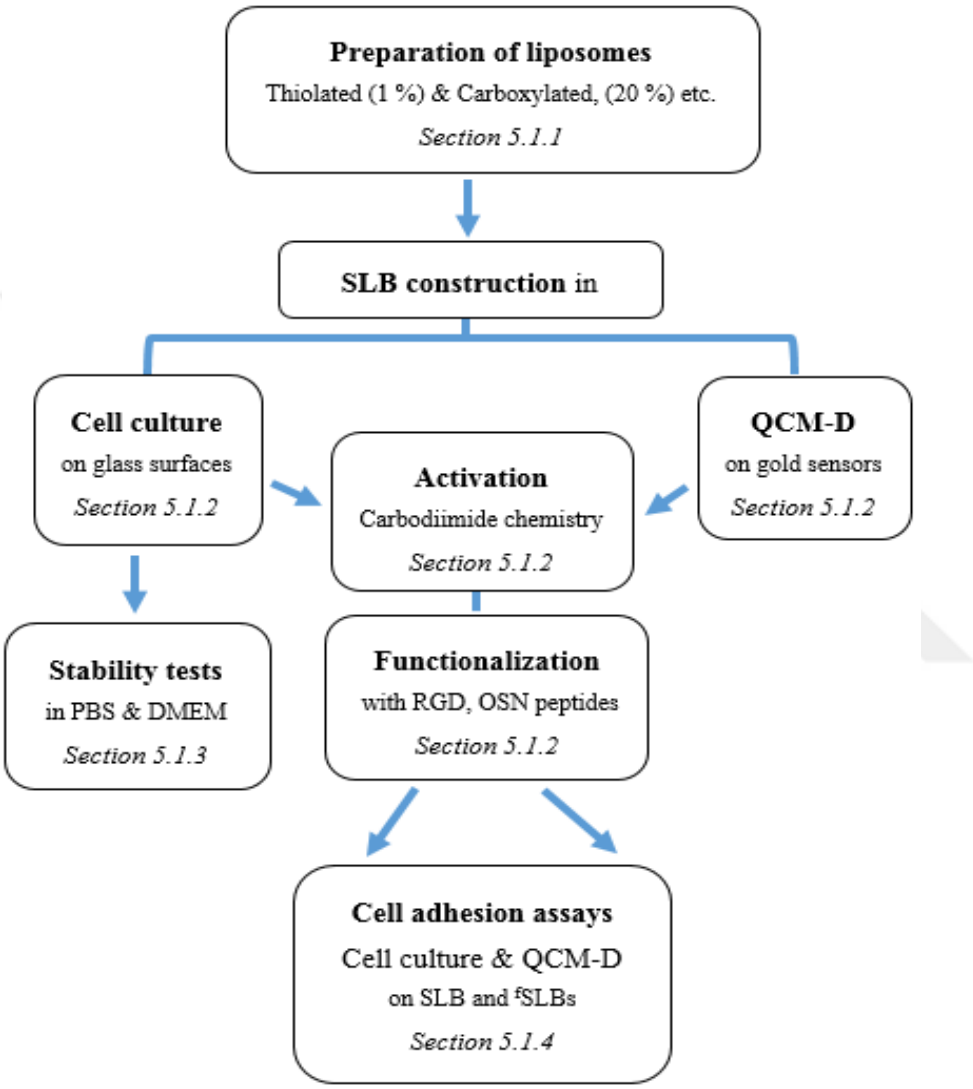

Figure 5.1 : Schematic of studies conducted during thesis.

5.1.1 Liposome production

Unilamellar PC-liposomes were prepared with the method described in Chapter 2. Differently, they were produced in *2-(N-morpholino)ethanesulfonic acid* (MES) buffer (pH = 5.5). To introduce sites for chemical modification, *1,2-dioleoyl-sn-glycero-3-phosphoethanolamine-N-(glutaryl) (sodium salt)* [18:1 Glutaryl PE] (DOPE-GA) lipids (20 % mol/mol) involving carboxylic acid groups at their headgroups, were included together with PC (Figure 5.2).

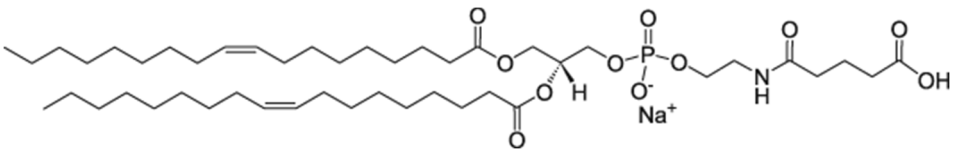

Figure 5.2 : The structure of DOPE-GA phospholipids

5.1.2 Activation and functionalization of SLBs

First SLBs were constructed in MES buffer, and then they were functionalized with either RGD or OSN peptides via carbodiimide chemistry. All events were monitored by QCM-D. Carboxyl groups (-COOH) on DOPE-GA lipids were activated in the presence of EDC/NHS (Figure 5.3). For this purpose, after bilayer formation and rinsing step, SLB was treated with mixed solution of 50 mM EDC and 50 mM NHS for 10 min in flow conditions (100 µL/min). Then, the buffer was exchanged and pH was raised to 7.4 with PBS. After the signal stabilization, peptide solutions at two different concentrations (50 and 500 µg/mL) were introduced to the activated SLB. For cell culture, glass surface was utilized for both ^{f}SLB (functionalized SLB) construction and nonspecific peptide coatings. Differently from QCM-D setup, all experimental steps, SLB construction, peptide modification (200 µg/mL for 2 hours), washing steps and cell studies, were conducted in no-flow conditions. During all subsequent step, care was taken to guarantee that the bilayer remained fully hydrated.

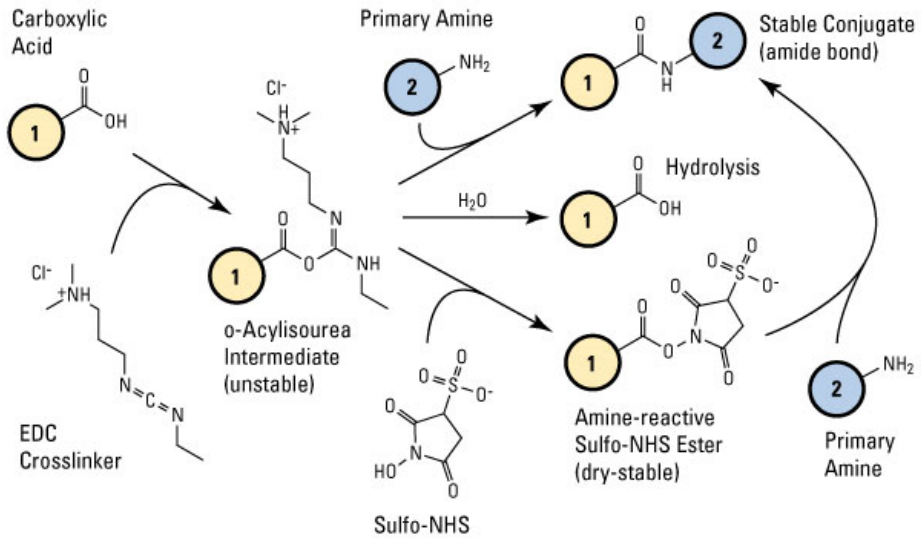

Figure 5.3 : Carboxyl-to-amine crosslinking using the carbodiimide EDC and NHS. Figure retrieved from [157].

5.1.3 Stability analysis of SLBs

The stability of phosphatidylcholine (PC) lipid bilayers on glass support in various medium conditions (PBS and DMEM supplemented with/without serum protein) were evaluated. Further, SLBs were enriched with different lipids to see their influence on stability: a negatively charged phospholipid, *phosphatidylserine* (PS, 25 %); a positively charged phospholipid, *1,2-dioleoyl-3-trimethylammonium-propane* (DOTAP, 50 %) and cholesterol (25 %). Liposomes were stained with 1 % *1,2-dioleoyl-sn-glycero-3-phosphoethanolamine-N-(lissamine rhodamine B sulfonyl) (ammonium salt)* (Liss Rhodamine PE*)* for imaging.

Before each assay, microscopic glass slides were cleaned through ultrasonication in *sodium dodecyl sulfate* (SDS) solution (2 % w/w), ethanol (70 % v/v) and MilliQ water (~18 µS), respectively. Then they were dried under stream of nitrogen. Using nail polish, a vial cap was mounted on microscopic slide to reduce the volume of vesicles required for an effective bilayer formation (Figure 5.4). Then, they were left to air dry for 30 min. The slides were exposed to UV-Ozone for 15 min to clean all remaining organic – hydrocarbon contaminations and make the surfaces more hydrophilic.

A small volume of liposome solution (100 µL) was incubated into the chambers in a darkroom. The slides were left for 1 h at 37 ºC to allow the formation of bilayers by vesicle fusion. At the end of 1 h, the chambers were rinsed with excess amount of PBS to remove all non-adhered vesicles, and aggregates. Imaging was done with an inverted fluorescence microscope using rhodamine fluorophore filter (Excitation/Emission wavelength 560nm/583nm). Series of SLB imaging was taken on different days (0 – 7).

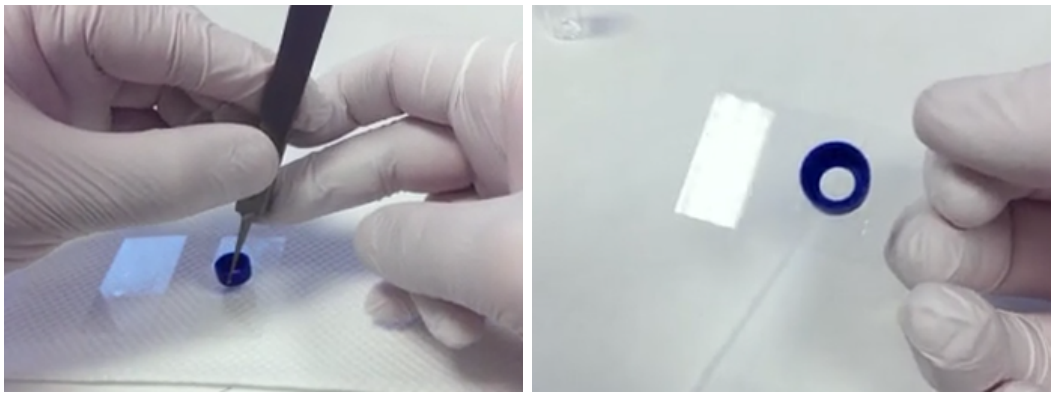

Figure 5.4 : Chamber Mounting

5.1.4 Cell adhesion assays

Cell adhesion on ^{f}SLBs were monitored via QCM-D. For cell adhesion tests in cell culture, sterile 8-well slides (Mattek) were used. After ^{f}SLBs preparations, hFOB cells seeded on surfaces at a density of 10,000 cells/cm^2 in serum-free conditions. Cell adhesion on glass surfaces with serum-supplemented medium was used as positive control. Initial cell attachment and longer-term adherence were evaluated at 4 and 18 h incubation, respectively, after rinsing non-adhered cells.

The average cell numbers for initial attachment were calculated by manually counting the cells under light microscopy from several spots. Cell morphologies and numbers for long-term incubation was evaluated using a general cell staining protocol. Cells were fixed with 4% (w/v) formaldehyde for 15 min. After washing with PBS three times, 0.5% Triton® X-100 (v/v) in PBS (15 min) was used for permeabilization. After washing with PBS three times, the cell nuclei were stained with *4',6-diamidino-2-phenylindole dihydrochloride* (DAPI; 100nM) in PBS for 15 min. Bovine serum albumin (3%, 1h) was used as blocking agent. To stain filamentous actin (F-actin), cells were incubated with Phalloidin CruzFluor™ 488 Conjugate (Excitation/Emission wavelength 493/517 nm) (Santa Cruz) for 20 min at room temperature. After washing with PBS three times, fluorescence images were captured using an inverted florescence microscope at several spots on each surface and the average number and surface area of the adhered cells were measured by ImageJ software.

5.2 Results & Discussion

5.2.1 Physical (nonspecific) adsorption of RGD and OSN peptides on gold

The signal shifts related to physical adsorption of both peptides at different concentrations onto gold surface and average surface mass densities were given in Figure 5.5 and Figure 5.6, respectively. Higher signal changes were recorded for OSN than that of RGD, which is reasonable for a higher molecular weighted peptide.

Representative D-f plot results for RGD peptides were given in Figure 5.7. At the end of physisorption of low concentration (50 µg/mL) RGD solution onto gold surface, Δf decreased and remained constant at -3.33 ± 0.58 Hz and ΔD increased and stabilized at $0.03 \pm 0.06 \times 10^{-6}$. The "hydrated" mass calculated according to Sauerbrey equation equals to $\Delta m = 59.0 \pm 10.22$ ng/cm^2. These results showed that RGD coverage at this

concentration on the surface is highly rigid due to near zero dissipation, which is expectable for a short peptide. When RGD concentration increased ten-fold (500 µg/mL), Δf stabilized at −8.18 ± 2.09 Hz and ΔD at 0.40 ± 0.14 × 10^{-6}. The total mass density equals to Δm = 144.7 ± 36.92 ng/cm^2. It can be seen that the low concentration was not sufficient to saturate the surface. RGD coverage at high concentration also showed rigid character with near zero dissipation. Slight increase in dissipation compared to low concentration coverage could be associated with the bound water within the packed peptide layer.

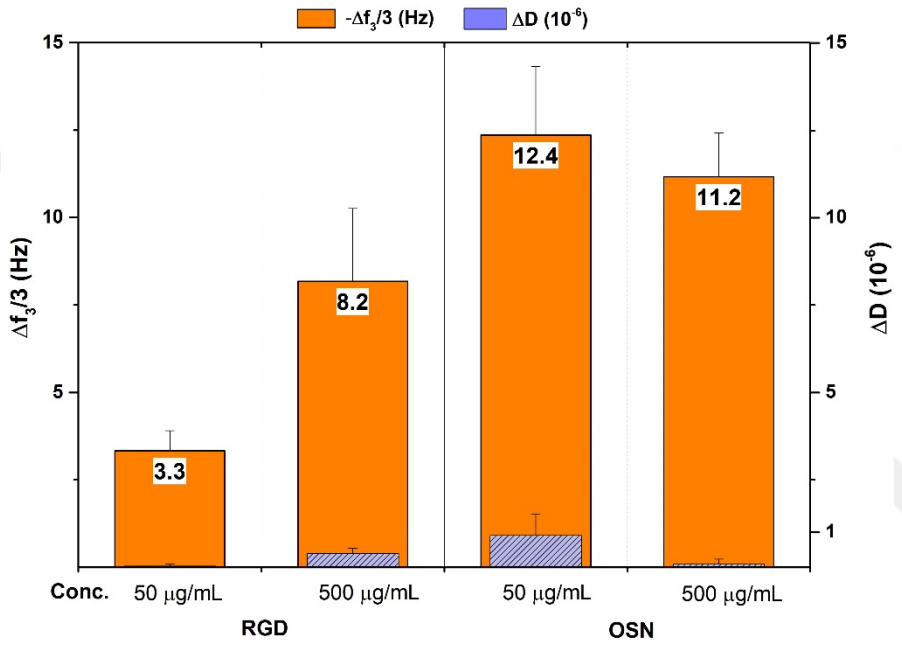

Figure 5.5 : ΔD and |Δf| values for physisorption of RGD and OSN peptides.

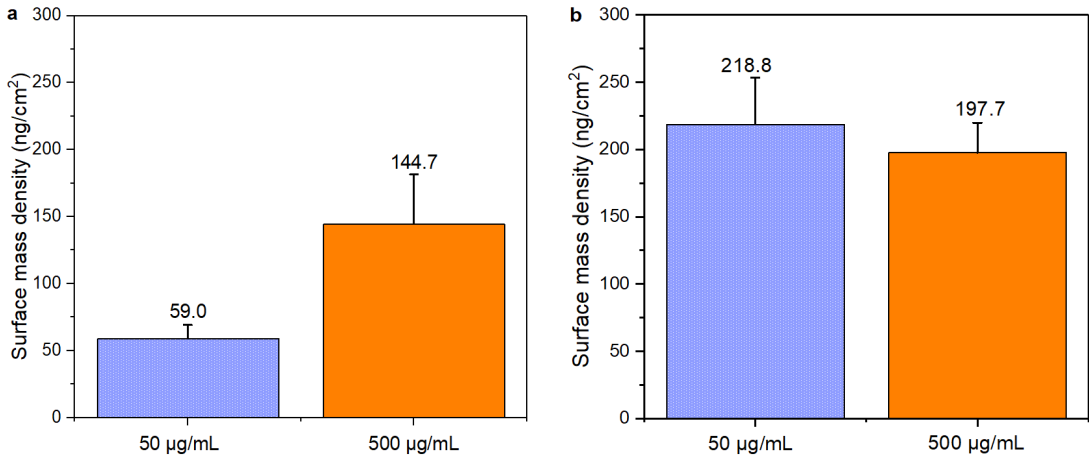

Figure 5.6 : Surface mass densities for a) RGD and b) OSN peptides used at different concentrations.

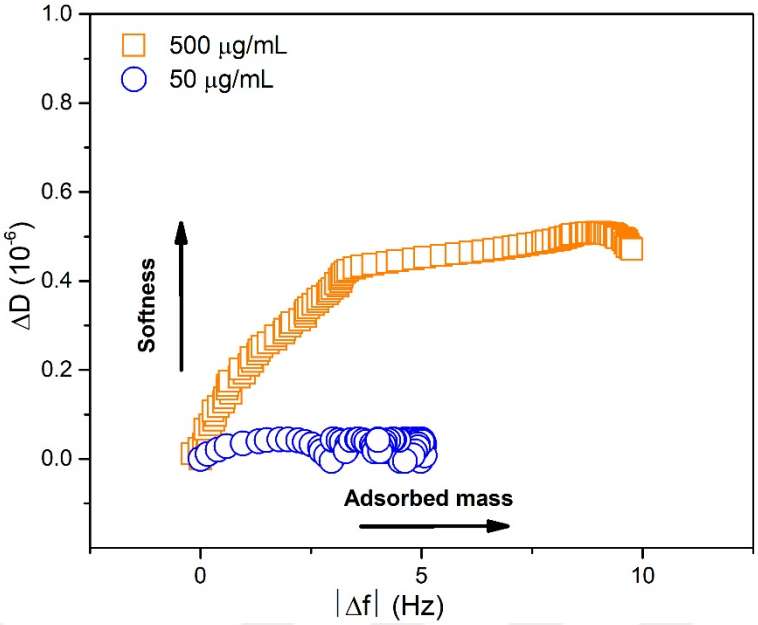

Figure 5.7 : Representative D-f plots for RGD peptides used at different concentrations.

Acoustic ratio (ΔD/Δf) is used to evaluate the viscoelasticity and structure of the adlayer. The D-f slope for high RGD concentration is higher than that of low RGD concentration, also indicating the increased amount of coupled water per adsorbed peptide. The increased amount of coupled water at high concentrations might be related to the aggregation of peptides.

Representative D-f plot results for OSN peptides were given in Figure 5.8. At the end of physisorption of low concentration (50 µg/mL) OSN solution onto gold surface, Δf was recorded as −12.36 ± 1.96 Hz and ΔD as 0.91 ± 0.61 × 10^{-6}. The "hydrated" mass calculated according to Sauerbrey equation equals to Δm = 218.77 ± 34.61 ng/cm^2. When peptide concentration increased ten-fold (500 µg/mL), Δf stabilized at −11.17 ± 1.26 Hz and ΔD at 0.08 ± 0.14 × 10^{-6} and respective total mass equals to Δm = 197.65 ± 22.27 ng/cm^2. The calculated mass is expected to be higher than that of RGD considering its higher molecular weight.

The difference between the adsorbed OSN peptide masses at different concentrations is statistically not significant so it could be said that the low concentration is sufficient to saturate the surface. In low concentration, on the other hand, slightly more viscoelastic layer was found to be obtained throughout the experiment. Both D-f plots showed two distinctive part indicating "two-step" conformational change of the molecules within the adlayer. At the first step, the dissipation/softness was increased

at both concentrations, but after a period, the dissipation noticeably approached to zero while frequency remained almost constant. It is known that the fractional trapped liquid among adsorbed molecules generally decreases with increasing coverage [116] so the decrease in dissipation is expected. This was the case also for RGD peptide (Figure 5.7), however, the decrease monitored for OSN is more pronounced. It was stated that the lateral organization and the height-to-width ratio of the adsorbed molecules affect the degree of fractional trapped liquid and its decrease rate with increasing coverage [116]. OSN is a linear (*i.e.,* high height-to-width ratio) and negatively charged peptide. Therefore, it could be suggested that at low surface coverages, OSN peptides adsorbed onto the surface in various orientations (randomly distributed on the surface) with low repulsive interactions among them. At high surface coverages, repulsive interactions increased within the adlayer and forced the peptides to laterally reorganize into a more ordered state with decreased trapped water.

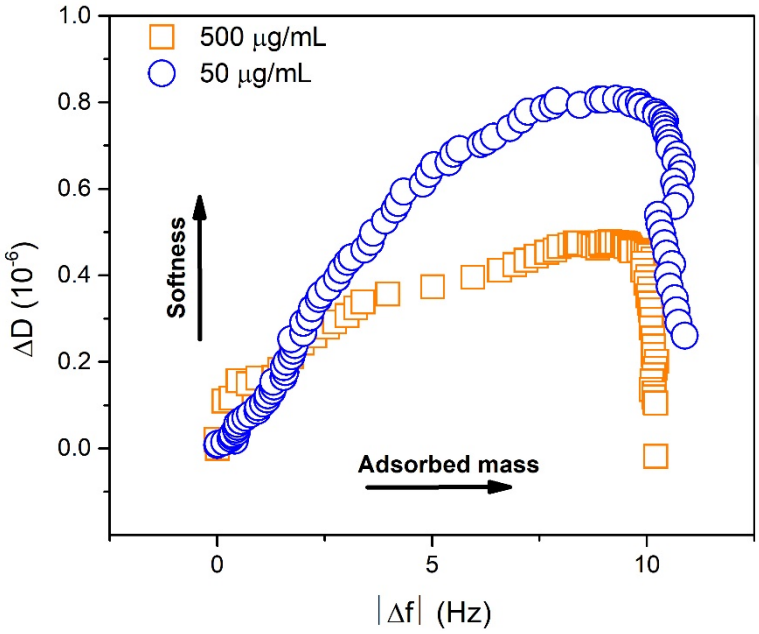

Figure 5.8 : Representative D-f plots for OSN peptides used at different concentrations.

5.2.2 Chemical attachment of RGD and OSN peptides onto SLB

Physical (nonspecific) adsorption has comparatively simple preparation steps; however, this type of passive adsorption methods of peptides/proteins do not provide a stable attachment onto the surface, because molecules might desorb in time. Moreover, there is possibility of structural changes for biomolecules in some cases, which could lead loss of function. Chemical attachment methods, on the other hand,

permanently couple molecules of interest onto the surface with improved stability. Using chemical linkers that react with certain functional groups on the molecules, reactions occur more specifically and in a controllable fashion (density of molecules can be optimized).

The signal shifts related to conjugation of both peptides to SLB were given in Figure 5.9. SLB formation, EDC/NHS activation were not shown and the values were normalized to zero. In addition, the results for both peptides at low concentrations were excluded for simplicity. Because RGD solution did not give pronounced changes at low concentrations. On the other hand, OSN solution at low concentrations gave similar values as for high concentrations (data not shown).

The quantification of peptide areal density on SLB was done according to Sauerbrey equation using QCM-D results (Figure 5.10). Since QCM-D also senses water content of adlayer, the calculated values are called as "hydrated" masses. Average adsorbed "hydrated" masses were 28.3 ± 5.3 and 104.4 ± 21.2 ng/cm^2 for RGD and OSN, respectively. For comparison, theoretical "dry" masses of peptides was additionally calculated assuming surface contact area of a phospholipid head as A_{lipid} = 70 A$^{\circ 2}$ in a bilayer, 1:1 coupling between carboxyl groups and peptides [79,81], and 100 % activation and conjugation efficiency. According to the calculations, "dry" masses equal to Δm = 16.49 and 74.70 ng/cm^2 for RGD and OSN, respectively. Since the exact "coupled water ratio" of the peptides is not known, it is not possible to determine the efficiency of the peptide conjugation via QCM-D method alone.

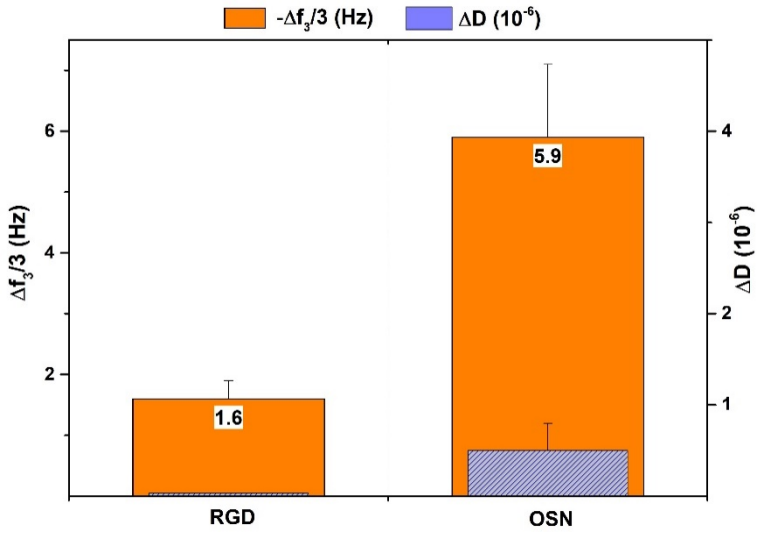

Figure 5.9 : ΔD and |Δf| values for chemical attachment of both peptides onto SLB.

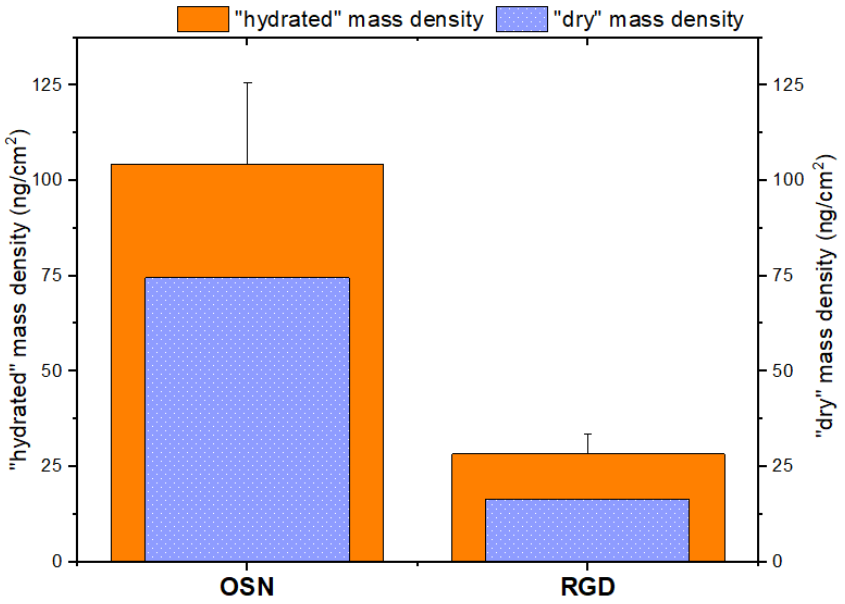

Figure 5.10 : Surface mass densities of peptides conjugated to SLB.

Comparing the mass densities for SLB (Figure 5.10) and gold (Figure 5.5) shows that more peptides adsorbed to gold compared to SLB. The frequency shift for passive RGD adsorption is nearly fivefold, and for OSN is nearly twofold higher. The peptides adsorb to gold surface nonspecifically, on the other hand, zwitterionic SLB surfaces prevent protein adsorption. Because of that non-fouling characteristic, peptides conjugate to SLB surface only via DOPE-GA phospholipids, which involve activated carboxylic acid groups at their headgroups and therefore, limited number of peptides could be linked to the SLB.

The amount of trapped water per adsorbed peptide, which could be tracked from D-f slope (or acoustic ratio), depends on the structure of the adlayer. Increased water content/softness is correlated with increased flexibility [158], i.e., higher acoustic ratio. Thus, to predict the structural differences of peptide adlayers, D-f slopes belonging to OSN peptide adsorption kinetics on both SLB and gold were compared (Figure 5.11). However, D-f slope for RGD peptide on SLB gave near zero values so this comparison could not be made for RGD. Acoustic ratio is higher for OSN peptide conjugated onto SLB indicating a higher structural flexibility and/or water content, which might lead orientation and more ordered state of the peptides on a mobile SLB surface. On the contrary, in passive adsorption OSN peptides were immobilized in a nonoriented, disordered state onto the gold surface and this reduces the flexibility of the adlayer.

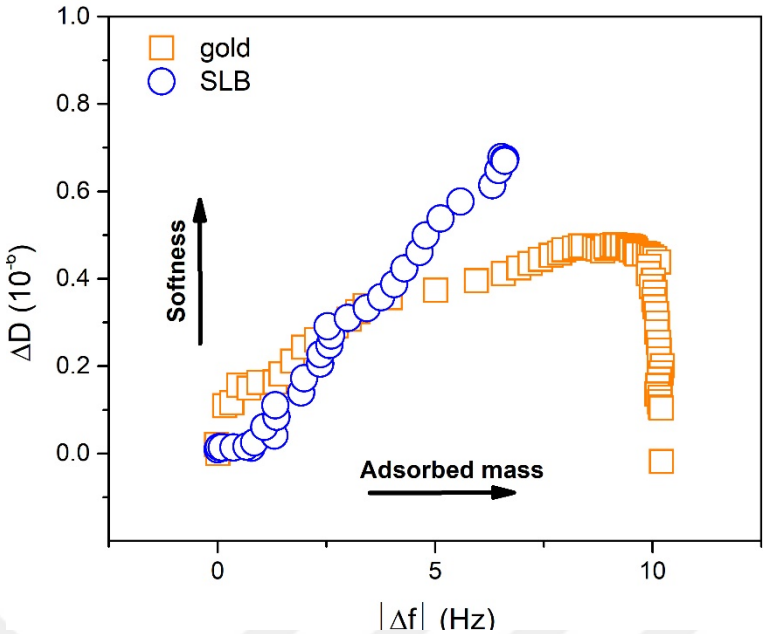

Figure 5.11 : Dissipation–frequency curves upon OSN adsorption onto the SLB and gold surface.

5.2.3 Cell Adhesion on Peptide Coatings

After the examination of peptide attachment on gold and SLB surfaces, cell adhesion on the same surfaces were monitored via QCM-D. Acoustic ratio, -Δf and ΔD values concerning cell adhesion on peptide coatings at the end of 1 and 18 hours were graphed in Figure 5.12. Cell adhesion on UV-ozone treated (hydrophilic) bare gold sensor was also included for better comparison.

As it was discussed in Chapter-3, frequency and dissipation changes are signs of attached cell number for the initial step (within the first hour) and change in surface contact area for longer times. Moreover, the change in dissipation per frequency change, i.e. acoustic ratio is correlated with integrin-mediated specific interactions, focal adhesion maturation and associated cytoskeletal changes [93]. At the end of first hour, cell number seemed to be slightly more on bare gold surface (though statistically insignificant) than low-density protein coatings. On the other hand, the difference with high-density coatings is significant. High-density peptide coatings on gold obviously reduced the attached cell number, which could be related to the need for a critical spacing between peptides. The need for critical density for selective cell adhesion has been previously described for RGD peptides, while higher densities was found to be not optimal [159-160]. It is noteworthy that, while acoustic ratios are similar for gold and OSN-coated surfaces, acoustic ratio and ΔD are significantly higher for RGD-

coated ones. RGD is binding motif of various ECM proteins to integrins so led to rapid establishment of specific interactions. OSN, on the other hand, is a peptide motif known to promote biomineralization, not cell adhesion, so this difference between to peptides is expected.

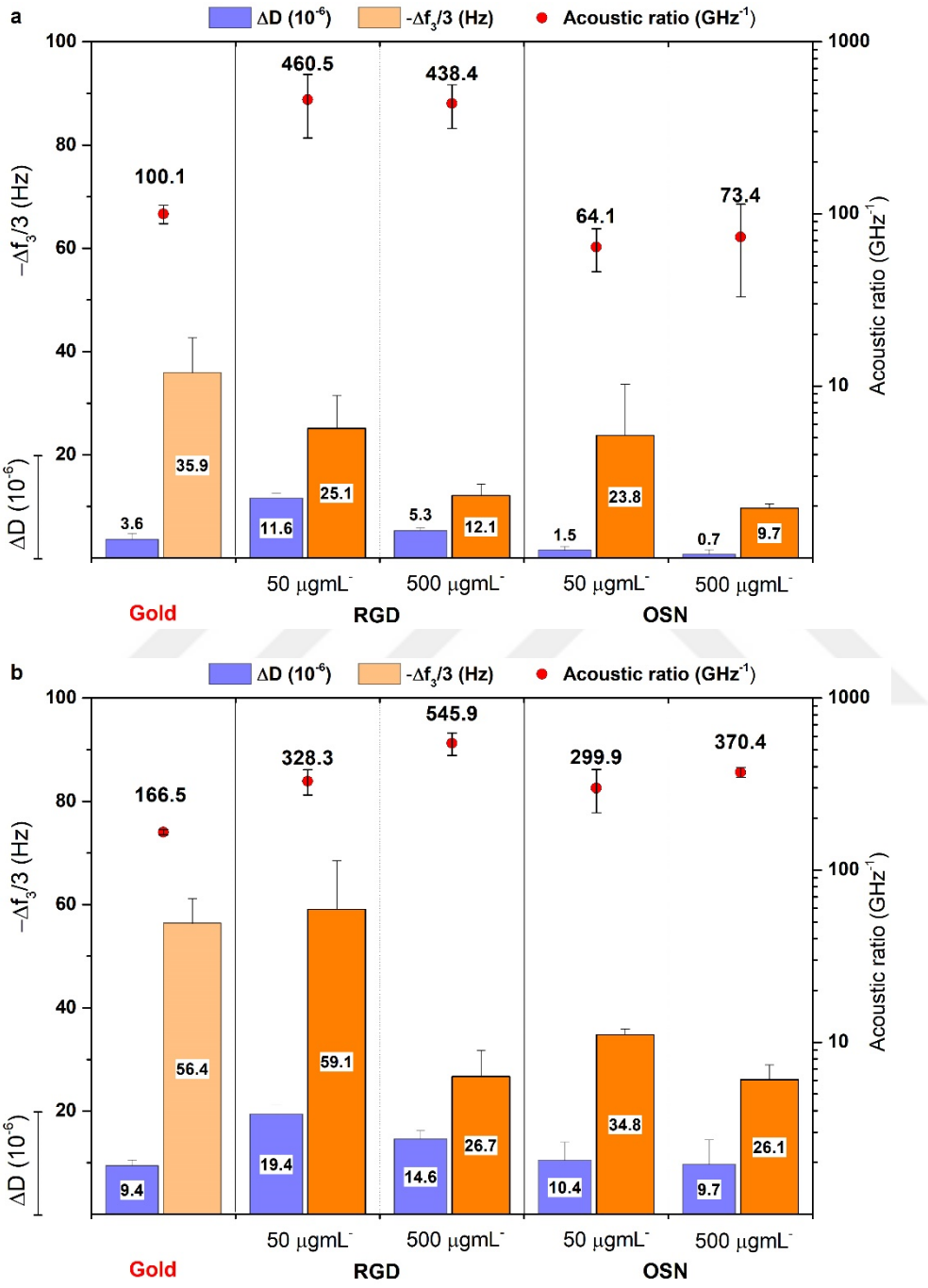

Figure 5.12 : -Δf, ΔD and acoustic ratio values at the end of a) 1 and b) 18 h for peptide coated and uncoated gold surfaces.

ΔD and -Δf values increased at the end of 18 h for all surfaces suggesting an increase in cell surface contact area (Figure 5.12b). The increase in acoustic ratios indicated

that spreading involves the aid of protein-mediated specific interactions. The acoustic ratio for RGD-coated surfaces remained high and the values did not change significantly compared to 1 h results. This observation can be interpreted as the early focal adhesion maturation (within 1 hour) of cells on RGD-coated surfaces. On the other hand, smaller frequency changes (*i.e.,* limited cell spread) was observed on OSN-coated surface, though acoustic ratios increased notably (*ca.* 5 fold). OSN peptide does not promote cell adhesion as mentioned; however, owing hydrophilic nature and net negative charge could provide electrostatic interactions between OSN-coating and biomolecules on the cell membrane, thus promoting nonspecific protein and cell attachment, which might have led increase in acoustic ratio.

5.2.4 Cell Adhesion on Functionalized SLB Surfaces

Acoustic ratio, -Δf and ΔD values for cell adhesion on ^{f}SLB surfaces at the end of 1 and 18 hours were graphed in Figure 5.13. Cells cannot adhere to pure *phosphatidylcholine* (PC) SLBs since it is cell resistant because of some factors such as surface electrostatics, surface hydration, and lateral mobility of the lipid molecules [9]. When cell adhesion was monitored on pure PC supported lipid layer, no attached cells were detected. A few weakly attached cells onto the layer were washed rapidly from the surface. SLBs modified with low concentration of RGD peptide solution did not give pronounced changes as well, so these results were excluded. Although frequency and dissipation changes were observed, the results for OSN at low concentrations were also not involved for meaningful comparison at the same concentration usages.

Cell adhesion was detected on both RGD and OSN-^{f}SLB surfaces contrary to control SLB surface. While attached cell numbers are similar (~Δf), dissipation change and acoustic ratios are higher at the end of 1 h for RGD-^{f}SLB compared to OSN-^{f}SLB demonstrating that cells immediately started protein-mediated specific interactions on RGD-^{f}SLB. Cells increased their surface contact area until the end of 18 h (higher Δf), but the change is more significant on RGD-^{f}SLB. Notable acoustic ratio increase was also monitored on OSN-^{f}SLB surface due to promoted nonspecific protein and cell attachment.

When Figure 5.12 and 5.13 are compared, it is obvious that more cells adsorbed to peptide-coated gold surfaces than to ^{f}SLB. This is probably the result of limited

number of peptides conjugated to the SLB as discussed before. The amount of peptide on gold and SLB are different, so to compare the results for different surfaces, the acoustic ratios were divided by peptide mass to normalize the results (Figure 5.14).

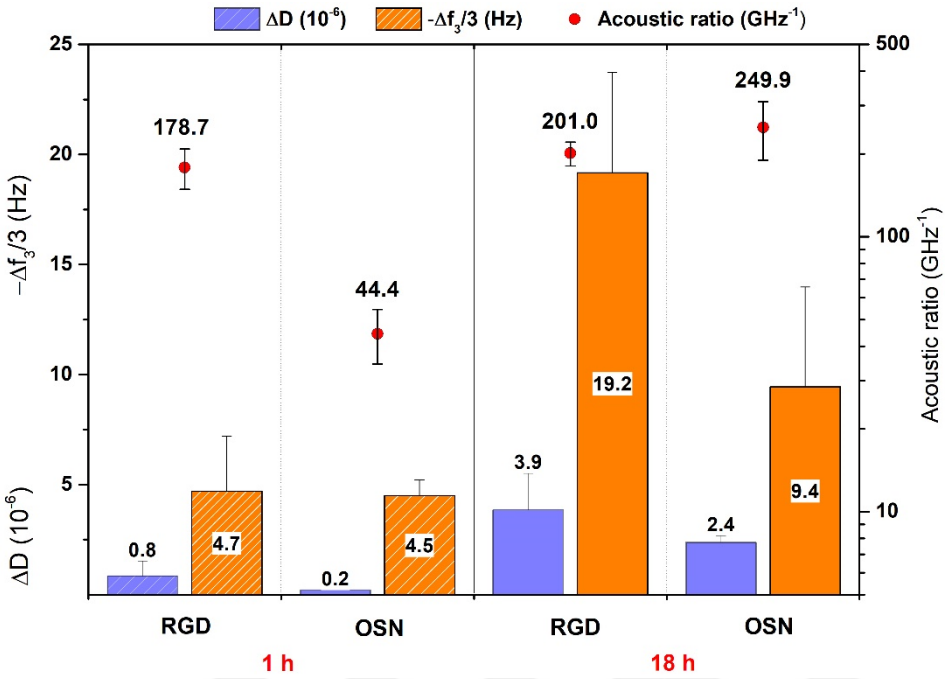

Figure 5.13 : -Δf, ΔD and acoustic ratio values for cell adhesion on ^{f}SLB surfaces at the end of 1 and 18 h.

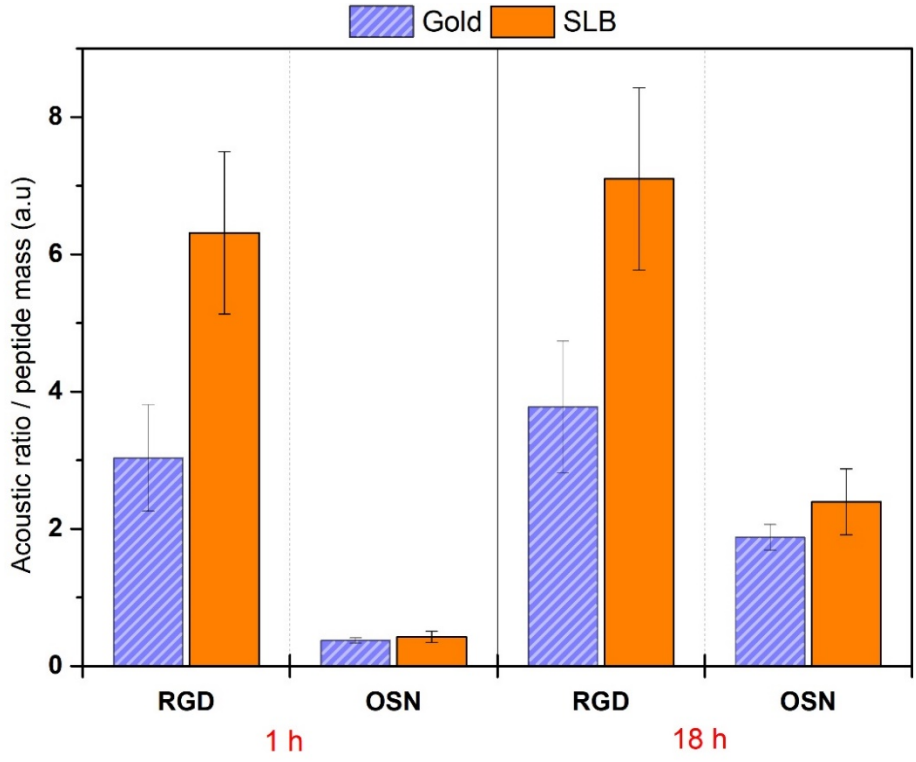

Figure 5.14 : Normalized comparison of cell-surface interactions measured on nonspecific coatings on gold and ^{f}SLB surfaces.

When normalized results were compared, acoustic ratios were higher for SLB compared to that of gold at each time point for both peptides. These results further verify that low density of mobile peptides on SLB platforms preserve their biological activity and promote cell adhesion more efficiently than high number of immobile peptides on gold surfaces. The difference at the normalized values between SLB and gold surfaces is significant for RGD peptide, but not for OSN. But, not to forget that OSN peptide showed higher structural flexibility on SLB (Figure 5.11). Conclusively, passive adsorption of peptides resulted in a non-oriented layer on the gold surface. Even the amount is higher, substantial ratio of peptides could become inaccessible to the cells, even denatured and their biological activities are reduced. Biomimetic microenvironment of SLB, on the other hand, provides mobility and consequently allow lateral rearrangement of peptides by cells. Moreover, higher percentages of peptides remain active and accessible.

5.2.5 Application of ^{f}SLBs to cell culture

Cell interactions with ^{f}SLBs were also observed in cell culture environment. A typical PC lipid bilayer formed on glass by vesicle fusion was seen in Figure 5.15a. The effect of partial dehydration to SLB was presented in Figure 5.15b. In this part, the stability of SLBs was tested since it is essential to predict their utility as cell culture platforms. To check the fluidity of the prepared SLB, fluorescence recovery after photobleaching (FRAP) measurements were performed and the diffusion coefficient was calculated.

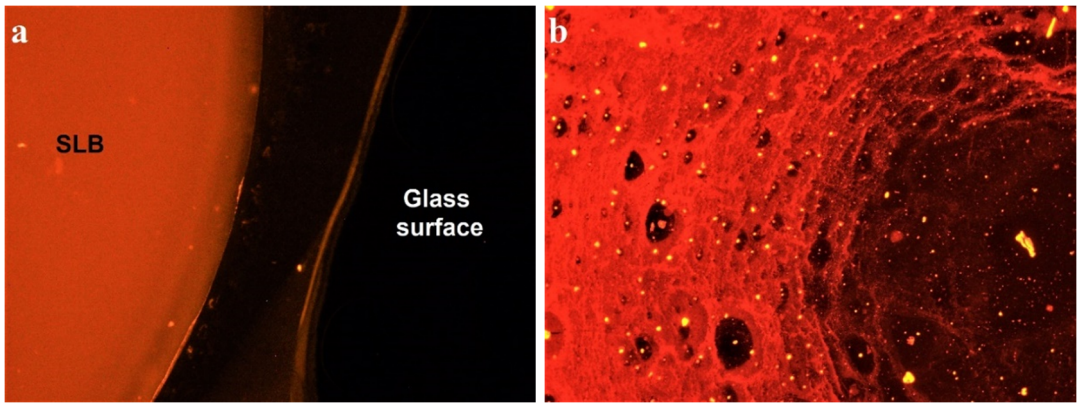

Figure 5.15 : a) Fluorescent image of SLB. The uniform fluorescence shows the presence of continuous and uniform layer b) the destructive effect of dehydration on SLB. Lipid aggregates are seen as bright dots.

5.2.6 Stability of the SLB

Long-term stability of SLBs are often desirable to utilize them for several applications such as cell culture platforms. Fluorescence techniques can be used to investigate the structural integrity of lipid bilayers on glass support in PBS and DMEM supplemented with/without serum protein.

The structural changes of PC lipid bilayers at 37 ºC in PBS over a week can be seen in Figure 5.16. The structural integrity was conserved until fifth day, and there was no aggregate or hole formation on the bilayer until seventh day. After fifth days, there were just local scratches, nubs and protrusions with irregular shapes in the sample indicating the stretching of SLB. This could be attributed to destabilization in the lipid bilayer with time due to heterogeneous diffusion of lipid molecules because of irregular cracks on glass surface. It is known that lipid molecules have tendency to move places where the lipid-surface interaction is stronger [161]. Deep and irregular cracks on glass surface may act as diffusion barriers of lipid lateral motion. Research on surface topography showed that lipid bilayer formation in the presence of curvature between 1.2 – 22 nm, yields loss of integrity and leads to pore formation and scratches through the curvature that enlarged in time [41].

When PC lipid bilayers were stored at 37 ºC under serum-supplemented medium, holes started to be formed beginning from the first day and their number and size increased rapidly in time (Figure 5.17). At the end of 7^{th} day, most of the bilayer was disrupted. These results showed the accelerated bilayer destruction in the presence of proteins. When the experiments were repeated in serum-free medium conditions as a control, disruption was lowered but still occurred beginning from the first day because of other probable factors in medium (data not shown).

To examine the effect of different lipid compositions on the stability, SLBs made up with PC:Cholesterol (4:1), PC: PS (4:1) and PC: DOTAP (1:1) were produced and incubated with serum containing media (Figure 5.18). Generally, all of the lipid types increased the stability of SLB to pure PC bilayer. Sterol molecules supply stiffness beside fluidity. It could be commented that cholesterol content provided increased rigidity to the membrane, caused higher stability, therefore reduced and delayed the destructive effects on lipid layer (Figure 5.18a).

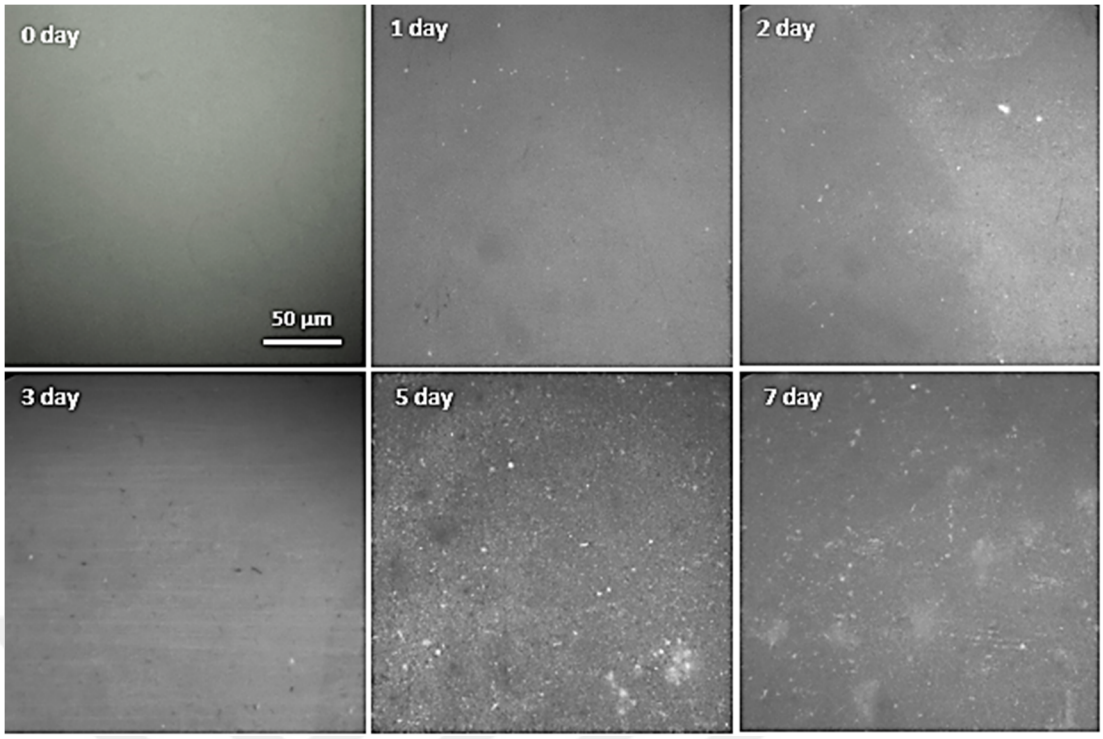

Figure 5.16 : Images of SLB on 0-7 days kept at 37ºC under PBS conditions.

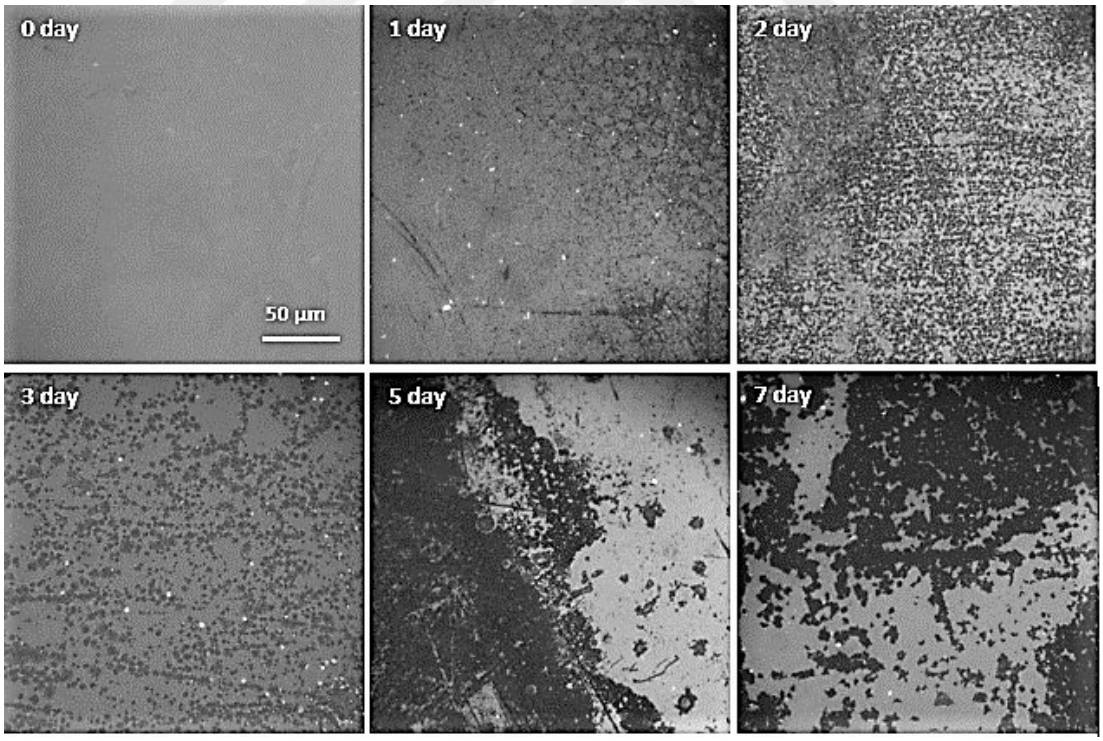

Figure 5.17 : Images of SLB kept at 37ºC under 10 % serum supplemented DMEM conditions.

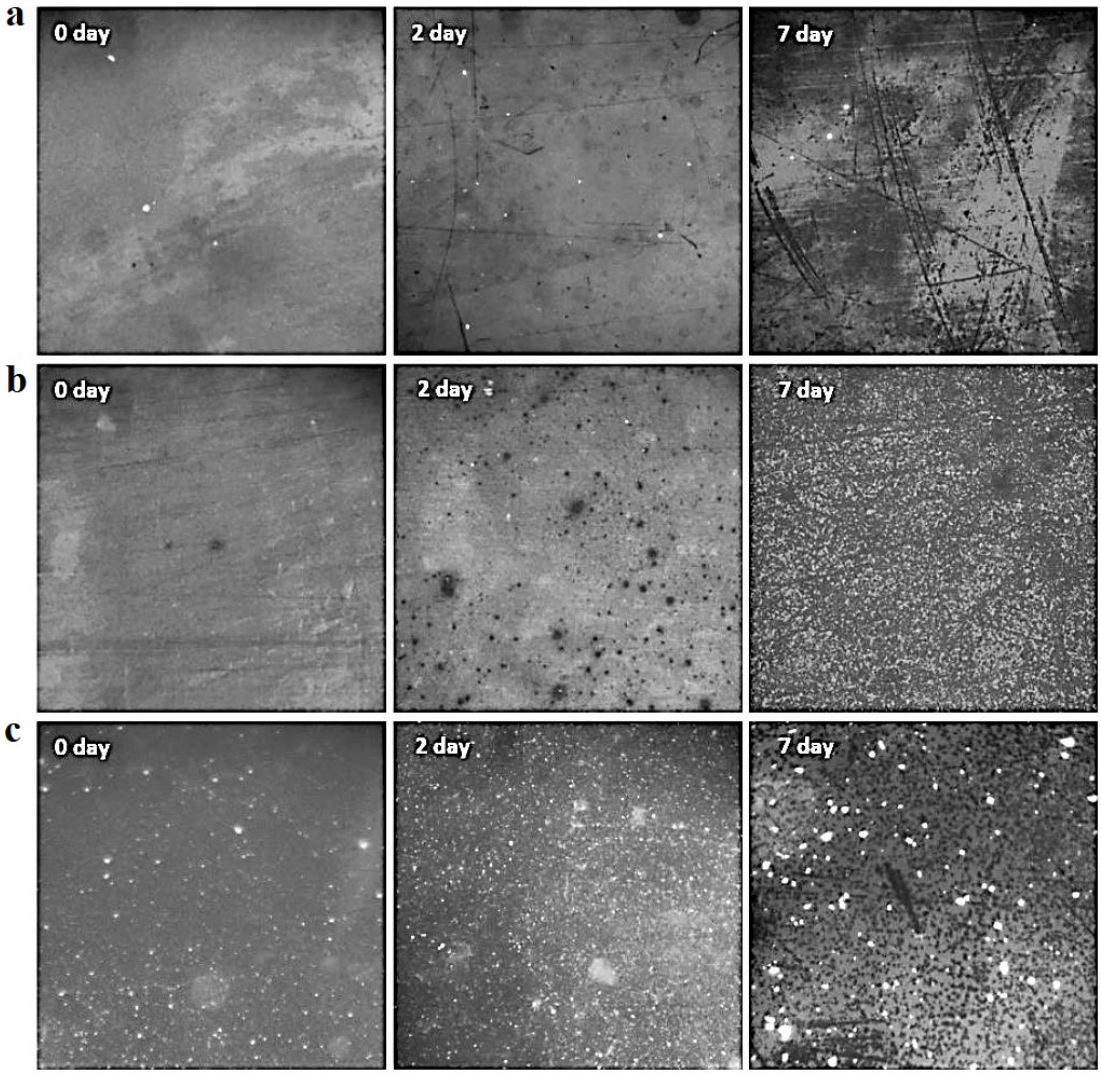

Figure 5.18 : Images of SLB made up with a) PC:Cholesterol (4:1), b) PC: PS (4:1) and c) PC: DOTAP (1:1) kept in cell culture medium with 10 % FBS at 37°C.

Positively charged bilayer structures also showed increased stability (Figure 5.18c). Charged lipids increase surface charge density of bilayers. Hence, the increased electrostatic attractive forces between the glass and headgroups of the lipids on the SLB surfaces decreased mobility of bilayer. The decreased mobility also decreases the interactions within the medium and provides incremented integrity to the bilayer [162]. Alternatively, the influence could be result of the denser packaging of phospholipids due to electrostatic interactions between biomolecules. Each effects might play role at the same time. When positively charged PC:DOTAP composition (1:1) compared with other results, it is seen that dense luminescent spots existed from the beginning probably as a result of lipid aggregation. Using high amount of positively charged DOTAP molecules within the liposomes may have caused some unstable reorganizations and hence these aggregations.

Negatively charged PS bilayers did not show high stability (Figure 5.18b). Negatively charged glass surface chemistry readily allows formation of bilayer composition but strong repulsive forces between the surface and negatively charged bilayer probably prevent to maintain the integrity of the bilayer for longer periods and increased the deformation. Despite this, it seems that PS involvement increased the stability to pure PC layer.

5.2.7 Fluidity of SLB

The lateral mobility of the lipid layer is significant for proper functions and dynamics of the membrane components. Model membrane systems must maintain the fluidity, i.e. lateral mobility of the lipid bilayer, to mimic the natural membrane. Fluorescence recovery after photobleaching (FRAP) is one of the most common techniques used for this purpose and it is based on the determination of the diffusion of fluorescently labeled lipids or proteins in supported bilayers. In this technique, the intense light/laser is focused onto a small field of the bilayer to bleach labeled molecules, then recovery of fluorescence due to Brownian motion in the bleached area caused by lateral diffusion is monitored over time. Finally, mobile and immobile fraction are obtained and the diffusion coefficient is calculated from the measurements.

For that purpose, the intense light was focused through a 40-x objective on the bilayer. A region of interest (ROI) around 0.5 mm diameter was bleached for 1 min, and then the field was monitored using a 5-x objective. Images were taken at 5 min intervals to monitor the recovery process (Figure 5.19-right). Fluorescent profiles at each time point were double normalized using equation 5.1:

$$I_{norm}\ (t) = \frac{I_{ref\_pre}}{I_{ref}\ (t)} \cdot \frac{I_{frap}\ (t)}{I_{frap\_pre}} \qquad (5.1)$$

Where I_{norm} (t) is normalized intensity; I_{frap} (t) is measured average intensity inside the bleached spot; I_{ref} (t) is measured average reference intensity; “pre” subscript is the mean intensity in the corresponding ROI before bleach moment. After double normalization, FRAP data was scaled between 0 to 1 (Figure 5.19-left).

Normalized data was then transferred to FRAP Analyzer software [163] for modelling and fitting FRAP experiments. “Diffusion circular spot” was selected as the diffusion model. The diffusion coefficient calculated by the fitting procedure was found as 1.16

± 0.19 $\mu m^2/s$, which is close to the data found in literature (1 $\mu m^2/s$ [164]). Complete recovery was not observed for the time scale of the experiment (30 min). The time required for complete recovery is calculated as 7.4 h using the equation 5.2:

$$D = r^2/4\tau \quad (5.2)$$

where D is the diffusion coefficient, r is the radius of the bleached ROI and τ is half recovery time of average fluorescent intensity.

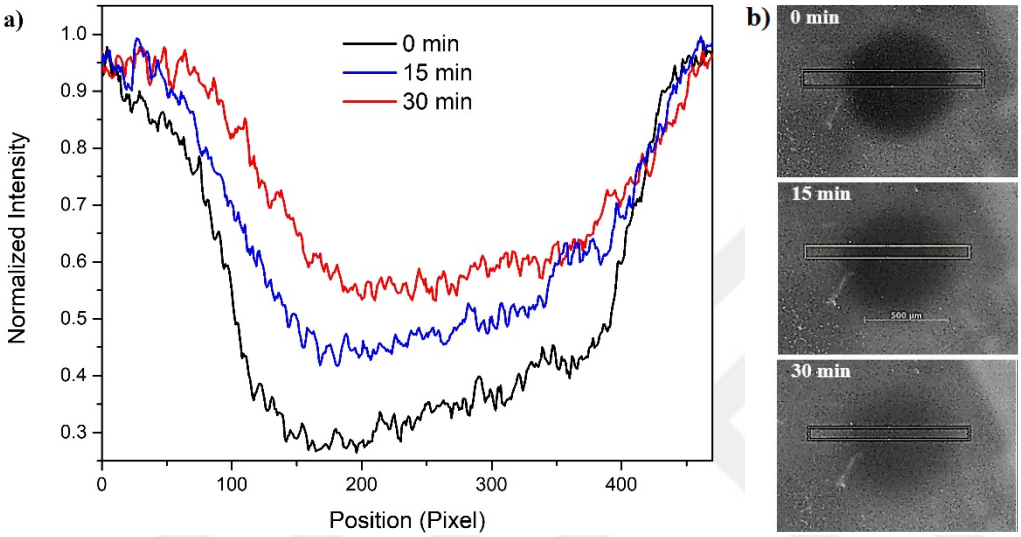

Figure 5.19 : a) Graph shows the normalized intensity and b) recovery of a bleached spot (~ 500-µm diameter) during 30 min.

5.2.8 Cell attachment on ^{f}SLB surfaces in cell culture environment

5.2.8.1 Initial (4 h) cell attachment

Initial cell attachment on RGD and OSN- ^{f}SLBs were observed at the end of 4 h incubation. Nonfunctional SLB and bare glass surfaces were used as control negative and positive controls, respectively. Cells seeded onto all surfaces at a density of 100 cells/mm^2 in serum-free conditions. This time point was thought to be sufficient for cells to adhere since endogenous matrix proteins are secreted by cells to mediate cell-surface interactions [79]. The medium itself did not contain serum, so ECM proteins solely come from the cells as in QCM-D experiments. After 4 h incubation, wells were carefully washed to remove non-adhered cells and adhered cell numbers were determined (Figure 5.20).

The number of cells attached onto SLB was significantly lower when compared to functionalized surfaces and control glass surface. That result also confirms the protein

and cell-resistant feature of zwitterionic PC SLBs. OSN- and RGD-^{f}SLBs showed similar cell densities. Even though OSN does not contain cell attachment motifs, it seemed to support to initial cell attachment but the nature of cell-surface interaction is uncertain from microscopic images. A correlation could be seen when the cell numbers were compared to 1 h - Δf changes of QCM-D results for both functionalized surfaces in Figure 5.13, reminding that frequency changes are signs of attached cell number for the initial attachment step (within the first hour). It could be deduced that the cell densities on both functionalized surfaces are similar within the sensing depth of QCM-D (~250 nm). It is known that the minimum distance between the surface and ventral cell membrane during initial cell attachment is 50 nm, and that proximity decreases to 10–20 nm afterward through integrin receptors binding to surface [137]. Since the acoustic ratio calculated for RGD-^{f}SLB were significantly higher, it could be suggested that even the cell densities were similar, the cells were in close contact with RGD-^{f}SLB surface and integrin-mediated specific interactions have already begun. Apparently, this was not the case for OSN-^{f}SLB and probably the reason for the cell attachment is related mainly to nonspecific interactions such as electrostatic interactions.

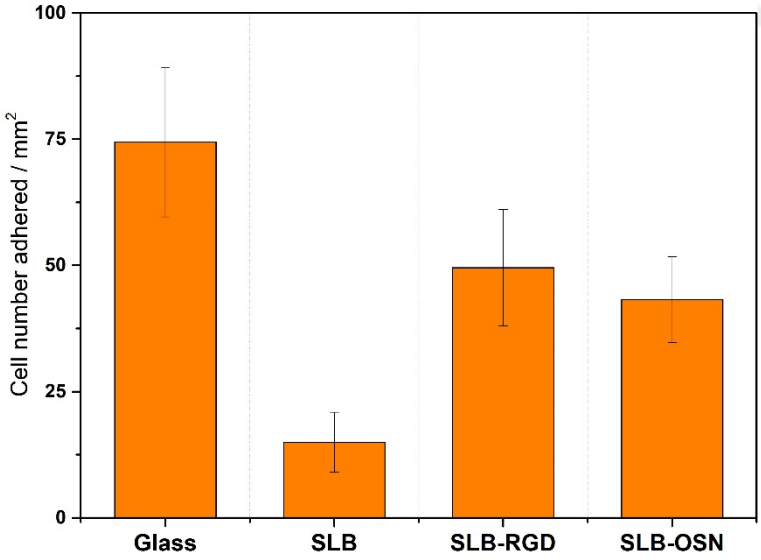

Figure 5.20 : Initial cell attachment on surfaces after 4 h incubation.

5.2.8.2 Long-term (18 h) cell attachment

In order to determine long-term adherence in parallel to QCM-D assays, cells were seeded on peptide-coated glass and ^{f}SLB surfaces at a density of 100 cells/mm^2 in serum-free conditions for 18 h. Cells on SLB were cultured in serum-supplemented

medium in a separate experiment in order to see the effect of serum proteins. Figure 5.21 (see also Figures in Appendix C) demonstrates the fluorescence images of cells attached to each surfaces after 18 h. The number and the area of adhered cells were quantified and shown in Figure 5.22 and Figure 5.23, respectively.

Limited number of cells attached on SLB and remained in rounded morphology and did not spread (Figure 21b). On the other hand, cells attached and spread well on RGD-^{f}SLB surfaces (Figure 21d). Quantitative analysis showed that there are 11.3 times higher mean cell density (~60 cells/mm^2) and 2.3 times larger mean cell surface area (~868 μm^2) on RGD-^{f}SLB surfaces than those on SLB surfaces.

The influence of RGD is obvious when cells adhered on RGD-coated glass surface (Figure 5.21c) compared to control glass surfaces (Figure 5.21a). As seen in quantitative results, cell number and cell surface area are significantly higher on RGD-coated glass surface. Mean cell density increased 1.2 times and mean cell surface area increased 1.7 times.

Cell number adhered to RGD-coated glass controls was slightly higher (~65 cells/mm^2) than that of RGD-^{f}SLB, but mean cell surface area (~1200 μm^2) was significantly larger. This difference in the area could be the consequence of fluidity of peptides on SLB, which are more prone to rearrangement when cells exerted forces on the surface. However, nonspecifically adsorbed peptides on glass are immobile and they are resistant to displacement. Since the amount of peptide coverage on glass was not known, normalization of the data could not be done to compare the cell adhesion on RGD-coated glass and RGD-^{f}SLB surfaces.

The cell number and spread area on OSN-^{f}SLB (Figure 5.21e) surfaces are significantly lower than that on RGD-^{f}SLB (Figure 5.21c). Since cells did not spread well on both OSN coated-glass and ^{f}SLB, it can be said that the higher acoustic ratios calculated for OSN in QCM-D runs contain minimal contribution from the spread of the cells. As discussed before, the increase in acoustic ratio for OSN coated surfaces might come from secreted endogenous ECM proteins of cells retained on surface nonspecifically with the aid of net negative charge of OSN peptide layer.

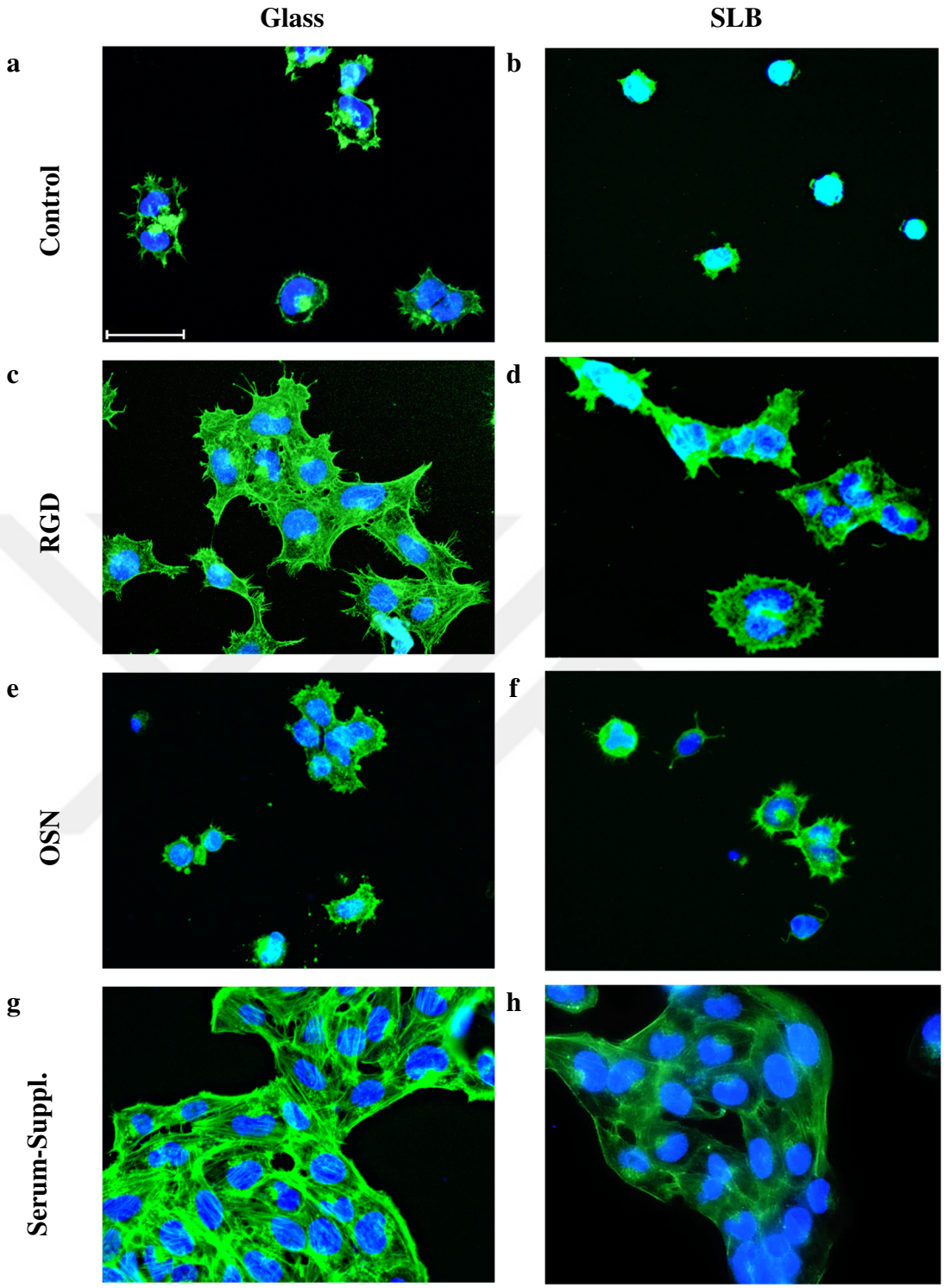

Figure 5.21 : Fluorescence images of cell morphologies attached on various surfaces after 18 h incubation; on a) control glass surface without any peptide coating, b) PC SLB c) RGD-coated glass, d) RGD-^{f}SLB, e) OSN-coated glass, f) OSN-^{f}SLB in serum-free conditions. Cell attachment was also checked in serum-supplemented medium on g) glass and h) SLB surfaces. Scale bar: 50 µm.

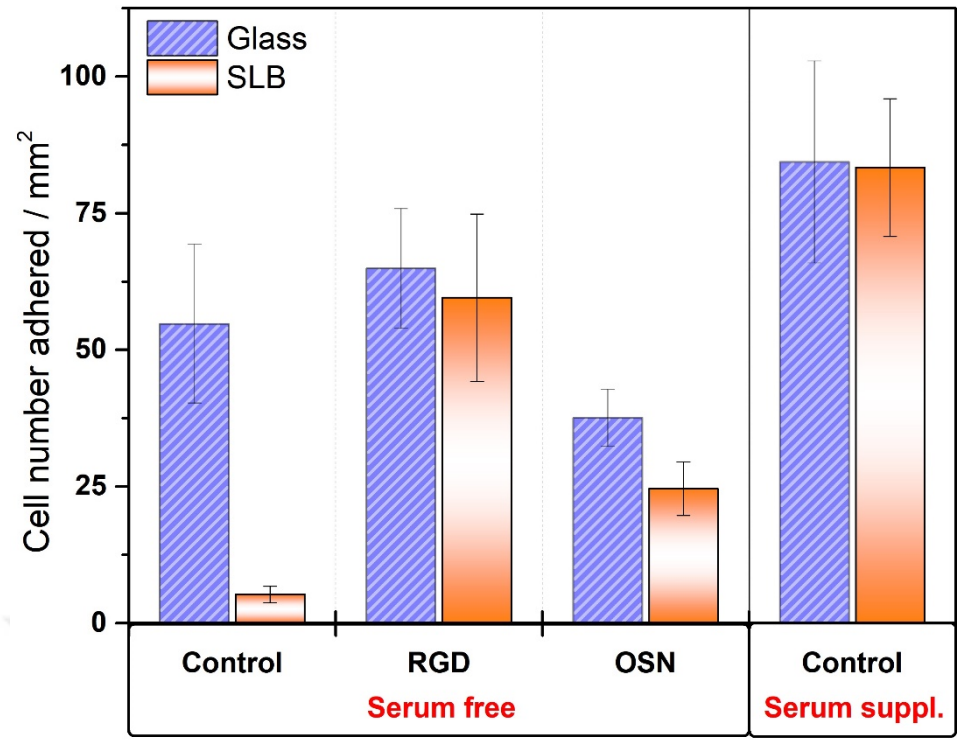

Figure 5.22 : Mean cell number on each surfaces after 18 h attachment.

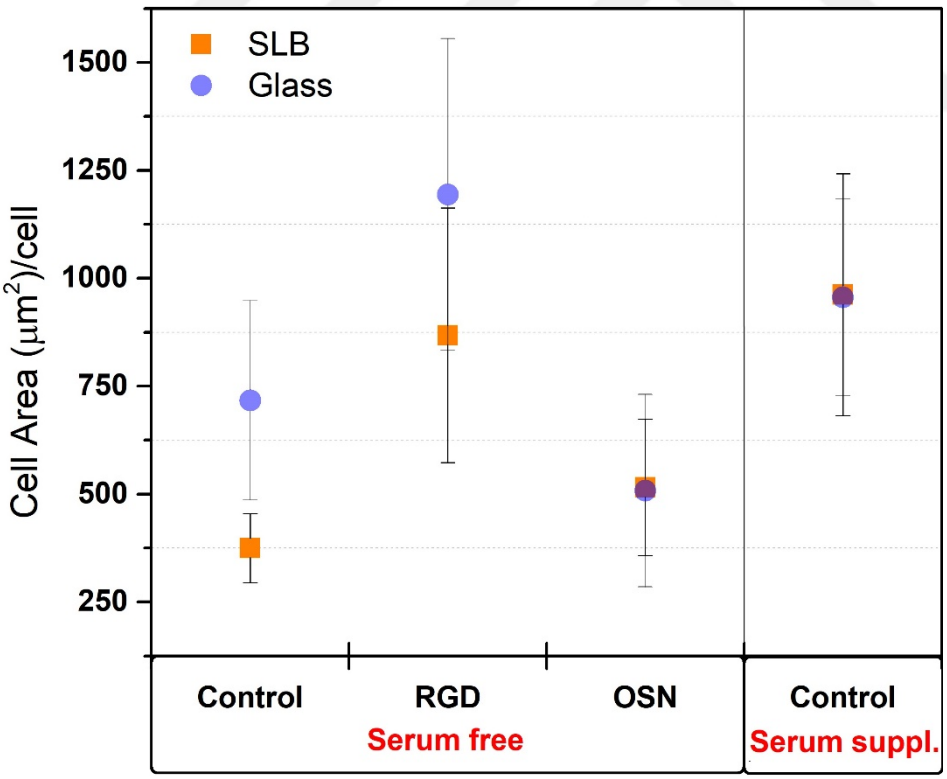

Figure 5.23 : Cell area on each surfaces after 18 h attachment.

Similar cell number and cell attachment were also observed on serum-supplemented glass (Figure 5.21g) and SLB (Figure 5.21h) surfaces. QCM-D studies had showed no

protein adsorption and cell attachment on SLB surfaces even in serum-supplemented medium (not shown). However, these experiments had been conducted in flow conditions. In cell culture counterparts, serum-supplemented medium was directly incubated (no-flow conditions) onto the surfaces. Serum proteins probably composed a thick layer on SLB surface and decreased the mobility of SLB, hence facilitated the cell attachment. Average cell spread area in serum-supplemented conditions is less than that found for RGD-coated glass and closer to RGD-^{f}SLB surfaces. However, the cell number is higher than both surfaces demonstrating that cells undergo proliferation in serum-supplemented conditions.

5.3 Conclusion

RGD and OSN peptides were used as model peptides for functionalization of SLBs to evaluate osteoblast cell-surface interactions via QCM-D monitoring. First, the stability of SLB in various medium conditions were evaluated. The structural integrity was conserved until fifth day in PBS, but hole formations started to form from the first day. When SLBs were enriched with different lipids (cholesterol, PS, DOTAP), all of the lipid compositions increased the stability of SLB to pure PC bilayer. Lateral mobility of the lipid bilayer was also demonstrated via FRAP method.

The kinetics of peptide attachment to SLBs were compared to their nonspecific adsorption onto gold surfaces and the behavior of resultant layers were analyzed via QCM-D. The results indicated that conjugation to SLB provide higher structural flexibility than passive adsorption. Then, cell-surface interaction studies were carried out in real time. Low density of mobile RGD peptides on SLB platforms preserved their biological activity and promoted cell adhesion more efficiently than high number of immobile peptides on gold surfaces. Cell attachment and spread on RGD-^{f}SLB surfaces were further confirmed in cell culture. On the other hand, bare SLBs supported limited number of cells with rounded morphology. Cells did not spread well on OSN-coated surfaces, and acoustic ratio measured on each OSN layers probably did not originate from adhesion of the cells, instead the negative charge of OSN could provide electrostatic interactions between surface and biomolecules on the cell membrane, thus promoting nonspecific protein and cell attachment.

In conclusion, nonfouling SLB surfaces were successfully functionalized and constructed ^{f}SLB platforms were shown to have the potential for real time and label-free monitoring of the specific cell – surface interactions via QCM-D.

6. CONCLUSIONS, CHALLENGES AND FUTURE PROSPECTS

Functionalized supported lipid bilayers with bioactive molecules are one of the most widely used platforms to study cell–cell and cell–material interactions and they can be successfully used to develop biosynthetic systems such as drug–screening platforms, membrane based biosensors, and utilized in medical diagnostics, biomaterial improvement, and various other biomedical assays. They allow the usage of various surface-sensitive characterization techniques such as QCM-D, SPR and AFM. QCM-D is an especially attractive technique commonly used for real-time monitoring, label-free evaluation of artificial lipid membrane studies and cell adhesion processes.

The aim of the thesis was to construct a functional SLB platform to investigate cell-surface interactions and to monitor whole process in real time via QCM-D system. At first, the effect of thiol-terminated phospholipid presence on SLB formation was determined. Using the quantitative $|\Delta D/\Delta f|$ results, the degree of the liquid trapped within the formed layer, or between the layer and the surface was predicted. Even at minor amounts (0.01%), DPPTE ensures the interaction of liposomes with gold surface whereas pure PC liposomes easily washed away. Lower thiol ratio (0.01 to 0.1%) resulted in an incomplete bilayer coverage together with unruptured liposomes. Whereas higher ratio (1–25%) yielded to the saturation of the surface and rupture of liposomes, not only as bilayer but also as multilayer islets in different depths through the continuous layer. Liposomes with 1% DPPTE was chosen as the optimized ratio since this is the lowest thiol content that generated appropriately rigid layer. The size of liposomes affected their behavior on the surface and there seemed to be a critical size in between 140 and 175 nm for them to rupture and form bilayer; bilayer formation is favored under 140 nm, whereas the liposomes seemed to flattened but not ruptured when the size is further increased (ca. 175 nm). The viscoelastic modelling results were combined with SPR and AFM experiments suggested that the resultant SLB was almost continuous but showed higher water content compared to an ideal bilayer due to partially fused liposomes. These partial fusions led the increase of membrane thickness average to ~7.0 nm. In sum, direct bilayer formation on bare gold surfaces can be achieved by well-known thiol-gold chemistry using low ratio of thiolated lipids

on liposomes. This procedure has a different dynamics than bilayer formation on modified gold and can further be explored by incorporating different membrane elements (different phospholipids, cholesterol, etc.) on the structure.

In second part, QCM-D method was used to investigate the dynamic adhesion behavior of human fetal osteoblastic bone cell lines on reference gold and various model surfaces. The initial cell sedimentation on various surfaces increased the acoustic ratio, which is the indication of nonspecific cell interactions on the surface. The increase of the signals when no other cells were introduced to the system was attributed to increasing surface contact area of the already attached cells. Extracellular matrix remodeling of the cells could be tracked from the adhesion kinetics as temporary increase in the rigidity at the interfacial layer. It was seen that while passive flattening also decreases Δf and increases ΔD signals, the acoustic ratio is not significantly affected. On the other hand, for protein-mediated specific interactions, higher acoustic ratios were observed due to increased contribution of the dissipative changes over frequency changes. RGD competition and trypsinization studies confirmed specific protein-mediated binding of cells to the surface. QCM-D results showed that cancerous cells interacted stronger with the hydrophilically treated surface and had higher viscoelastic characteristics than the healthy cells. The cluster of the average values was plotted to obtain fingerprints for both cell types and clear distinction of cancer cell signals from the healthy ones suggest potential use of this method in cell screening tests.

In the last part, RGD and OSN peptides were used as model peptides for functionalization of SLBs to evaluate osteoblast cell-surface interactions via QCM-D monitoring. First, the stability of SLB in various medium conditions were evaluated. The structural integrity was conserved until fifth day in PBS, but hole formations started to form from the first day. When SLBs were enriched with different lipids (cholesterol, PS, DOTAP), all of the lipid compositions increased the stability of SLB to pure PC bilayer. Lateral mobility of the lipid bilayer was also demonstrated via FRAP method.

The kinetics of peptide attachment to SLBs were compared to their nonspecific adsorption onto gold surfaces and the behavior of resultant layers were analyzed via QCM-D. The results indicated that conjugation to SLB provide higher structural flexibility than passive adsorption. Then, cell-surface interaction studies were carried

out in real time. Low density of mobile RGD peptides on SLB platforms preserved their biological activity and promoted cell adhesion more efficiently than high number of immobile peptides on gold surfaces. Cell attachment and spread on RGD-^{f}SLB surfaces were further confirmed in cell culture. On the other hand, bare SLBs supported limited number of cells with rounded morphology. Cells did not spread well on OSN-coated surfaces, and acoustic ratio measured on each OSN layers probably did not originate from adhesion of the cells, instead the negative charge of OSN could provide electrostatic interactions between surface and biomolecules on the cell membrane, thus promoting protein and cell attachment.

In conclusion, nonfouling SLB surfaces were successfully functionalized and constructed ^{f}SLB platforms were presented to have the potential for real time and label-free monitoring of the specific cell – surface interactions via QCM-D.

Biomimetic membranes generally suffer from structural defects, hole formations as demonstrated. When a scale-up is needed, the challenge in the preparation of defect-free membranes becomes more pronounced. In this thesis, the stability of SLB in various medium conditions and with different lipid types (cholesterol, PS, DOTAP) were evaluated till 7th day, but more thorough research should be done in this field to be able to monitor long-term experiments, such as cell differentiation.

Another important challenge is the complexity and the diversity of biomembranes. SLB platforms have been constructed with one or two lipid types. This is not sufficient to catch the actual, extensive lipid diversity and for precise modeling and to mimic the main structure and dynamics of the plasma membrane. The trials to increase SLB complexity with cholesterol, PS, DOTAP was successful on glass used for cell culture conditions, however cholesterol and negatively charged lipid (PS) was found to prevent the formation of PC bilayer on gold probably due to steric hindrance and repulsive energy barrier between gold and liposome surfaces.

As future prospect, these platforms could be constructed as multi-functional systems by including multiple peptides/proteins at defined densities, providing synergistic effects on cell behavior. The preparation of those multifunctional bilayers on spatially arrayed and/or patterned surfaces will provide high-throughput and fast analytical systems enabling parallel measurements. SLB arrays may speed up proteomic research based on membrane-associated proteins and drug screening. Integration of SLBs in

microfluidic systems will be needed to design miniaturized and automated devices for commercialization.

REFERENCES

[1] **Harvey Lodish, A. B., S. Lawrence Zipursky, Paul Matsudaira, David Baltimore and James Darnell**. (2001). Biomembranes and Cell Architecture *Molecular Cell Biology (4th edition)* (Vol. 29, pp. 126-128). Freeman & Co., New York, NY, 2000, 1084 pp.: Elsevier BV.

[2] **Clare O'Connor, J. U. A., Jennifer Fairman**. (2010). *Essentials of Cell Biology*. Cambridge, MA: NPG Education.

[3] **Ehud Gazit, A. M.** (2013). *Natural Biological Assembly at the Nanometric Scale* (Second ed.): Imperial College Press.

[4] **van Weerd, J., Karperien, M., & Jonkheijm, P.** (2015). Supported Lipid Bilayers for the Generation of Dynamic Cell-Material Interfaces. *Adv Healthc Mater, 4*(18), 2743-2779. doi: 10.1002/adhm.201500398

[5] **Richter, R. P., Him, J. L. K., & Brisson, A.** (2003). Supported lipid membranes. *Materials Today, 6*(11), 32-37. doi: 10.1016/s1369-7021(03)01129-5

[6] **Kiessling, V., Domanska, M. K., Murray, D., Wan, C., & Tamm, L. K.** (2008). Supported Lipid Bilayers: Development and Applications in Chemical Biology. *Wiley Encyclopedia of Chemical Biology*. doi: 10.1002/9780470048672.wecb663

[7] **Afanasenkau, D.** (2012). *Supported Lipid Bilayer as a Biomimetic Platform for Neuronal Cell Culture.* (PhD), Peter Grünberg Institute, Germany.

[8] **Reimhult, E., Kasemo, B., & Hook, F.** (2009). Rupture pathway of phosphatidylcholine liposomes on silicon dioxide. *Int J Mol Sci, 10*(4), 1683-1696. doi: 10.3390/ijms10041683

[9] **Afanasenkau, D., & Offenhausser, A.** (2012). Positively charged supported lipid bilayers as a biomimetic platform for neuronal cell culture. *Langmuir, 28*(37), 13387-13394. doi: 10.1021/la302500r

[10] **Hardy, G. J., Nayak, R., & Zauscher, S.** (2013). Model cell membranes: Techniques to form complex biomimetic supported lipid bilayers via vesicle fusion. *Curr Opin Colloid Interface Sci, 18*(5), 448-458. doi: 10.1016/j.cocis.2013.06.004

[11] **Li, X., Wang, R., Wicaksana, F., Zhao, Y., Tang, C., Torres, J., & Fane, A. G.** (2013). Fusion behaviour of aquaporin Z incorporated proteoliposomes investigated by quartz crystal microbalance with dissipation (QCM-D). *Colloids Surf B Biointerfaces, 111*, 446-452. doi: 10.1016/j.colsurfb.2013.06.008

[12] **Inci, F., Celik, U., Turken, B., Ozer, H. O., & Kok, F. N.** (2015). Construction of P-glycoprotein incorporated tethered lipid bilayer membranes. *Biochem Biophys Rep, 2*, 115-122. doi: 10.1016/j.bbrep.2015.05.012

[13] **Keller, C. A., & Kasemo, B.** (1998). Surface specific kinetics of lipid vesicle adsorption measured with a quartz crystal microbalance. *Biophys J, 75*(3), 1397-1402. doi: 10.1016/S0006-3495(98)74057-3

[14] **Keller, C. A., Glasmastar, K., Zhdanov, V. P., & Kasemo, B.** (2000). Formation of supported membranes from vesicles. *Phys Rev Lett, 84*(23), 5443-5446. doi: 10.1103/PhysRevLett.84.5443

[15] **Cho, N. J., Cho, S. J., Cheong, K. H., Glenn, J. S., & Frank, C. W.** (2007). Employing an amphipathic viral peptide to create a lipid bilayer on Au and TiO2. *J Am Chem Soc, 129*(33), 10050-10051. doi: 10.1021/ja0701412

[16] **Groves, J. T., Mahal, L. K., & Bertozzi, C. R.** (2001). Control of Cell Adhesion and Growth with Micropatterned Supported Lipid Membranes. *Langmuir, 17*(17), 5129-5133. doi: 10.1021/la010481f

[17] **Svedhem, S., Dahlborg, D., Ekeroth, J., Kelly, J., Höök, F., & Gold, J.** (2003). In Situ Peptide-Modified Supported Lipid Bilayers for Controlled Cell Attachment. *Langmuir, 19*(17), 6730-6736. doi: 10.1021/la034172w

[18] **Choi, S. E., Greben, K., Wordenweber, R., & Offenhausser, A.** (2016). Positively charged supported lipid bilayer formation on gold surfaces for neuronal cell culture. *Biointerphases, 11*(2), 021003. doi: 10.1116/1.4945306

[19] **Reimhult, E., & Kumar, K.** (2008). Membrane biosensor platforms using nano- and microporous supports. *Trends Biotechnol, 26*(2), 82-89. doi: 10.1016/j.tibtech.2007.11.004

[20] **Arslan Yildiz, A., Kang, C., & Sinner, E. K.** (2013). Biomimetic membrane platform containing hERG potassium channel and its application to drug screening. *Analyst, 138*(7), 2007-2012. doi: 10.1039/c3an36159d

[21] **Evans, S. F., Docheva, D., Bernecker, A., Colnot, C., Richter, R. P., & Knothe Tate, M. L.** (2013). Solid-supported lipid bilayers to drive stem cell fate and tissue architecture using periosteum derived progenitor cells. *Biomaterials, 34*(8), 1878-1887. doi: 10.1016/j.biomaterials.2012.09.024

[22] **Castellana, E. T., & Cremer, P. S.** (2006). Solid supported lipid bilayers: From biophysical studies to sensor design. *Surface Science Reports, 61*(10), 429-444. doi: 10.1016/j.surfrep.2006.06.001

[23] **Jackman, J., Knoll, W., & Cho, N.-J.** (2012). Biotechnology Applications of Tethered Lipid Bilayer Membranes. *Materials, 5*(12), 2637-2657. doi: 10.3390/ma5122637

[24] **McCabe, I. P., & Forstner, M. B.** (2013). Polymer Supported Lipid Bilayers. *Open Journal of Biophysics, 03*(01), 59-69. doi: 10.4236/ojbiphy.2013.31A008

[25] **Knoll, W., Köper, I., Naumann, R., & Sinner, E.-K.** (2008). Tethered bimolecular lipid membranes—A novel model membrane platform. *Electrochimica Acta, 53*(23), 6680-6689. doi: 10.1016/j.electacta.2008.02.121

[26] **Coutable, A., Thibault, C., Chalmeau, J., Francois, J. M., Vieu, C., Noireaux, V., & Trevisiol, E.** (2014). Preparation of tethered-lipid bilayers on gold surfaces for the incorporation of integral membrane proteins synthesized by cell-free expression. *Langmuir, 30*(11), 3132-3141. doi: 10.1021/la5004758

[27] **Hertrich, S., Stetter, F., Ruhm, A., Hugel, T., & Nickel, B.** (2014). Highly hydrated deformable polyethylene glycol-tethered lipid bilayers. *Langmuir, 30*(31), 9442-9447. doi: 10.1021/la4045804

[28] **Atanasov, V., Knorr, N., Duran, R. S., Ingebrandt, S., Offenhausser, A., Knoll, W., & Koper, I.** (2005). Membrane on a chip: a functional tethered lipid bilayer membrane on silicon oxide surfaces. *Biophys J, 89*(3), 1780-1788. doi: 10.1529/biophysj.105.061374

[29] **Wagner, M. L., & Tamm, L. K.** (2000). Tethered Polymer-Supported Planar Lipid Bilayers for Reconstitution of Integral Membrane Proteins: Silane-Polyethyleneglycol-Lipid as a Cushion and Covalent Linker. *Biophysical journal, 79*(3), 1400-1414. doi: 10.1016/s0006-3495(00)76392-2

[30] **Lin, Y.-H., Minner, D., Herring, V., & Naumann, C.** (2012). Physisorbed Polymer-Tethered Lipid Bilayer with Lipopolymer Gradient. *Materials, 5*(12), 2243-2257. doi: 10.3390/ma5112243

[31] **Wallin, M., Choi, J. H., Kim, S. O., Cho, N. J., & Andersson, M.** (2015). Peptide-induced formation of a tethered lipid bilayer membrane on mesoporous silica. *Eur Biophys J, 44*(1-2), 27-36. doi: 10.1007/s00249-014-0998-1

[32] **Rebaud, S., Maniti, O., & Girard-Egrot, A. P.** (2014). Tethered bilayer lipid membranes (tBLMs): interest and applications for biological membrane investigations. *Biochimie, 107 Pt A*, 135-142. doi: 10.1016/j.biochi.2014.06.021

[33] **He, L., Robertson, J. W., Li, J., Karcher, I., Schiller, S. M., Knoll, W., & Naumann, R.** (2005). Tethered bilayer lipid membranes based on monolayers of thiolipids mixed with a complementary dilution molecule. 1. Incorporation of channel peptides. *Langmuir, 21*(25), 11666-11672. doi: 10.1021/la051771p

[34] **Purrucker, O., Hillebrandt, H., Adlkofer, K., & Tanaka, M.** (2001). Deposition of highly resistive lipid bilayer on silicon–silicon dioxide electrode and incorporation of gramicidin studied by ac impedance spectroscopy. *Electrochimica Acta, 47*(5), 791-798. doi: 10.1016/s0013-4686(01)00759-9

[35] **Reimhult, E., Zach, M., Hook, F., & Kasemo, B.** (2006). A multitechnique study of liposome adsorption on Au and lipid bilayer formation on SiO2. *Langmuir, 22*(7), 3313-3319. doi: 10.1021/la0519554

[36] **Ramos, J. J., & Moya, S. E.** (2011). Water content of hydrated polymer brushes measured by an in situ combination of a quartz crystal microbalance with dissipation monitoring and spectroscopic ellipsometry. *Macromol Rapid Commun, 32*(24), 1972-1978. doi: 10.1002/marc.201100455

[37] **Yang, T., Baryshnikova, O. K., Mao, H., Holden, M. A., & Cremer, P. S.** (2003). Investigations of bivalent antibody binding on fluid-supported phospholipid membranes: the effect of hapten density. *J Am Chem Soc, 125*(16), 4779-4784. doi: 10.1021/ja029469f

[38] **Tamm, L. K., & Tatulian, S. A.** (1997). Infrared spectroscopy of proteins and peptides in lipid bilayers. *Q Rev Biophys, 30*(4), 365-429. doi: 10.1017/s0033583597003375

[39] **Ferreira, G. N., da-Silva, A. C., & Tome, B.** (2009). Acoustic wave biosensors: physical models and biological applications of quartz crystal microbalance. *Trends Biotechnol, 27*(12), 689-697. doi: 10.1016/j.tibtech.2009.09.003

[40] **Goksu, E. I., Hoopes, M. I., Nellis, B. A., Xing, C., Faller, R., Frank, C. W., . . . Longo, M. L.** (2010). Silica xerogel/aerogel-supported lipid bilayers: consequences of surface corrugation. *Biochim Biophys Acta, 1798*(4), 719-729. doi: 10.1016/j.bbamem.2009.09.007

[41] **Roiter, Y., Ornatska, M., Rammohan, A. R., Balakrishnan, J., Heine, D. R., & Minko, S.** (2008). Interaction of nanoparticles with lipid membrane. *Nano Lett, 8*(3), 941-944. doi: 10.1021/nl0800801

[42] **Davis, R. W., Flores, A., Barrick, T. A., Cox, J. M., Brozik, S. M., Lopez, G. P., & Brozik, J. A.** (2007). Nanoporous microbead supported bilayers: stability, physical characterization, and incorporation of functional transmembrane proteins. *Langmuir, 23*(7), 3864-3872. doi: 10.1021/la062576t

[43] **Mashaghi, A., Mashaghi, S., Reviakine, I., Heeren, R. M., Sandoghdar, V., & Bonn, M.** (2014). Label-free characterization of biomembranes: from structure to dynamics. *Chem Soc Rev, 43*(3), 887-900. doi: 10.1039/c3cs60243e

[44] **Attwood, S. J., Choi, Y., & Leonenko, Z.** (2013). Preparation of DOPC and DPPC Supported Planar Lipid Bilayers for Atomic Force Microscopy and Atomic Force Spectroscopy. *Int J Mol Sci, 14*(2), 3514-3539. doi: 10.3390/ijms14023514

[45] **Richter, R., Mukhopadhyay, A., & Brisson, A.** (2003). Pathways of lipid vesicle deposition on solid surfaces: a combined QCM-D and AFM study. *Biophys J, 85*(5), 3035-3047. doi: 10.1016/S0006-3495(03)74722-5

[46] **Kanazawa, K., & Cho, N.-J.** (2009). Quartz Crystal Microbalance as a Sensor to Characterize Macromolecular Assembly Dynamics. *Journal of Sensors, 2009*, 1-17. doi: 10.1155/2009/824947

[47] **Sauerbrey, G.** (1959). Verwendung von Schwingquarzen zur Wägung dünner Schichten und zur Mikrowägung. [Use of quartz crystal units for weighing thin films and Microweighing]. *Zeitschrift für Physik, 155*(2), 206-222. doi: 10.1007/bf01337937

[48] **Cooper, M. A., & Singleton, V. T.** (2007). A survey of the 2001 to 2005 quartz crystal microbalance biosensor literature: applications of acoustic

physics to the analysis of biomolecular interactions. *J Mol Recognit, 20*(3), 154-184. doi: 10.1002/jmr.826

[49] **Dixon, M. C.** (2008). Quartz crystal microbalance with dissipation monitoring: enabling real-time characterization of biological materials and their interactions. *Journal of Biomolecular Techniques, 19*(3), 151–158.

[50] **Viitala, T.** (2005). Modeling the Mechanical Properties of Adsorbed Deposited Layers At Air-Solid And Liquid-Solid Interfaces With The Dissipative KSV QCM-Z500 (pp. 1-33): KSV Instruments Ltd., Helsinki.

[51] **Hook, F., Kasemo, B., Nylander, T., Fant, C., Sott, K., & Elwing, H.** (2001). Variations in coupled water, viscoelastic properties, and film thickness of a Mefp-1 protein film during adsorption and cross-linking: a quartz crystal microbalance with dissipation monitoring, ellipsometry, and surface plasmon resonance study. *Anal Chem, 73*(24), 5796-5804.

[52] **Miller, M. M., & Lazarides, A. A.** (2005). Sensitivity of metal nanoparticle surface plasmon resonance to the dielectric environment. *J Phys Chem B, 109*(46), 21556-21565. doi: 10.1021/jp054227y

[53] **Willets, K. A., & Van Duyne, R. P.** (2007). Localized surface plasmon resonance spectroscopy and sensing. *Annu Rev Phys Chem, 58*(1), 267-297. doi: 10.1146/annurev.physchem.58.032806.104607

[54] **Homola, J.** (2008). Surface plasmon resonance sensors for detection of chemical and biological species. *Chem Rev, 108*(2), 462-493. doi: 10.1021/cr068107d

[55] **Reimhult, E., Larsson, C., Kasemo, B., & Hook, F.** (2004). Simultaneous surface plasmon resonance and quartz crystal microbalance with dissipation monitoring measurements of biomolecular adsorption events involving structural transformations and variations in coupled water. *Anal Chem, 76*(24), 7211-7220. doi: 10.1021/ac0492970

[56] **Chot, N. J., Kanazawa, K. K., Glenn, J. S., & Frank, C. W.** (2007). Employing two different quartz crystal microbalance models to study changes in viscoelastic behavior upon transformation of lipid vesicles to a bilayer on a gold surface. *Analytical Chemistry, 79*(18), 7027-7035.

[57] **Larsson, C., Rodahl, M., & Hook, F.** (2003). Characterization of DNA immobilization and subsequent hybridization on a 2D arrangement of streptavidin on a biotin-modified lipid bilayer supported on SiO2. *Anal Chem, 75*(19), 5080-5087.

[58] **Saitakis, M., & Gizeli, E.** (2012). Acoustic sensors as a biophysical tool for probing cell attachment and cell/surface interactions. *Cell Mol Life Sci, 69*(3), 357-371. doi: 10.1007/s00018-011-0854-8

[59] **Glasmastar, K., Larsson, C., Hook, F., & Kasemo, B.** (2002). Protein adsorption on supported phospholipid bilayers. *J Colloid Interface Sci, 246*(1), 40-47. doi: 10.1006/jcis.2001.8060

[60] **Faxalv, L., Hume, J., Kasemo, B., & Svedhem, S.** (2011). Imaging of blood plasma coagulation at supported lipid membranes. *J Colloid Interface Sci, 364*(2), 582-587. doi: 10.1016/j.jcis.2011.08.041

[61] **Richter, R. P., Maury, N., & Brisson, A. R.** (2005). On the effect of the solid support on the interleaflet distribution of lipids in supported lipid bilayers. *Langmuir, 21*(1), 299-304. doi: 10.1021/la0478402

[62] **Wikstrom, A., & Deinum, J.** (2007). Probing the interaction of coagulation factors with phospholipid vesicle surfaces by surface plasma resonance. *Anal Biochem, 362*(1), 98-107. doi: 10.1016/j.ab.2006.12.009

[63] **Heath, G. R., Johnson, B. R., Olmsted, P. D., Connell, S. D., & Evans, S. D.** (2013). Actin assembly at model-supported lipid bilayers. *Biophys J, 105*(10), 2355-2365. doi: 10.1016/j.bpj.2013.10.007

[64] **Milhiet, P. E., Giocondi, M. C., Baghdadi, O., Ronzon, F., Roux, B., & Le Grimellec, C.** (2002). Spontaneous insertion and partitioning of alkaline phosphatase into model lipid rafts. *EMBO Rep, 3*(5), 485-490. doi: 10.1093/embo-reports/kvf096

[65] **Sengur-Tasdemir, R., Aydin, S., Turken, T., Genceli, E. A., & Koyuncu, I.** (2015). Biomimetic Approaches for Membrane Technologies. *Separation & Purification Reviews, 45*(2), 122-140. doi: 10.1080/15422119.2015.1035443

[66] **Qi, S., Wang, R., Chaitra, G. K. M., Torres, J., Hu, X., & Fane, A. G.** (2016). Aquaporin-based biomimetic reverse osmosis membranes: Stability and long term performance. *Journal of Membrane Science, 508*, 94-103. doi: 10.1016/j.memsci.2016.02.013

[67] **Ding, W., Cai, J., Yu, Z., Wang, Q., Xu, Z., Wang, Z., & Gao, C.** (2015). Fabrication of an aquaporin-based forward osmosis membrane through covalent bonding of a lipid bilayer to a microporous support. *Journal of Materials Chemistry A, 3*(40), 20118-20126. doi: 10.1039/c5ta05751e

[68] **Kongsuphol, P., Fang, K. B., & Ding, Z.** (2013). Lipid bilayer technologies in ion channel recordings and their potential in drug screening assay. *Sensors and Actuators B: Chemical, 185*, 530-542. doi: 10.1016/j.snb.2013.04.119

[69] **Krishna, G., Schulte, J., Cornell, B. A., Pace, R. J., & Osman, P. D.** (2003). Tethered Bilayer Membranes Containing Ionic Reservoirs: Selectivity and Conductance. *Langmuir, 19*(6), 2294-2305. doi: 10.1021/la026238d

[70] **Andersson, M., Keizer, H. M., Zhu, C., Fine, D., Dodabalapur, A., & Duran, R. S.** (2007). Detection of single ion channel activity on a chip using tethered bilayer membranes. *Langmuir, 23*(6), 2924-2927. doi: 10.1021/la063503c

[71] **Sinner, E. K., Reuning, U., Kok, F. N., Sacca, B., Moroder, L., Knoll, W., & Oesterhelt, D.** (2004). Incorporation of integrins into artificial planar lipid membranes: characterization by plasmon-enhanced fluorescence spectroscopy. *Anal Biochem, 333*(2), 216-224. doi: 10.1016/j.ab.2004.05.022

[72] **Kaufmann, S., Sobek, J., Textor, M., & Reimhult, E.** (2011). Supported lipid bilayer microarrays created by non-contact printing. *Lab Chip, 11*(14), 2403-2410. doi: 10.1039/c1lc20073a

[73] **Jackman, J. A., & Cho, N. J.** (2012). Model membrane platforms for biomedicine: case study on antiviral drug development. *Biointerphases, 7*(1-4), 18. doi: 10.1007/s13758-011-0018-2

[74] **Harishchandra, R. K., Neumann, B. M., Gericke, A., & Ross, A. H.** (2015). Biophysical methods for the characterization of PTEN/lipid bilayer interactions. *Methods, 77-78*, 125-135. doi: 10.1016/j.ymeth.2015.02.004

[75] **Bailey, C. M., Kamaloo, E., Waterman, K. L., Wang, K. F., Nagarajan, R., & Camesano, T. A.** (2015). Size dependence of gold nanoparticle interactions with a supported lipid bilayer: A QCM-D study. *Biophys Chem, 203-204*, 51-61. doi: 10.1016/j.bpc.2015.05.006

[76] **Goreham, R. V., Thompson, V. C., Samura, Y., Gibson, C. T., Shapter, J. G., & Koper, I.** (2015). Interaction of silver nanoparticles with tethered bilayer lipid membranes. *Langmuir, 31*(21), 5868-5874. doi: 10.1021/acs.langmuir.5b00586

[77] **Lu, B., Smith, T., & Schmidt, J. J.** (2015). Nanoparticle-lipid bilayer interactions studied with lipid bilayer arrays. *Nanoscale, 7*(17), 7858-7866. doi: 10.1039/c4nr06892k

[78] **Andersson, A. S., Glasmastar, K., Sutherland, D., Lidberg, U., & Kasemo, B.** (2003). Cell adhesion on supported lipid bilayers. *J Biomed Mater Res A, 64*(4), 622-629. doi: 10.1002/jbm.a.10442

[79] **Ananthanarayanan, B., Little, L., Schaffer, D. V., Healy, K. E., & Tirrell, M.** (2010). Neural stem cell adhesion and proliferation on phospholipid bilayers functionalized with RGD peptides. *Biomaterials, 31*(33), 8706-8715. doi: 10.1016/j.biomaterials.2010.07.104

[80] **Stroumpoulis, D., Zhang, H., Rubalcava, L., Gliem, J., & Tirrell, M.** (2007). Cell adhesion and growth to Peptide-patterned supported lipid membranes. *Langmuir, 23*(7), 3849-3856. doi: 10.1021/la062375p

[81] **Thid, D., Holm, K., Eriksson, P. S., Ekeroth, J., Kasemo, B., & Gold, J.** (2008). Supported phospholipid bilayers as a platform for neural progenitor cell culture. *J Biomed Mater Res A, 84*(4), 940-953. doi: 10.1002/jbm.a.31358

[82] **Huang, C. J., Cho, N. J., Hsu, C. J., Tseng, P. Y., Frank, C. W., & Chang, Y. C.** (2010). Type I collagen-functionalized supported lipid bilayer as a cell culture platform. *Biomacromolecules, 11*(5), 1231-1240. doi: 10.1021/bm901445r

[83] **Ghosh Moulick, R., Afanasenkau, D., Choi, S. E., Albers, J., Lange, W., Maybeck, V., . . . Offenhausser, A.** (2016). Reconstitution of Fusion Proteins in Supported Lipid Bilayers for the Study of Cell Surface Receptor-Ligand Interactions in Cell-Cell Contact. *Langmuir, 32*(14), 3462-3469. doi: 10.1021/acs.langmuir.5b04644

[84] **Kam, L., & Boxer, S. G.** (2001). Cell adhesion to protein-micropatterned-supported lipid bilayer membranes. *J Biomed Mater Res, 55*(4), 487-495.

[85] **Sandrin, L., Coche-Guerente, L., Bernstein, A., Basit, H., Labbe, P., Dumy, P., & Boturyn, D.** (2010). Cell adhesion through clustered ligand on fluid supported lipid bilayers. *Org Biomol Chem, 8*(7), 1531-1534. doi: 10.1039/b924523e

[86] **Zhu, X., Wang, Z., Zhao, A., Huang, N., Chen, H., Zhou, S., & Xie, X.** (2014). Cell adhesion on supported lipid bilayers functionalized with RGD peptides monitored by using a quartz crystal microbalance with dissipation. *Colloids Surf B Biointerfaces, 116*, 459-464. doi: 10.1016/j.colsurfb.2014.01.032

[87] **Reiss, B., Janshoff, A., Steinem, C., Seebach, J., & Wegener, J.** (2003). Adhesion Kinetics of Functionalized Vesicles and Mammalian Cells: A Comparative Study†. *Langmuir, 19*(5), 1816-1823. doi: 10.1021/la0261747

[88] **Berat, R., Remy-Zolghadry, M., Gounou, C., Manigand, C., Tan, S., Salto, C., . . . Brisson, A. R.** (2007). Peptide-presenting two-dimensional protein matrix on supported lipid bilayers: an efficient platform for cell adhesion. *Biointerphases, 2*(4), 165-172. doi: 10.1116/1.2821954

[89] **Tymchenko, N., Nileback, E., Voinova, M. V., Gold, J., Kasemo, B., & Svedhem, S.** (2012). Reversible changes in cell morphology due to cytoskeletal rearrangements measured in real-time by QCM-D. *Biointerphases, 7*(1-4), 43. doi: 10.1007/s13758-012-0043-9

[90] **Atienza, J. M., Zhu, J., Wang, X., Xu, X., & Abassi, Y.** (2005). Dynamic monitoring of cell adhesion and spreading on microelectronic sensor arrays. *J Biomol Screen, 10*(8), 795-805. doi: 10.1177/1087057105279635

[91] **Da-Silva, A. C., Rodrigues, R., Rosa, L. F., de-Carvalho, J., Tome, B., & Ferreira, G. N.** (2012). Acoustic detection of cell adhesion on a quartz crystal microbalance. *Biotechnol Appl Biochem, 59*(6), 411-419. doi: 10.1002/bab.1041

[92] **Zhou, T., Marx, K. A., Dewilde, A. H., McIntosh, D., & Braunhut, S. J.** (2012). Dynamic cell adhesion and viscoelastic signatures distinguish normal from malignant human mammary cells using quartz crystal microbalance. *Anal Biochem, 421*(1), 164-171. doi: 10.1016/j.ab.2011.10.052

[93] **Iturri, J., Garcia-Fernandez, L., Reuning, U., Garcia, A. J., del Campo, A., & Salierno, M. J.** (2015). Synchronized cell attachment triggered by photo-activatable adhesive ligands allows QCM-based detection of early integrin binding. *Sci Rep, 5*, 9533. doi: 10.1038/srep09533

[94] **Chen, J. Y., Tsai, W. S., Shao, H. J., Wu, J. C., Lai, J. M., Lu, S. H., . . . Chang, Y. C.** (2016). Sensitive and Specific Biomimetic Lipid Coated Microfluidics to Isolate Viable Circulating Tumor Cells and Microemboli for Cancer Detection. *PLoS One, 11*(3), e0149633. doi: 10.1371/journal.pone.0149633

[95] **Lee, I. C., Liu, Y. C., Tsai, H. A., Shen, C. N., & Chang, Y. C.** (2014). Promoting the selection and maintenance of fetal liver stem/progenitor cell colonies by layer-by-layer polypeptide tethered supported lipid bilayer. *ACS Appl Mater Interfaces, 6*(23), 20654-20663. doi: 10.1021/am503928u

[96] **Hook, F., Kasemo, B., Grunze, M., & Zauscher, S.** (2008). Quantitative biological surface science: challenges and recent advances. *Acs Nano, 2*(12), 2428-2436. doi: 10.1021/nn800800v

[97] **Tiefenauer, L., & Demarche, S.** (2012). Challenges in the Development of Functional Assays of Membrane Proteins. *Materials, 5*(12), 2205-2242. doi: 10.3390/ma5112205

[98] **Lind, T. K., & Cardenas, M.** (2016). Understanding the formation of supported lipid bilayers via vesicle fusion-A case that exemplifies the need for the complementary method approach (Review). *Biointerphases, 11*(2), 020801. doi: 10.1116/1.4944830

[99] **Shen, Y.-x., Saboe, P. O., Sines, I. T., Erbakan, M., & Kumar, M.** (2014). Biomimetic membranes: A review. *Journal of Membrane Science, 454*, 359-381. doi: 10.1016/j.memsci.2013.12.019

[100] **Sachse, R., Dondapati, S. K., Fenz, S. F., Schmidt, T., & Kubick, S.** (2014). Membrane protein synthesis in cell-free systems: from bio-mimetic systems to bio-membranes. *FEBS Lett, 588*(17), 2774-2781. doi: 10.1016/j.febslet.2014.06.007

[101] **Adams, P. G., Swingle, K. L., Paxton, W. F., Nogan, J. J., Stromberg, L. R., Firestone, M. A., . . . Montano, G. A.** (2015). Exploiting lipopolysaccharide-induced deformation of lipid bilayers to modify membrane composition and generate two-dimensional geometric membrane array patterns. *Sci Rep, 5*, 10331. doi: 10.1038/srep10331

[102] **Watanabe, R., Soga, N., Yamanaka, T., & Noji, H.** (2014). High-throughput formation of lipid bilayer membrane arrays with an asymmetric lipid composition. *Sci Rep, 4*, 7076. doi: 10.1038/srep07076

[103] **Arslan Yildiz, A., Yildiz, U. H., Liedberg, B., & Sinner, E. K.** (2013). Biomimetic membrane platform: fabrication, characterization and applications. *Colloids Surf B Biointerfaces, 103*, 510-516. doi: 10.1016/j.colsurfb.2012.10.066

[104] **Kilic, A., & Kok, F. N.** (2016). Biomimetic lipid bilayers on solid surfaces: models for biological interactions. *Surface Innovations, 4*(3), 141-157. doi: 10.1680/jsuin.16.00008

[105] **Moya, S., Richter, W., Leporatti, S., Baumler, H., & Donath, E.** (2003). Freeze-fracture electron microscopy of lipid membranes on colloidal polyelectrolyte multilayer coated supports. *Biomacromolecules, 4*(3), 808-814. doi: 10.1021/bm034013r

[106] **Lang, H., Duschl, C., & Vogel, H.** (1994). A new class of thiolipids for the attachment of lipid bilayers on gold surfaces. *Langmuir, 10*(1), 197-210. doi: 10.1021/la00013a029

[107] **Marques, J. T., de Almeida, R. F. M., & Viana, A. S.** (2014). Lipid bilayers supported on bare and modified gold - Formation, characterization and relevance of lipid rafts. *Electrochimica Acta, 126*, 139-150. doi: 10.1016/j.electacta.2013.07.117

[108] **Cho, N. J., Frank, C. W., Kasemo, B., & Hook, F.** (2010). Quartz crystal microbalance with dissipation monitoring of supported lipid bilayers on various substrates. *Nat Protoc, 5*(6), 1096-1106. doi: 10.1038/nprot.2010.65

[109] **Pawlowski, J., Juhaniewicz, J., Guzeloglu, A., & Sek, S.** (2015). Mechanism of Lipid Vesicles Spreading and Bilayer Formation on a Au(111) Surface. *Langmuir, 31*(40), 11012-11019. doi: 10.1021/acs.langmuir.5b01331

[110] **Marquês, J. T., de Almeida, R. F. M., & Viana, A. S.** (2012). Biomimetic membrane rafts stably supported on unmodified gold. *Soft Matter, 8*(6), 2007-2016. doi: 10.1039/c2sm06738b

[111] **Steinem, C., Janshoff, A., Ulrich, W. P., Sieber, M., & Galla, H. J.** (1996). Impedance analysis of supported lipid bilayer membranes: a scrutiny of different preparation techniques. *Biochim Biophys Acta, 1279*(2), 169-180. doi: 10.1016/0005-2736(95)00274-x

[112] **Ekeroth, J., Konradsson, P., & Höök, F.** (2002). Bivalent-Ion-Mediated Vesicle Adsorption and Controlled Supported Phospholipid Bilayer Formation on Molecular Phosphate and Sulfate Layers on Gold. *Langmuir, 18*(21), 7923-7929. doi: 10.1021/la026131q

[113] **Lundström, I.** (1994). Real-time biospecific interaction analysis. *Biosensors and Bioelectronics, 9*(9-10), 725-736. doi: 10.1016/0956-5663(94)80071-5

[114] **Pera, I., & Fritz, J.** (2007). Sensing lipid bilayer formation and expansion with a microfabricated cantilever array. *Langmuir, 23*(3), 1543-1547. doi: 10.1021/la0624337

[115] **McCubbin, G. A., Praporski, S., Piantavigna, S., Knappe, D., Hoffmann, R., Bowie, J. H., . . . Martin, L. L.** (2011). QCM-D fingerprinting of membrane-active peptides. *Eur Biophys J, 40*(4), 437-446. doi: 10.1007/s00249-010-0652-5

[116] **Reviakine, I., Johannsmann, D., & Richter, R. P.** (2011). Hearing what you cannot see and visualizing what you hear: interpreting quartz crystal microbalance data from solvated interfaces. *Anal Chem, 83*(23), 8838-8848. doi: 10.1021/ac201778h

[117] **Wang, K. F., Nagarajan, R., & Camesano, T. A.** (2014). Antimicrobial peptide alamethicin insertion into lipid bilayer: a QCM-D exploration. *Colloids Surf B Biointerfaces, 116*, 472-481. doi: 10.1016/j.colsurfb.2014.01.036

[118] **Viitala, T., Hautala, J. T., Vuorinen, J., & Wiedmer, S. K.** (2007). Structure of anionic phospholipid coatings on silica by dissipative quartz crystal microbalance. *Langmuir, 23*(2), 609-618. doi: 10.1021/la060923t

[119] **Malmstrom, J., Agheli, H., Kingshott, P., & Sutherland, D. S.** (2007). Viscoelastic modeling of highly hydrated laminin layers at homogeneous and nanostructured surfaces: quantification of protein layer properties using QCM-D and SPR. *Langmuir, 23*(19), 9760-9768. doi: 10.1021/la701233y

[120] **Serro, A. P., Carapeto, A., Paiva, G., Farinha, J. P. S., Colaço, R., & Saramago, B.** (2012). Formation of an intact liposome layer adsorbed on oxidized gold confirmed by three complementary techniques: QCM-D, AFM and confocal fluorescence microscopy. *Surface and Interface Analysis, 44*(4), 426-433. doi: 10.1002/sia.3820

[121] **Macakova, L., Blomberg, E., & Claesson, P. M.** (2007). Effect of adsorbed layer surface roughness on the QCM-D response: focus on trapped water. *Langmuir, 23*(24), 12436-12444. doi: 10.1021/la7014308

[122] **Salamon, Z., & Tollin, G.** (2001). Optical anisotropy in lipid bilayer membranes: coupled plasmon-waveguide resonance measurements of molecular orientation, polarizability, and shape. *Biophys J, 80*(3), 1557-1567. doi: 10.1016/S0006-3495(01)76128-0

[123] **Innes, R. A., & Sambles, J. R.** (1987). Optical characterisation of gold using surface plasmon-polaritons. *Journal of Physics F: Metal Physics, 17*(1), 277-287. doi: 10.1088/0305-4608/17/1/031

[124] **Jung, L. S., Campbell, C. T., Chinowsky, T. M., Mar, M. N., & Yee, S. S.** (1998). Quantitative Interpretation of the Response of Surface Plasmon Resonance Sensors to Adsorbed Films. *Langmuir, 14*(19), 5636-5648. doi: 10.1021/la971228b

[125] **Feiler, A. A., Sahlholm, A., Sandberg, T., & Caldwell, K. D.** (2007). Adsorption and viscoelastic properties of fractionated mucin (BSM) and bovine serum albumin (BSA) studied with quartz crystal microbalance (QCM-D). *J Colloid Interface Sci, 315*(2), 475-481. doi: 10.1016/j.jcis.2007.07.029

[126] **Richter, R. P., Berat, R., & Brisson, A. R.** (2006). Formation of solid-supported lipid bilayers: an integrated view. *Langmuir, 22*(8), 3497-3505. doi: 10.1021/la052687c

[127] **Granéli, A., Rydström, J., Kasemo, B., & Höök, F.** (2003). Formation of Supported Lipid Bilayer Membranes on SiO2from Proteoliposomes Containing Transmembrane Proteins. *Langmuir, 19*(3), 842-850. doi: 10.1021/la026231w

[128] **Ferhan, A. R., Jackman, J. A., & Cho, N. J.** (2017). Investigating how vesicle size influences vesicle adsorption on titanium oxide: a competition between steric packing and shape deformation. *Phys Chem Chem Phys, 19*(3), 2131-2139. doi: 10.1039/c6cp07930j

[129] **Reimhult, E., Hook, F., & Kasemo, B.** (2002). Vesicle adsorption on SiO2 and TiO2: Dependence on vesicle size. *Journal of Chemical Physics, 117*(16), 7401-7404. doi: 10.1063/1.1513230

[130] **Khalili, A. A., & Ahmad, M. R.** (2015). A Review of Cell Adhesion Studies for Biomedical and Biological Applications. *Int J Mol Sci, 16*(8), 18149-18184. doi: 10.3390/ijms160818149

[131] **Michaelis, S., Robelek, R., & Wegener, J.** (2012). Studying cell-surface interactions in vitro: a survey of experimental approaches and techniques. *Adv Biochem Eng Biotechnol, 126*, 33-66. doi: 10.1007/10_2011_112

[132] **Palacio, M. L., & Bhushan, B.** (2012). Bioadhesion: a review of concepts and applications. *Philos Trans A Math Phys Eng Sci, 370*(1967), 2321-2347. doi: 10.1098/rsta.2011.0483

[133] **Mechler, A., Praporski, S., Atmuri, K., Boland, M., Separovic, F., & Martin, L. L.** (2007). Specific and selective peptide-membrane interactions revealed using quartz crystal microbalance. *Biophys J, 93*(11), 3907-3916. doi: 10.1529/biophysj.107.116525

[134] **Watarai, E., Matsuno, R., Konno, T., Ishihara, K., & Takai, M.** (2012). QCM-D analysis of material–cell interactions targeting a single cell during initial cell attachment. *Sensors and Actuators B: Chemical, 171-172*, 1297-1302. doi: 10.1016/j.snb.2012.05.010

[135] **Lord, M. S., Modin, C., Foss, M., Duch, M., Simmons, A., Pedersen, F. S., . . . Besenbacher, F.** (2006). Monitoring cell adhesion on tantalum and oxidised polystyrene using a quartz crystal microbalance with dissipation. *Biomaterials, 27*(26), 4529-4537. doi: 10.1016/j.biomaterials.2006.04.006

[136] **Tagaya, M.** (2015). In situ QCM-D study of nano-bio interfaces with enhanced biocompatibility. *Polymer Journal, 47*(9), 599-608. doi: 10.1038/pj.2015.43

[137] **Lord, M. S., Modin, C., Foss, M., Duch, M., Simmons, A., Pedersen, F. S., . . . Milthorpe, B. K.** (2008). Extracellular matrix remodelling during cell adhesion monitored by the quartz crystal microbalance. *Biomaterials, 29*(17), 2581-2587. doi: 10.1016/j.biomaterials.2008.03.002

[138] **Modin, C., Stranne, A. L., Foss, M., Duch, M., Justesen, J., Chevallier, J., . . . Besenbacher, F.** (2006). QCM-D studies of attachment and differential spreading of pre-osteoblastic cells on Ta and Cr surfaces. *Biomaterials, 27*(8), 1346-1354. doi: 10.1016/j.biomaterials.2005.09.022

[139] **Knerr, R., Weiser, B., Drotleff, S., Steinem, C., & Gopferich, A.** (2006). Measuring cell adhesion on RGD-modified, self-assembled PEG monolayers using the quartz crystal microbalance technique. *Macromol Biosci, 6*(10), 827-838. doi: 10.1002/mabi.200600106

[140] **Chen, J. Y., Shahid, A., Garcia, M. P., Penn, L. S., & Xi, J.** (2012). Dissipation monitoring for assessing EGF-induced changes of cell adhesion. *Biosens Bioelectron, 38*(1), 375-381. doi: 10.1016/j.bios.2012.06.018

[141] **Tagaya, M., Ikoma, T., Takemura, T., Hanagata, N., Okuda, M., Yoshioka, T., & Tanaka, J.** (2011). Detection of interfacial phenomena with osteoblast-like cell adhesion on hydroxyapatite and oxidized polystyrene by the quartz crystal microbalance with dissipation. *Langmuir, 27*(12), 7635-7644. doi: 10.1021/la200008z

[142] **Fatisson, J., Azari, F., & Tufenkji, N.** (2011). Real-time QCM-D monitoring of cellular responses to different cytomorphic agents. *Biosens Bioelectron, 26*(7), 3207-3212. doi: 10.1016/j.bios.2010.12.027

[143] **Westas, E., Svanborg, L. M., Wallin, P., Bauer, B., Ericson, M. B., Wennerberg, A., . . . Andersson, M.** (2015). Using QCM-D to study the adhesion of human gingival fibroblasts on implant surfaces. *J Biomed Mater Res A, 103*(10), 3139-3147. doi: 10.1002/jbm.a.35458

[144] **Wegener, J., Seebach, J., Janshoff, A., & Galla, H. J.** (2000). Analysis of the composite response of shear wave resonators to the attachment of mammalian cells. *Biophys J, 78*(6), 2821-2833. doi: 10.1016/S0006-3495(00)76825-1

[145] **Fredriksson, C., Kihlman, S., Rodahl, M., & Kasemo, B.** (1998). The Piezoelectric Quartz Crystal Mass and Dissipation Sensor: A Means of Studying Cell Adhesion. *Langmuir, 14*(2), 248-251. doi: 10.1021/la9710051

[146] **Li, F., Wang, J. H., & Wang, Q. M.** (2007). Monitoring cell adhesion by using thickness shear mode acoustic wave sensors. *Biosens Bioelectron, 23*(1), 42-50. doi: 10.1016/j.bios.2007.03.018

[147] **Kilic, A., Fazeli Jadidi, M., Ozer, H. O., & Kok, F. N.** (2017). The effect of thiolated phospholipids on formation of supported lipid bilayers on gold substrates investigated by surface-sensitive methods. *Colloids Surf B Biointerfaces, 160*, 117-125. doi: 10.1016/j.colsurfb.2017.09.016

[148] **Marx, K. A., Zhou, T., Montrone, A., McIntosh, D., & Braunhut, S. J.** (2005). Quartz crystal microbalance biosensor study of endothelial cells and their extracellular matrix following cell removal: Evidence for transient cellular stress and viscoelastic changes during detachment and the elastic behavior of the pure matrix. *Anal Biochem, 343*(1), 23-34. doi: 10.1016/j.ab.2005.05.013

[149] **Da-Silva, A. C., Soares, S. S., & Ferreira, G. N.** (2013). Acoustic detection of cell adhesion to a coated quartz crystal microbalance - implications for studying the biocompatibility of polymers. *Biotechnol J, 8*(6), 690-698. doi: 10.1002/biot.201200320

[150] **Seker, S., Elcin, A. E., & Elcin, Y. M.** (2016). Real-time monitoring of mesenchymal stem cell responses to biomaterial surfaces and to a model drug by using quartz crystal microbalance. *Artif Cells Nanomed Biotechnol, 44*(7), 1722-1732. doi: 10.3109/21691401.2015.1089255

[151] **Wan, X., Kim, S. Y., Guenther, L. M., Mendoza, A., Briggs, J., Yeung, C., . . . Helman, L.** (2009). Beta4 integrin promotes osteosarcoma metastasis and interacts with ezrin. *Oncogene, 28*(38), 3401-3411. doi: 10.1038/onc.2009.206

[152] **Chronaki, D., Stratiotis, D. I., Tsortos, A., Anastasiadou, E., & Gizeli, E.** (2016). Screening between normal and cancer human thyroid cells through comparative adhesion studies using the Quartz Crystal Microbalance. *Sensing and Bio-Sensing Research, 11*, 99-106. doi: 10.1016/j.sbsr.2016.10.001

[153] **Sobiepanek, A., Milner-Krawczyk, M., Lekka, M., & Kobiela, T.** (2017). AFM and QCM-D as tools for the distinction of melanoma cells with a different metastatic potential. *Biosens Bioelectron, 93*, 274-281. doi: 10.1016/j.bios.2016.08.088

[154] **Nowacki, L., Follet, J., Vayssade, M., Vigneron, P., Rotellini, L., Cambay, F., . . . Rossi, C.** (2015). Real-time QCM-D monitoring of cancer cell death early events in a dynamic context. *Biosens Bioelectron, 64*, 469-476. doi: 10.1016/j.bios.2014.09.065

[155] **Ruoslahti, E.** (1996). RGD and other recognition sequences for integrins. *Annu Rev Cell Dev Biol, 12*, 697-715. doi: 10.1146/annurev.cellbio.12.1.697

[156] **Hosseini, S., Naderi-Manesh, H., Vali, H., & Faghihi, S.** (2014). Improved surface bioactivity of stainless steel substrates using osteocalcin mimetic peptide. *Materials Chemistry and Physics, 143*(3), 1364-1371. doi: 10.1016/j.matchemphys.2013.11.047

[157] **Inc., T. F. S.** Carbodiimide Crosslinker Chemistry. from https://www.thermofisher.com/us/en/home/life-science/protein-biology/protein-biology-learning-center/protein-biology-resource-library/pierce-protein-methods/carbodiimide-crosslinker-chemistry.html

[158] **Su, X., Zong, Y., Richter, R., & Knoll, W.** (2005). Enzyme immobilization on poly(ethylene-co-acrylic acid) films studied by quartz crystal microbalance with dissipation monitoring. *J Colloid Interface Sci, 287*(1), 35-42. doi: 10.1016/j.jcis.2005.01.089

[159] **Sandrin, L., Thakar, D., Goyer, C., Labbé, P., Boturyn, D., & Coche-Guérente, L.** (2015). Controlled surface density of RGD ligands for cell adhesion: evidence for ligand specificity by using QCM-D. *Journal of Materials Chemistry B, 3*(27), 5577-5587. doi: 10.1039/c5tb00420a

[160] **Le Saux, G., Magenau, A., Bocking, T., Gaus, K., & Gooding, J. J.** (2011). The relative importance of topography and RGD ligand density for endothelial cell adhesion. *PLoS One, 6*(7), e21869. doi: 10.1371/journal.pone.0021869

[161] **Tamm, L. K., & McConnell, H. M.** (1985). Supported phospholipid bilayers. *Biophys J, 47*(1), 105-113. doi: 10.1016/S0006-3495(85)83882-0

[162] **Campbell, R. B., Balasubramanian, S. V., & Straubinger, R. M.** (2001). Phospholipid-cationic lipid interactions: influences on membrane and vesicle properties. *Biochim Biophys Acta, 1512*(1), 27-39. doi: https://doi.org/10.1016/S0005-2736(01)00290-5

[163] **Luxembourg, U. o.** FRAP Analyser. from http://actinsim.uni.lu/eng/Downloads

[164] **Bruce Alberts, A. J., Julian Lewis, Martin Raff, Keith Roberts, and Peter Walter.** (2002). The Lipid Bilayer *Molecular Biology of the Cell* (4th edition ed.): Garland Science.

[165] **Marquês, J. T., de Almeida, R. F. M., & Viana, A. S.** (2014). Lipid bilayers supported on bare and modified gold – Formation, characterization and relevance of lipid rafts. *Electrochimica Acta, 126*, 139-150. doi: 10.1016/j.electacta.2013.07.117

[166] **Hopfner, M., Rothe, U., & Bendas, G.** (2008). Biosensor-based evaluation of liposomal behavior in the target binding process. *J Liposome Res, 18*(1), 71-82. doi: 10.1080/08982100801894000

APPENDICES

APPENDIX A: Supporting Information for Chapter 3.

APPENDIX B: Supporting Information for Chapter 4.

APPENDIX C: Supporting Information for Chapter 5.

APPENDIX A

A.1. Preparation of hydrophilic and hydrophobic self-assembled monolayer (SAM) sensor surfaces

Bare, untreated gold surfaces are in hydrophobic nature [165]. Hydrophilic gold surfaces were obtained by oxidization, *i.e.,* subjecting sensors to two cycles of UV-Ozone exposure for 10 min, rinsing with excess water, and drying under nitrogen. For the preparation of SAM, gold surfaces were immersed in 1 mM DPPTE phospholipids in ethanol/chloroform (1:1) solution and left for 48 hours. Before use, QCM-D crystals were rinsed with pure ethanol and excess distilled water and dried under N_2.

After each measurement, the crystals were soaked in mild detergent and ethanol (70 %) solutions and then rinsed with water, dried under nitrogen, and stored in a desiccator until reuse. To remove the thiol residuals from the gold surfaces, the crystals were separately cleaned with H_2O:NH_3(25 %):H_2O_2 (30 %) (5:1:1) solution for 5 min in 75°C, then they were treated under UV-Ozone chamber for 15 min.

A.2. Acoustic ratio of rigid and viscoelastic layers

It is practical to evaluate dissipation per frequency ratio, acoustic ratio, *i.e.,* $|\Delta D/\Delta f|$, to compare the distinct outcomes for liposomal binding behavior during the whole process. In order to assess the success of bilayer formation, firstly two representative rigid and two viscoelastic layers were constructed on the surface and their acoustic ratio (GHz^{-1}) results were used as a reference (Figure A.1).

Firstly, as a rigid protein monolayer example [166], Bovine Serum Albumin (BSA) (50 µg/mL) adsorption was monitored on an untreated, *i.e.,* hydrophobic gold surface. Low ΔD, $|\Delta f|$ and acoustic ratio values for BSA adsorption (Figure A.1a) corresponded to a rigid monolayer on the surface. Taking into consideration the theoretical mass of fully saturated BSA monolayer coverage in a particular conformation (aspect ratio, e = 3.5) on the sensor surface area (197 $ng.cm^{-2}$), mass calculated via Sauerbrey equation [48] corresponding to the obtained $|\Delta f|$ value (12 ± 1 Hz) is reasonable (212.4 ± 18 $ng.cm^{-2}$) and in agreement with the literature [125]. Secondly, to get a rigid phospholipid monolayer, PC liposomes was sent onto the gold surface premodified with SAM [13]. Despite the high liposome concentration (10x), the total absolute frequency shift was only 13.5 ± 1 Hz as expected, which indicates formation of an additional lipid monolayer on SAM as suggested in literature [13] (Figure A.1b).

In the second part of the experiment set, acoustic ratio values of viscoelastic liposomal layers were investigated. Pure PC liposomes are expected to be adsorbed without rupturing on the oxidized surface thanks to the strong electrostatic attraction of the oxidized gold surface [13]. High ΔD (12.5 ± 1), $|\Delta f|$ (77 ± 5 Hz) and $|\Delta D/\Delta f|$ values (162.3 ± 10 GHz^{-1}) suggests a soft liposomal layer with high liquid content (Figure A.1c). Lastly, interaction of negatively charged liposomes (zeta potential -24 ± 0.9 mV) prepared by PC and *phosphatidylserine* (PS) at the same ratio, with the unoxidized gold surfaces was monitored (Figure A.1d). Low $|\Delta f|$ value reflects that the intensity of binding is weak, indicating low number of liposomes adhered onto the surface. However, high acoustic ratio (298 ± 21 GHz^{-1}) points out high viscoelasticity meaning that formed liposome layer did not flatten, but remained almost intact on the surface.

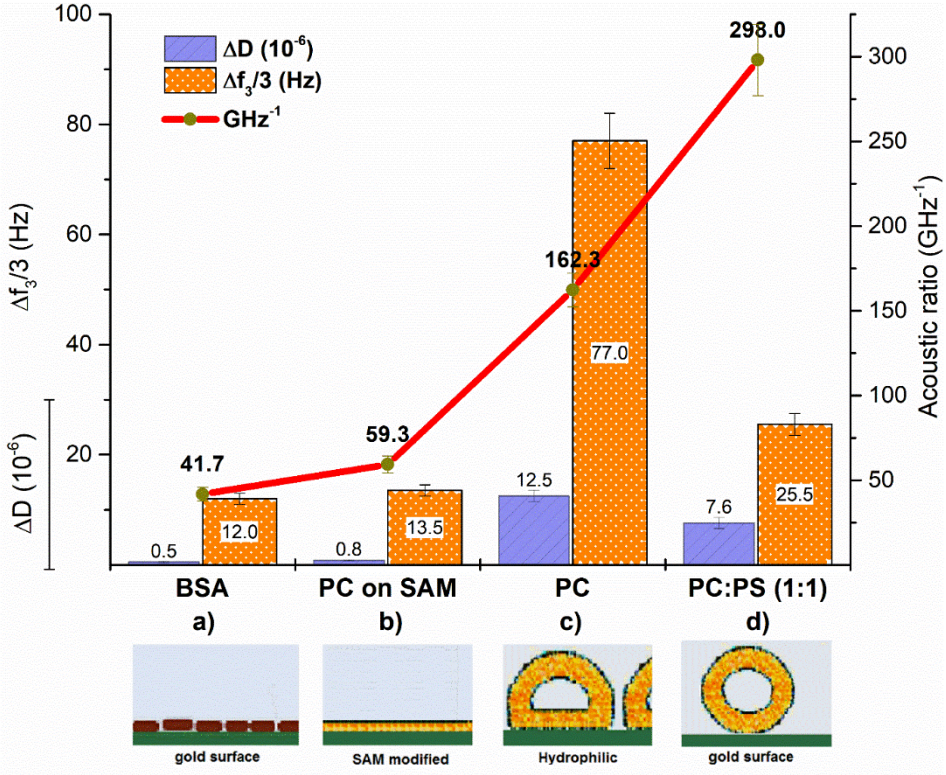

Figure A.1 : ΔD, |Δf| and acoustic ratio values and representative figures (not to scale) of rigid: a) BSA monolayer on hydrophobic gold surface and b) PC lipid monolayer on SAM modified gold surface; and viscoelastic layers: c) flattened PC liposomes on oxidized gold surfaces and d) intact PC:PS (1:1) liposomes on hydrophobic gold surface.

A.3. Figure for DPPTE liposomes

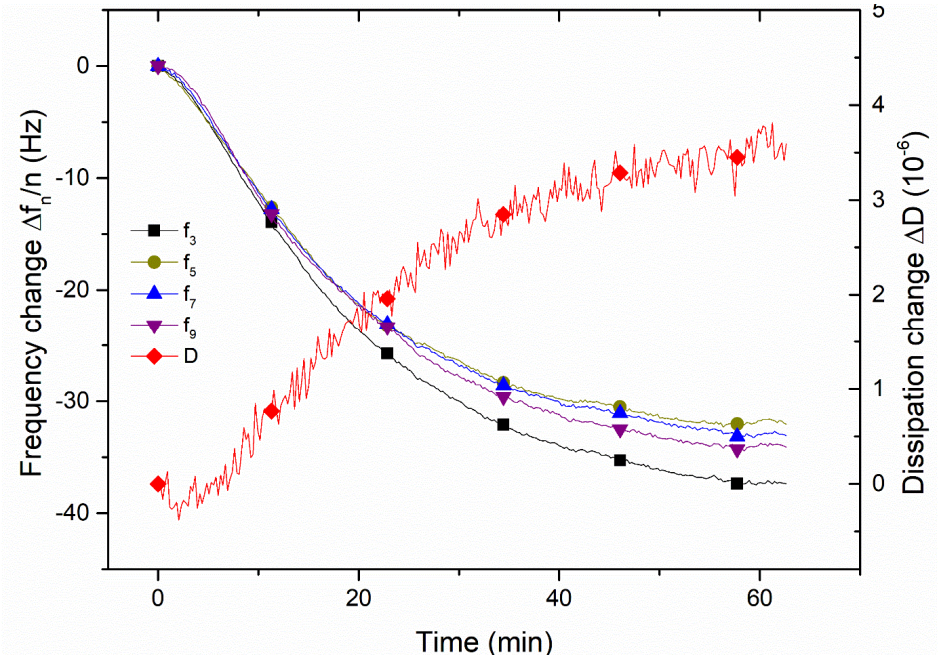

Figure A.2 : Normalized frequency (in various harmonics) and dissipation changes versus time for the adsorption of pure DPPTE liposomes sensor surface.

A.4. SPR kinetics

Angle shift for each liposome type (Figure A.3) multiplied by the mass density for lipids calculated in section 3.3.2 SPR measurements section and used in conversion of SPR response to the adsorbed mass.

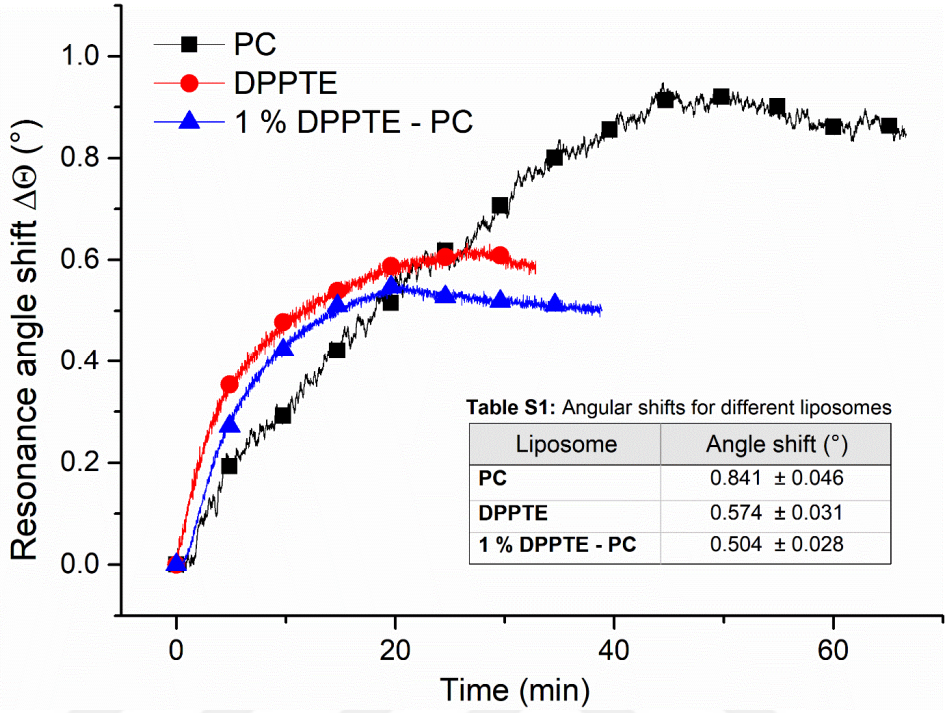

Table S1: Angular shifts for different liposomes

Liposome	Angle shift (°)
PC	0.841 ± 0.046
DPPTE	0.574 ± 0.031
1 % DPPTE - PC	0.504 ± 0.028

Figure A.3 : Kinetic plot of SPR angle shifts for different liposomes.

APPENDIX B

B.1. The correlation of Δf and ΔD changes with injected cell number

Effect of injected cell number on Δf and ΔD was determined with hfOB cells at varying amounts (60 - 2500 × 10^3 in 6 mL in serum-free medium) using untreated gold surfaces. The data at the end of an hour flow showed that Δf and ΔD varied with the seeding density of the cell suspensions in a power-law behavior (Figure B.1). A pronounced increase (~ 40-fold) in the number of cells caused a marginal increase on -Δf, from 25 to 35 Hz, but 3-fold increase was seen on ΔD (from 1.5 × 10^{-6} to 4.5 × 10^{-6}).

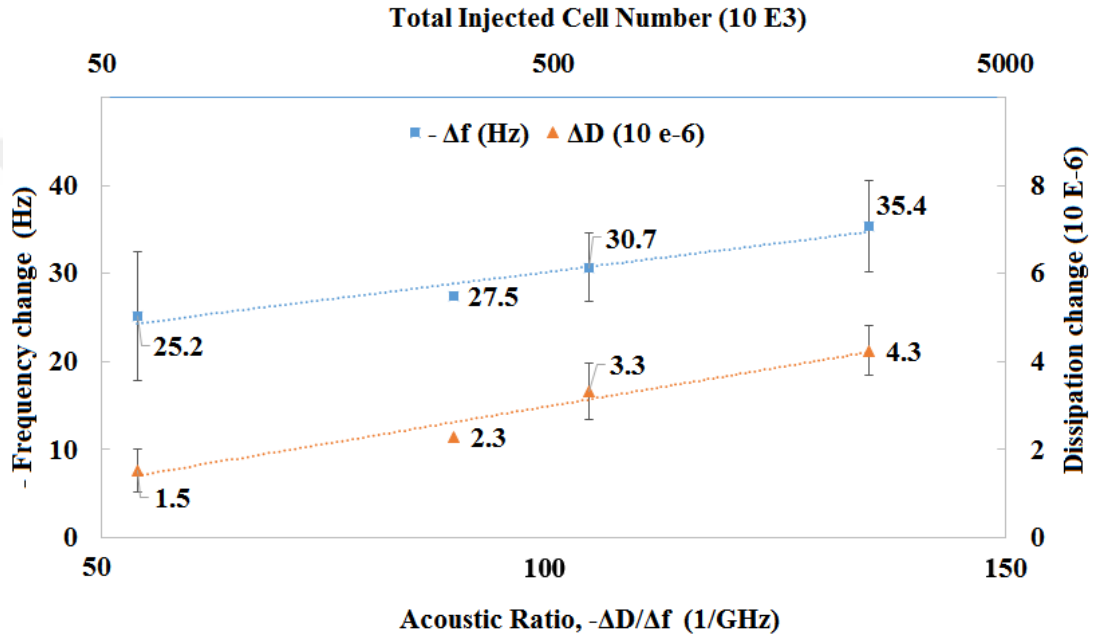

Figure B.1 : The correlation between injected hfOB cell number, acoustic ratio and -Δf and ΔD values under 1 h continuous flow.

The experiment was also conducted in no flow conditions with direct incubation of cells onto the sensor. In this case, Δf dropped rapidly and stabilized within few ten minutes for all cell numbers. The interval of 25 – 35 Hz corresponded to 50 – 80 × 10^3 cells (Figure B.2). In the flow system, however, effect of gravitational force seemed to be reduced so not all cells can reach the surface for attachment and some of them might be attached onto the walls of the tubings or washed away from the system. It is also important to state that, the adhesion stages of the cells on the surface at the beginning and the end of 1 h may be different in the flow system; thereby the source of the signals will not only convolutes the results of the initial attachment, but also further stages.

The calculated acoustic ratio, -ΔD/Δf (dissipated energy per mass), is independent from cell density on the surface (unless approached to the confluency). However, it is significantly affected from introduced cell concentration, especially at low values (50 – 500 × 10^3), but not changed considerably at higher ones (500 – 5000 × 10^3). This might be an indication of cell–cell interactions affecting the cell morphology and therefore dissipation signal [152].

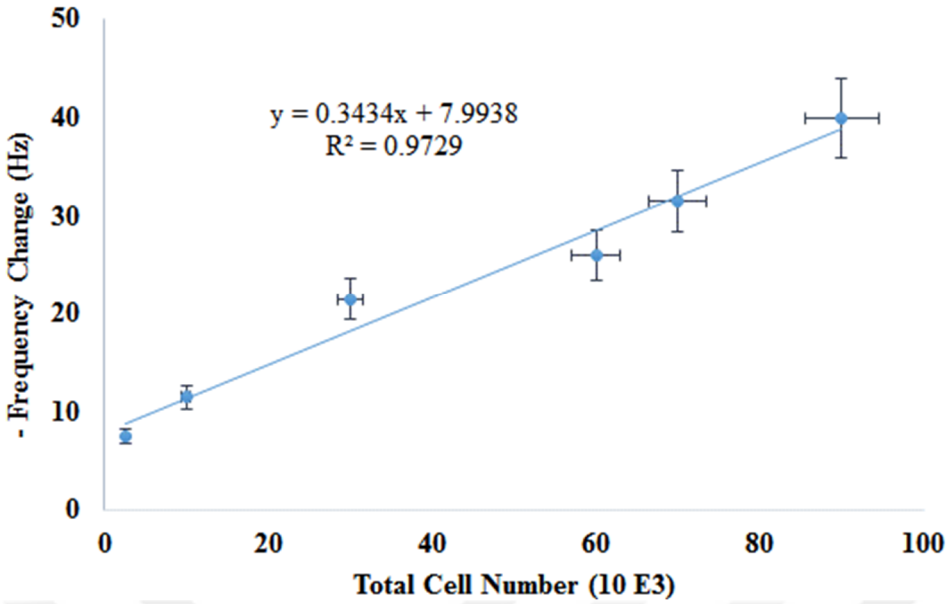

Figure B.2 : The correlation between hfOB cell number on untreated gold surface and -Δf values for 10 min of incubation in no flow conditions.

In no flow conditions, there was linear correlation between the introduced cell density and frequency change on untreated surfaces (Figure B.2). This is generally consistent with the literature for short-term experiments (< 1 h) with non-confluent cell layers [138]. In the flow system, on the other hand, a power-law correlation was observed between the seeding density and frequency change.

B.2. Cell morphologies in a standard cell culture well plate

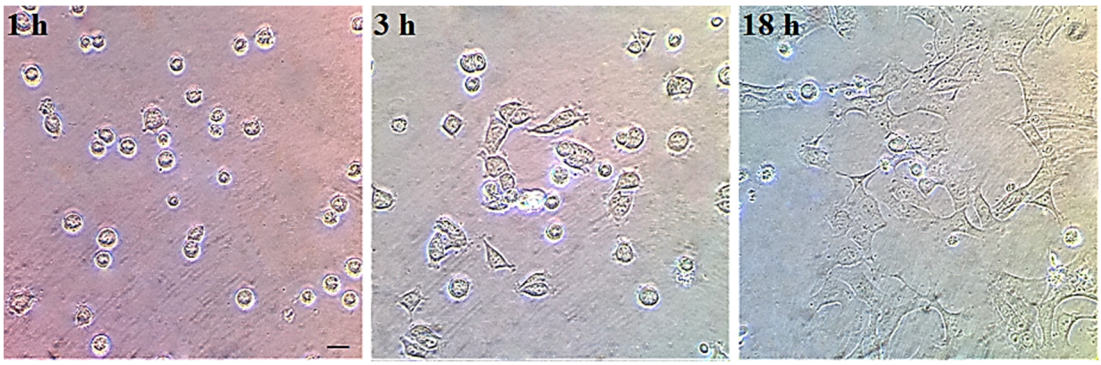

Figure B.3 : Cell morphologies in a standard cell culture well plate with similar density (in serum-free media). Scale bar is 20 µm.

B.3. Monitoring cell behavior during trypsin treatment

After the cell attachment, spreading and rinsing steps, the effect of trypsinization on cell behavior was tested in untreated surfaces (Figure B.4). It can be seen that trypsin–EDTA treatment decreased the sensed mass and Δf and ΔD approached to their initial values (-25 Hz and 1.2×10^{-6}, respectively) indicating disruption of protein-mediated anchorage of the live cells. It can be concluded that even in untreated surfaces where the cell adhesion is less favored, live cells established protein-mediated connections with the surface.

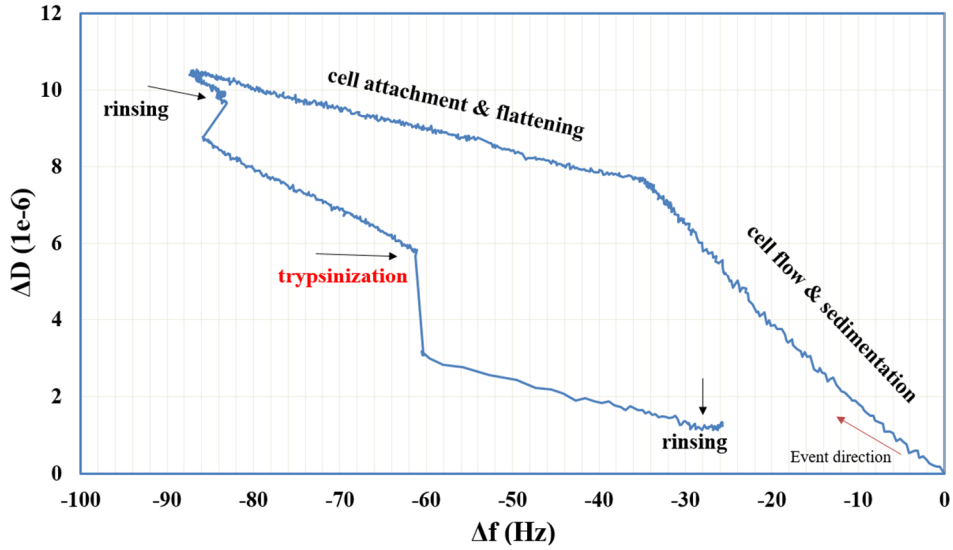

Figure B.4 : The effect of trypsinization on hfOB cells attached on untreated surface.

B.4. Protein coating onto the sensor surfaces

Table B.1 : The -Δf and ΔD changes and calculated adsorbed areal mass according to Sauerbrey equation [118] for each protein coating.

	-Δf (Hz)	ΔD (10^{-6})	Δmass (ng/cm^2)
FN (2.5 µg/mL)	13.8 ± 2.5	1.0 ± 0.1	244.3 ± 44.3
BSA (200 µg/mL)	13.2 ± 1.6	0.4 ± 0.2	233.6 ± 28.3
PLL (100 µg/mL)	18.2 ± 4.0	0.8 ± 0.3	322.1 ± 70.8

B.5. Cancerous cell adhesion on untreated and hydrophilic gold surfaces

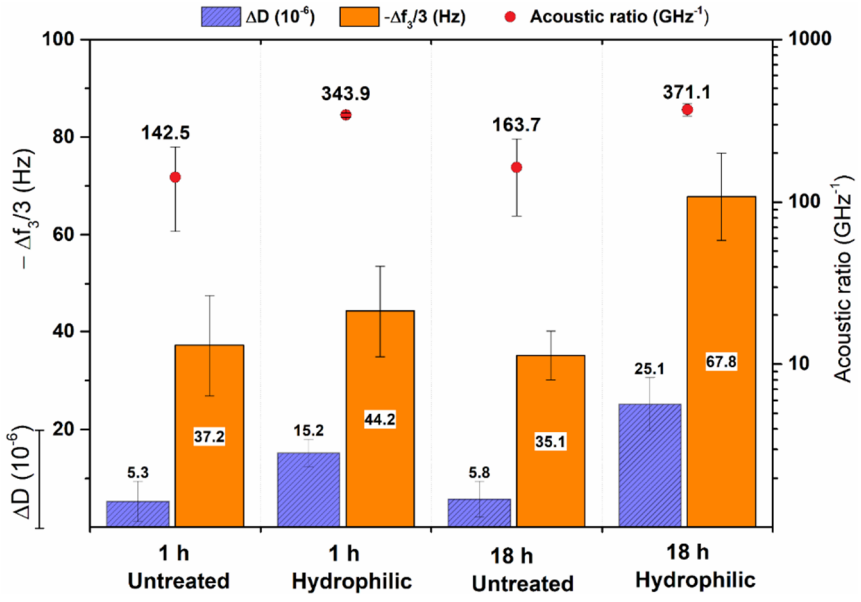

Figure B.5 : -Δf, ΔD and -ΔD/Δf values at the end of 1 and 18 hours on both untreated and hydrophilically treated gold surfaces for SaOS-2 cells.

APPENDIX C

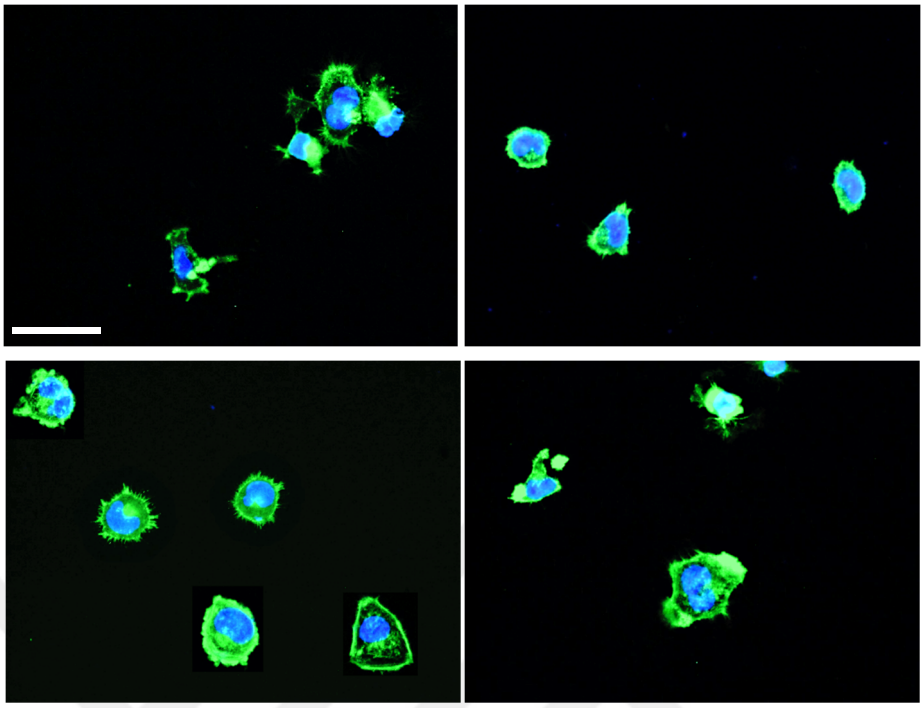

Figure C.1 : Fluorescence images of cell morphologies attached on control glass surface without any peptide coating. Scale bar: 50 µm.

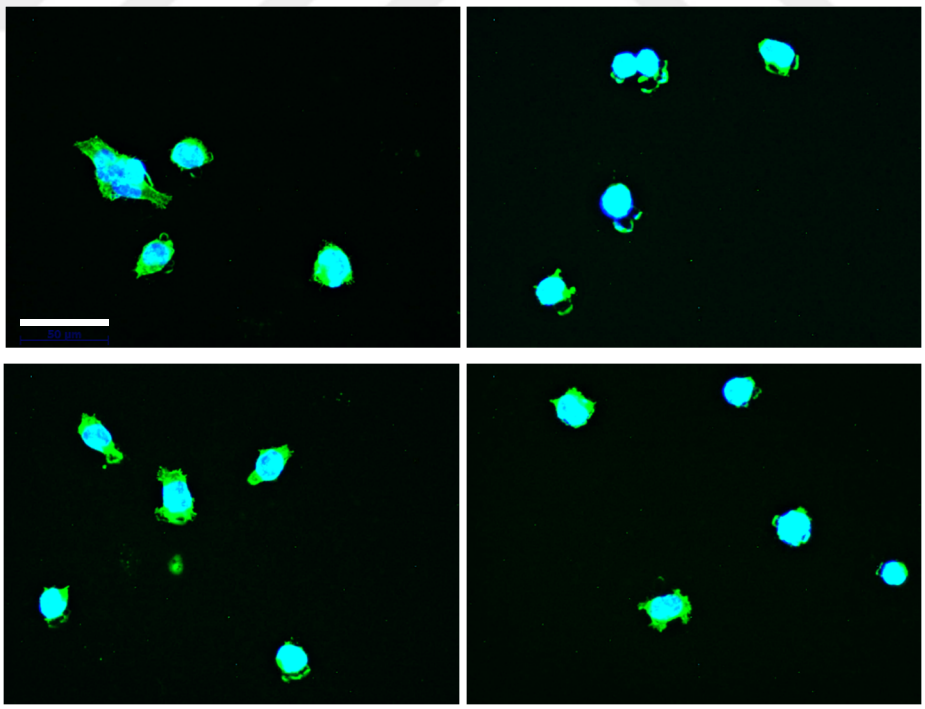

Figure C.2 : Fluorescence images of cell morphologies attached on PC SLB. Scale bar: 50 µm.

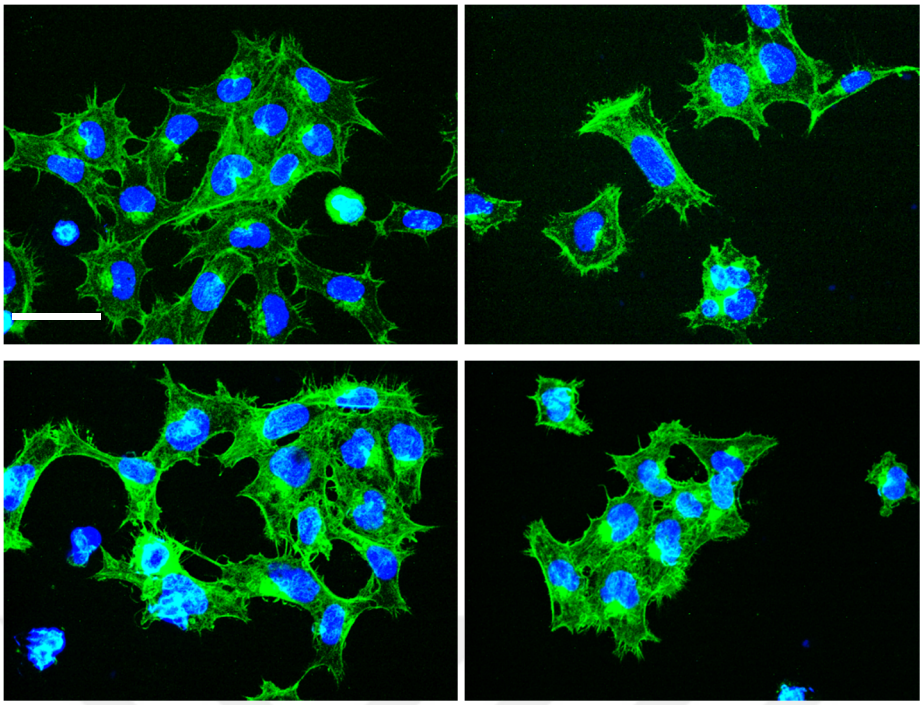

Figure C.3 : Fluorescence images of cell morphologies attached on RGD-coated glass. Scale bar: 50 µm.

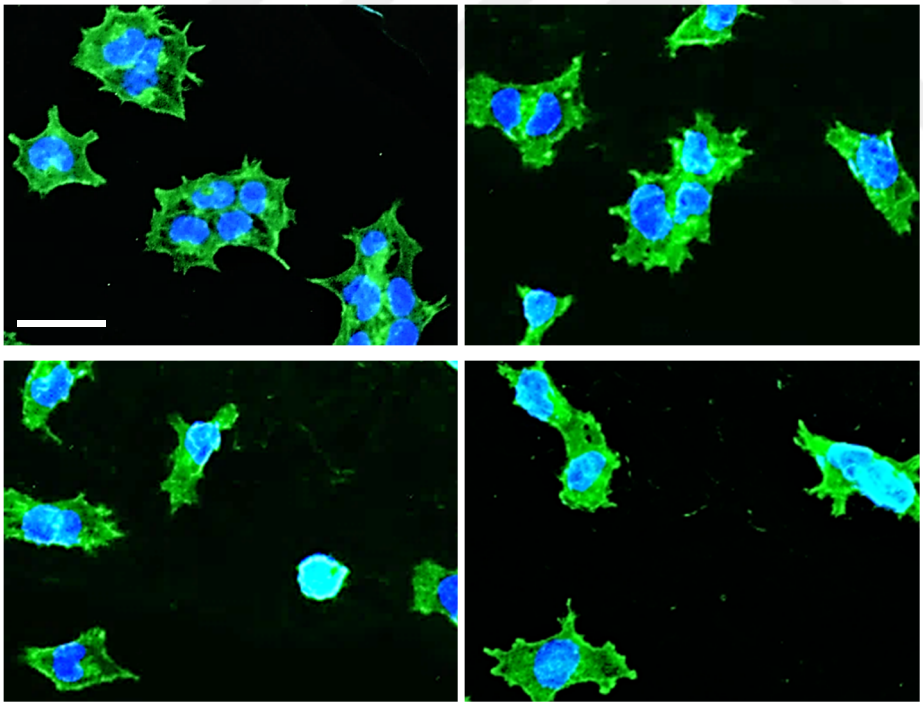

Figure C.4 : Fluorescence images of cell morphologies attached on RGD-^{f}SLB. Scale bar: 50 µm.

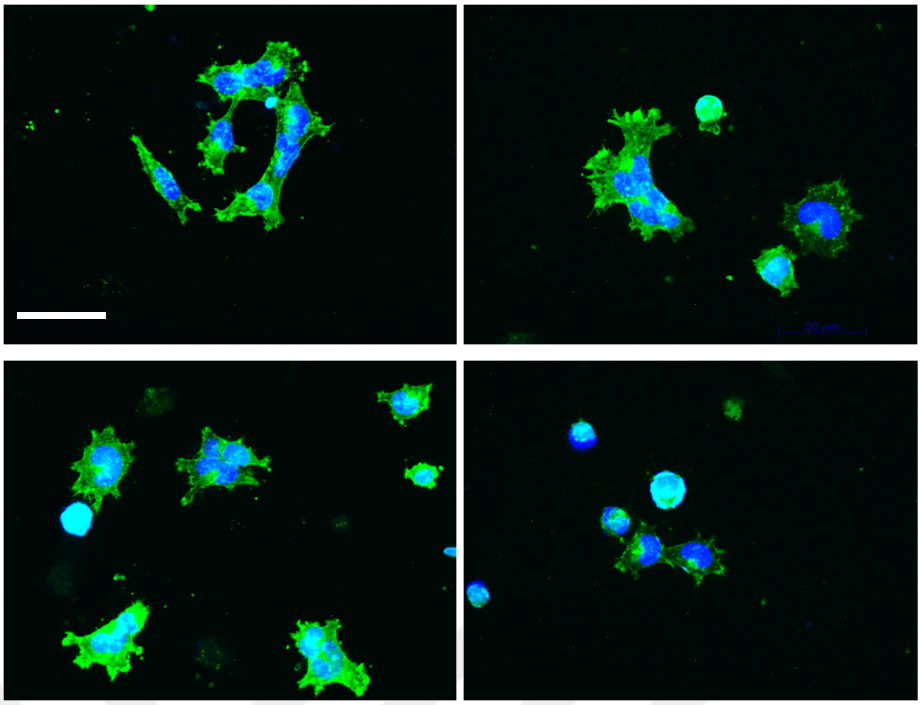

Figure C.5 : Fluorescence images of cell morphologies attached on OSN-coated glass. Scale bar: 50 µm.

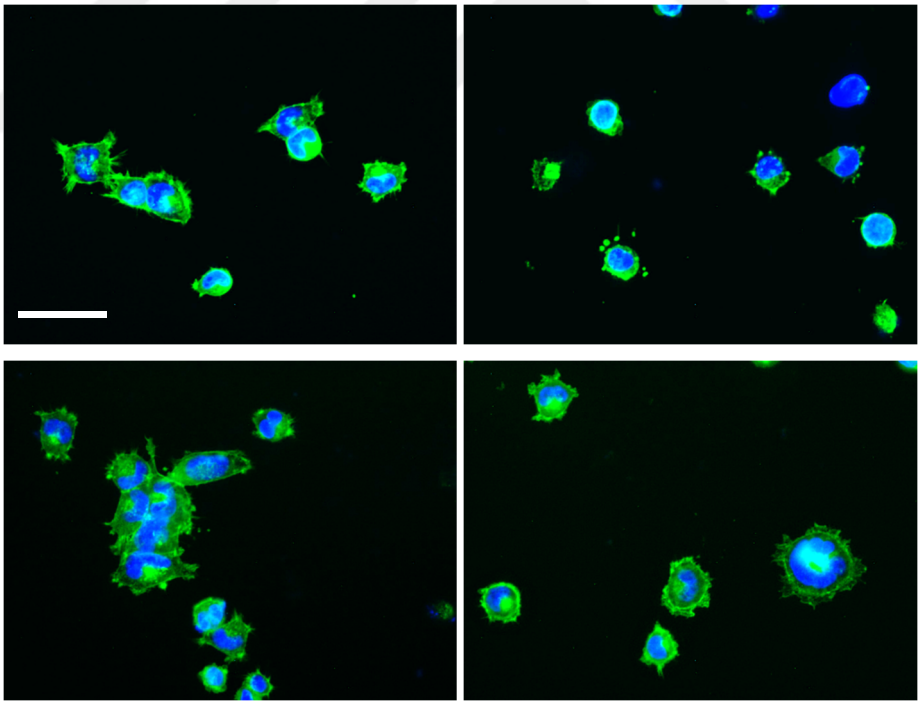

Figure C.6 : Fluorescence images of cell morphologies attached on OSN-^{f}SLB. Scale bar: 50 µm.

CURRICULUM VITAE

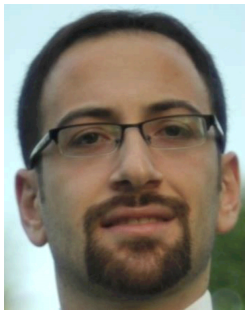

Name Surname **:** Abdulhalim KILIÇ

Place and Date of Birth **:** Trabzon / 08.12.1984

E-Mail **:** kilicabd@itu.edu.tr

EDUCATION

B.Sc. : 2008, Istanbul Technical University, Molecular Biology and Genetics Programme

M.Sc. : 2012, Istanbul Technical University, Molecular Biology-Genetics and Biotechnology Programme

PROFESSIONAL EXPERIENCE:

- 2009-2018, Research Assistant, Istanbul Technical University (ITU), Graduate School of Science, Technology and Engineering

PUBLICATIONS AND PRESENTATIONS ON THE THESIS:

- **A. Kilic,** F.N. Kok. Quartz crystal microbalance with dissipation as a biosensing platform to evaluate cell-surface interactions of osteoblast cells, *Biointerphases*, *13 (2017)* 011001.DOI: 10.1116/1.5000752.
- **A. Kilic**, M. F. Jadidi, H.O. Ozer, F.N. Kok. The effect of thiolated phospholipids on formation of supported lipid bilayers on gold substrates investigated by surface-sensitive methods, *Colloids Surf B Biointerfaces*, *160 (2017)* 117-125. DOI: 10.1016/j.colsurfb.2017.09.016.
- **A. Kilic**, F.N. Kok. Biomimetic lipid bilayers on solid surfaces: models for biological interactions, *Surf Innov*, *4 (2016)* 141-157. Themed issue on bio–nano interfaces and their engineering applications. DOI: 10.1680/jsuin.16.00008.

- **A. Kilic**, F.N. Kok. Real-time measurement of cell adhesion on model proteins-coated surfaces. *4th International Symposium of Materials on Regenerative Medicine (2017 ISOMRM)*, 23 – 26 August 2017, Taiwan.
- **A. Kilic**, Ş. Üstünel, F.N. Kok. QCM-D as a Biosensing Platform to Evaluate Cell – Surface Interactions of Model Cancerous and Healthy Cells. *BIOMED 2017 The 22nd International Biomedical Science and Technology Symposium,* 12-14 May 2017, Ankara, Turkey.
- **A. Kilic**, E. Güney, F.N. Kok. The Effect of Negatively Charged Phospholipid On Liposome Behavior. *BIOMED 2017 The 22nd International Biomedical Science and Technology Symposium*, 12-14 May 2017, Ankara, Turkey.
- **A. Kilic**, G. Çelebi, F.N. Kok. Analysis of the stability of supported lipid bilayers for cell culture studies. *The FEBS Journal, Volume 283, Issue Supplement S1 Special Issue: 41st FEBS Congress, Molecular and Systems Biology for a Better Life*, Ephesus/Kuşadasi, Turkey, September 3-8, 2016 September 2016. Pages: 127–427 DOI: 10.1111/febs.13808.
- **A. Kilic**, F.N. Kok. Monitoring of cell adhesion on different surfaces by quartz crystal microbalance sensor. *12th Nanoscience and Nanotechnology Conference (NanoTR 12)*, 03-05 June 2016, Kocaeli, Turkey.
- **A. Kilic**, F.N. Kok. Characterization of a Supported Lipid Membrane Model by Quartz Crystal Microbalance and Surface Plasmon Resonance Techniques. *12th Nanoscience and Nanotechnology Conference (NanoTR 12),* 03-05 June 2016, Kocaeli, Turkey.
- **A. Kilic**, M. Fazeli Jadidi, H.O. Ozer, F.N. Kok. Construction and Characterization of Supported Lipid Membranes to mimic Cell-Surface Interactions. *BIOMED 2015 The 21st International Biomedical Science and Technology Symposium*, 22-24 October 2015, Antalya, Turkey.
- **A. Kilic**, D. Bozkurt, E. Yener, F.N. Kok. Detection of Liposome Stability with Quartz Crystal Microbalance with Dissipation (QCM-D) Analysis. *BIOMED 2015 The 21st International Biomedical Science and Technology Symposium*, 22-24 October 2015, Antalya, Turkey.

OTHER PUBLICATIONS AND PRESENTATIONS:

- U. Celik, **A. Kilic**, F.N. Kok, H.O. Ozer, F. Bakan, A. Oral. Characterization of Au (111) Supported Artificial Lipid Membranes in the Study of Cell Membrane Related Proteins by nc-AFM. *15th International Conference on non-Contact Atomic Force Microscopy*, July 1-5 2012, Cesky Krumlov (Czech Republic).
- **A. Kilic**, F.N. Kok. Supported Lipid Bilayers with Thiolated Lipids. *17th International Symposium on Biomedical Science and Technology (BIOMED 2011)*, November 23-25, 2011 Ankara, Turkey.
- Ince O., Kolukirik M., **A. Kilic**, Gozdereliler E., Ince B. K. FISH versus Q-PCR to quantify Sulfate Reducing Bacteria and Methanogens in a Marine Sediment. *Advances and Applications of FISH Technology: drinking water, environmental and foodstuff analysis Workshop*. December 10-11, 2007. Riga-Latvia.